LA-SUB--97-48

Modification of the Finite Element Heat and Mass Transfer Code (FEHM) to Model Multicomponent Reactive Transport

Hari Selvi Viswanathan

Los Alamos
NATIONAL LABORATORY
Los Alamos, New Mexico 87545

ACKNOWLEDGMENTS

I would like to thank Professor Albert Valocchi, Dr. Bruce Robinson and Dr. George Zyvoloski for making this work possible. Professor Valocchi was nice enough to take me in as his student and spent a lot of time assisting me with my work. His expertise in reactive transport modeling was vital to the numerical techniques presented. Dr. Bruce Robinson played an equally important role by sharing his expert knowledge on FEHMN and on transport modeling at Yucca Mountain. Many of the ideas contained within this document have their roots within Professor Valocchi and Dr. Bruce Robinson. George Zyvoloski is responsible for making the collaboration with Los Alamos National Laboratory and the University of Illinois possible. Thanks to George, I was allowed to concentrate on the technical work rather than having to constantly worry about funding.

Thanks also go to Dr. Andy Wolfsberg who thoroughly reviewed this document and provided many helpful comments. Appreciation is also expressed to Caroline Tebes who aided in the FEHMN verification studies presented in this document.

Financial support for this project is gratefully acknowledged to the Earth and Environmental Sciences Division at Los Alamos National Laboratory.

TABLE OF CONTENTS

LIST OF FIGURES

LIST OF TABLES

MODIFICATION OF THE FINITE ELEMENT HEAT AND MASS TRANSFER CODE (FEHMN) TO MODEL MULTICOMPONENT REACTIVE TRANSPORT

by

Hari Selvi Viswanathan

ABSTRACT

The finite element code FEHMN, developed by scientists at Los Alamos National Laboratory (LANL), is a three-dimensional finite element heat and mass transport simulator that can handle complex stratigraphy and nonlinear processes such as vadose zone flow, heat flow and solute transport. Scientists at LANL have been developing hydrologic flow and transport models of the Yucca Mountain site using FEHMN. Previous FEHMN simulations have used an equivalent K_d model to model solute transport. In this thesis, FEHMN is modified making it possible to simulate the transport of a species with a rigorous chemical model. Including the rigorous chemical equations into FEHMN simulations should provide for more representative transport models for highly reactive chemical species.

A fully kinetic formulation is chosen for the FEHMN reactive transport model. Several methods are available to computationally implement a fully kinetic formulation. Different numerical algorithms are investigated in order to optimize computational efficiency and memory requirements of the reactive transport model. The best algorithm of those investigated is then incorporated into FEHMN. The algorithm chosen requires for the user to place strongly coupled species into groups which are then solved for simultaneously using FEHMN. The complete reactive transport model is verified over a wide variety of problems and is shown to be working properly.

The new chemical capabilities of FEHMN are illustrated by using Los Alamos National Laboratory's site scale model of Yucca Mountain to model two-dimensional, vadose zone ^{14}C transport. The simulations demonstrate that gas flow and carbonate chemistry can significantly affect ^{14}C transport at Yucca Mountain. The simulations also prove that the new capabilities of FEHMN can can be used to refine and buttress already existing Yucca Mountain radionulcide transport studies.

1. INTRODUCTION

1.1 Overview

Yucca Mountain, Nevada, has been chosen by the Department of Energy (DOE) as a possible site for the nation's first high level radioactive waste repository. The DOE must demonstrate that a repository will isolate waste for at least 10,000 years. The probability of radionuclide release into the groundwater and atmosphere must be determined, and these probabilities are then to be compared to regulatory release limits to assess the suitability of the site. In order to predict these probabilities, the complex flow and transport of contaminants must be modeled for at least 10,000 years.

Coupled air-water flow, heat flow, and contaminant transport are among the important processes that need to be modeled in the saturated and unsaturated zones of Yucca Mountain. The Yucca Mountain Project Review, an external review committee appointed by the DOE, has selected three unsaturated zone codes for further development and application (Reeves et al., 1994). These codes are Finite Element Heat and Mass Transfer Code (FEHMN) and TRACR3D of Los Alamos National Laboratory, and TOUGH of Lawrence Berkeley Laboratory. Of these codes, FEHMN is the only one that combines coupled thermal and stress capabilities with multiphase flow and transport (Zyvoloski, 1994).

Scientists at Los Alamos National Laboratory (LANL) have been developing hydrologic flow and transport models of the Yucca Mountain site using FEHMN. Coupled heat, flow and transport simulations have been used to model the transport of natural environmental isotopes. Simulations of ^{14}C and ^{36}Cl transport have already been conducted using half life models to simulate the decay of the radionuclides (Robinson, 1995). Repository breach simulations of ^{237}Np have also been carried out using sorption isotherms and decay models (Robinson, 1995). These simulations provide estimates for parameters such as the effective K_d and the retardation factor of a contaminant which can be then be used to predict probabilities of radionuclide release into the groundwater system at Yucca Mountain.

More complex chemical interactions with ^{237}Np and ^{14}C have not been possible. Specifically, ^{237}Np speciation studies have shown that different ^{237}Np complexes differ greatly in sorption behavior (Benson et al., 1994). Specifically, negatively charged ^{237}Np carbonate complexes do not strongly sorb to Yucca Mountain mineral surfaces, whereas positively charged species such as NpO_2^+ strongly sorb to many Yucca Mountain mineral surfaces. The species NpO_2^+ has also been shown to participate in an ion exchange reaction with Ca^{2+}. These complex interactions may not be representable with an equivalent K_d because the retardation of ^{237}Np will be a function of the water chemistry which is spatially variant throughout the mountain. ^{14}C also participates in numerous chemical reactions in the Yucca Mountain groundwater system. Numerous aqueous carbonate species (e.g. H_2CO_3, HCO_3^-, CO_3^{2-}) and carbonate minerals (e.g. calcite) exist in the Yucca Mountain groundwater system and all of these species may play an important role in the transport of ^{14}C (Meijer, 1993). Again, these chemical interactions may display nonlinear effects which cannot be modeled by an equivalent K_d.

FEHMN does not have the capability to model more complicated processes such as complexation, dissolution/precipitation and kinetic sorption processes. In fact, the majority of transport problems in the groundwater field are simulated as either nonreactive or are simulated with linear retardation and first order decay models. More complex models have not been widely used due to the substantial computational demands and human effort required to simulate these problems (Walter et al., 1994).

The increase in relatively inexpensive computational power in the last few years has made the problem of multidimensional and multicomponent reaction and transport feasible (Steefel and Lasaga, 1994). FEHMN can now be modified to include more complex chemical processes in the transport model while maintaining reasonable computational efficiency. These complex processes should provide more representative models of radionuclide transport than the simple decay and linear retardation models used in previous studies.

The topics covered in this thesis pertain to enhancing FEHMN's reactive transport capabilities. The enhancements will make it possible to include more complicated reaction sequences into the radionuclide transport models. By treating the chemical system more rigorously, more representative predictions of radionuclide transport should be possible. In addition, the equivalent K_d approach of modeling solute transport used in previous transport studies can be buttressed by these more rigorous calculations.

1.2 Background

This section provides a brief summary of the techniques used to model reactive transport. Some of the relevant papers are presented to develop the history of reactive transport modeling.

In a reactive transport code, the transport of a species is modeled with a partial differential equation (PDE) which describes the advection, dispersion and sources/sinks in the model domain. The method in which transport codes incorporate the chemistry varies depending on the particular code. In general, the chemistry of the system can be modeled using either a kinetic, equilibrium or mixed kinetic-equilibrium formulation.

The equilibrium formulation relies on the local equilibrium assumption (LEA). LEA can be invoked when the reaction time scale is sufficiently faster than the transport time scale. A great deal of work has been done to examine the validity of the assumption (Lasaga and Rye, 1993; Steefel and Cappellen, 1990; Knapp, 1989; Bahr and Rubin, 1987; Valocchi, 1985). The simplification which arises from applying LEA often results in a mixed differential/algebraic equation set (Zysett et al, 1994) because all the reaction source/sink terms can be described by algebraic equations if LEA is invoked.

A kinetic formulation is always the more general approach to describing any reactive system, and allows for both equilibrium and kinetic reactions to be modeled with the same general formulation. In kinetic formulations, the chemical equations are incorporated into the transport PDE as a source/sink term. This source/sink term due to chemical reaction is often dependent on the concentrations of many chemical species. Therefore, a kinetic formulation results in a system of

coupled PDEs and ODEs which are computationally more intensive to solve than the equations which result from the equilibrium formulation (Zysett et al., 1994).

The first codes that coupled complex chemistry with transport typically assumed that all chemical species in the system were in local equilibrium (Engesgaard and Kipp, 1992; Yeh and Tripathi, 1988; Cederberg et al., 1985; Rubin , 1983). Papers by Yeh and Tripathi (1989) and Liu and Narasimhan (1989) review many of these models and discuss their approaches. Due to computational limitations and the virtually nonexistent data base of mineral-water reaction rates, the local equilibrium assumption was a necessity until recently. The current trend in reactive transport codes has been to include kinetic formulations for certain types of chemistry. Studies have shown that equilibrium conditions do not always exist in the subsurface (Steefel and Lasaga, 1994; Friedly and Rubin, 1992). Friedly and Rubin cite numerous studies which provide experimental evidence that disequilibrium can exist in the field and especially in laboratory column experiments. Experimental evidence of kinetic limitations is shown in: Wood et al. (1990), Brusseau et al. (1989), Nicoud and Schweich (1989), van der Zee et al. (1989), Goltz and Roberts (1986), and Hutzler et al. (1986). In general, multi-phase reactions, such as rock-water interactions, often take place over extremely long time scales relative to the typical groundwater transport time scales making it necessary to account for the kinetics of the system for these processes. With a rapidly increasing data base on mineral-water reaction rates and with the enormous increase in inexpensive computational power, multidimensional kinetic and equilibrium reactive transport problems are now feasible (Steefel and Lasaga, 1994).

Various approaches have been taken to model combined kinetic and equilibrium transport systems. These approaches will be referred to as mixed equilibrium-kinetic formulations in this thesis. Liu and Narasimhan (1989) include kinetic solid dissolution in their otherwise equilibrium transport code. Steefel and Lasaga (1994) and Valocchi and Pastor (1994) assume aqueous phase reactions are in local equilibrium but include kinetic models for rock-water interactions. Friedly and Rubin (1992) provide a general framework for modeling mixed systems of kinetic and equilibrium reactions. Their method allows for kinetic and equilibrium formulations to be used interchangeably by

performing certain transformations on the matrix equations. Friedly and Rubin found that under certain conditions, equilibrium conditions are most efficiently simulated by solving the kinetic equations with relatively large rate constants rather than mixing kinetic and equilibrium formulations. Although, many cases exist in which a equilibrium formulation mixed with a kinetic formulation is the most efficient formulation.

None of the models reported in the literature review are capable of modeling chemical reactions coupled to processes such as heat flow and multiphase flow. All of these processes may be important in modeling radionuclide transport at Yucca Mountain. Specifically, the potential repository is to be located in the unsaturated zone of Yucca Mountain requiring an unsaturated flow model. A heat flow model is also necessary because the containers placed in the repository will release large amounts of heat due to radioactive decay of the waste. The heat flow will influence the groundwater flow near the repository (Ross, 1987). Including a chemical model into FEHMN will make it possible to study the interaction between the chemical transport processes and the groundwater flow and heat flow processes at Yucca Mountain. These processes may be time variant requiring that the flow and transport models are coupled as they are in FEHMN.

1.3 Purpose and Scope

This thesis discusses the development of a general reaction module that is capable of modeling kinetic and equilibrium reactions within a single framework. In Chapter 2, the formulation framework for the reactive transport model is chosen and developed for a one-dimensional, saturated flow transport code. Various solution algorithms are constructed to determine the best method for solving the transport and chemical equation sets. Chapter 3 reports the evaluation of these solution strategies. In Chapter 4, the most efficient scheme is then incorporated into FEHMN and the reactive transport model is thoroughly tested and verified. After the model is verified, the new chemical capabilities of FEHMN will be illustrated in Chapter 5 by using LANL's site scale model of Yucca Mountain to model unsaturated zone ^{14}C transport.

2. DEVELOPMENT OF THE REACTIVE TRANSPORT MODEL

2.1 Overview

In this chapter, the reactive transport model is developed. First, the type of formulation is chosen for the reactive transport model. Various iterative schemes are then proposed to solve the system of equations which result from the reactive transport formulation. To facilitate comparisons between the different iterative schemes, a one-dimensional saturated flow finite difference code was written.

2.2 Choice of Model Formulation

FEHMN is to be used for large-scale, two and three dimensional flow and transport simulations with many nodes and will not be used to perform large geochemical calculations (i.e. 50 or more chemical species). As stated previously, FEHMN combines coupled thermal and stress capabilities with multiphase porous media flow and transport. Since the Yucca Mountain FEHMN simulations are already very computer intensive, it would probably be infeasible to couple a full geochemical model to FEHMN. In addition, major code revisions would be necessary to couple a geochemical code to FEHMN. Instead, information from large geochemical codes will be distilled down to 10 or fewer species which can then be modeled by FEHMN. The guiding principle behind the FEHMN reactive transport model is that a "good" model does not consider every possible reaction and species; instead, the user of the model must apply insight in order to identify the reactions and species that are truly significant.

The FEHMN reactive transport model should be capable of modeling several types of chemical processes, specifically, radioactive decay, aqueous complexation, precipitation/dissolution, and adsorption. Each of these reaction types can display different characteristics in a groundwater system. Aqueous phase complexation reactions often take place over a short time scale relative to a typical groundwater transport time scale (Steefel and Lasaga, 1994). Therefore, these reactions can usually be treated as equilibrium reactions which leads to more simplified models. Mineral rock interactions such as adsorption and precipitation/dissolution often display kinetic limitations in many groundwater systems (Steefel and Lasaga, 1994). Therefore, these processes may have to be modeled as kinet-

ic reactions since the local equilibrium assumption may not always apply. Since adsorption and precipitation/dissolution reactions are important in modeling many geochemical systems, a kinetic or mixed equilibrium-kinetic formulation will be required for the FEHMN reactive transport model (recall that a full equilibrium model cannot model kinetic reactions).

Several options are available to add kinetic and equilibrium reaction capability to FEHMN. For example, Friedly and Rubin (1992) provide a general framework for modeling both equilibrium and kinetic reactions. However, their method requires a transformation of solution variables which would be difficult to implement practically for a large existing code like FEHMN.

Another common technique adopted by mixed equilibrium-kinetic reactive transport codes is the reduction of the number of independent variables by using the idea of chemical components. A set of chemical components is defined as the minimum number of species that uniquely describe the chemical system (Mangold and Tsang, 1991). Most large reactive transport codes simulate the transport of components and use an algebraic mass action expression to obtain concentrations of the chemical species in equilibrium with each component. By transporting components rather than species, the number of coupled PDEs is reduced. Specifically, the number of independent components in a system is given by:

$$N_c = N_{tot} - N_r$$

where N_c is the number of independent components, N_r number of equilibrium reactions, and N_{tot} is the total number of species in the simulation (Steefel and Lasaga, 1994). For large geochemical systems, N_{tot} can exceed fifty species making it necessary to simplify the system by assuming local equilibrium for certain types of reactions while retaining kinetic capability for other reaction types. For example, Lasaga and Steefel (1994) assume local equilibrium for all aqueous reactions, but model mineral-rock water interactions kinetically. They state that this assumption is widely accepted to be valid for all aqueous phase reactions except for some very low temperature redox reactions. Incorporating the idea of components into FEHMN would require significant software restructuring of the code. An equilibrium speciation routine would need to be constructed or borrowed

from another code. In addition, solute transport model of FEHMN would have to be modified to transport chemical components rather than chemical species. However, with major software restructuring, this type of mixed equilibrium-kinetic formulation is an option.

Another option for the FEHMN reactive transport model is to use a fully kinetic formulation to model both equilibrium and kinetic reactions. The software structure for a fully kinetic formulation already exists within the code. Therefore, major software restructuring would not be necessary to develop the reactive transport model. The primary disadvantage of this formulation is that number of species in the system is not reduced by applying the idea of components and LEA. Therefore, due to computational limitations, the maximum number of species which can be modeled simultaneously would be much less than that of codes which apply LEA to model aqueous phase reactions.

A clear tradeoff exists between either implementing a mixed equilibrium-kinetic formulation and a fully kinetic formulation. The mixed formulation solves for fewer coupled PDEs and will therefore be more computationally efficient than the fully kinetic formulation. However, this option requires major software restructuring of FEHMN. A fully kinetic formulation is computationally less efficient than the mixed formulation but would be easier to implement. In weighing both options, the fully kinetic formulation appears to be the better one when considering that FEHMN will only be used to model relatively small chemical systems.

Using a fully kinetic formulation to model both kinetic and equilibrium reactions has several minor advantages over the mixed formulation. Since each chemical species is transported individually, the transport parameters of each species can be different. For example, a free radionuclide can be given different dispersion properties than a radionuclide which has sorbed onto a colloid. An additional advantage is that any reaction can be modeled with either kinetic or equilibrium models. As previously stated, low temperature aqueous phase reactions could be kinetically limited. Most mixed kinetic-equilibrium formulations would be incapable of modeling any aqueous phase reactions with a kinetic model.

Several methods are available to computationally implement a fully kinetic formulation into FEHMN. The rest of the chapter will discuss different numerical algorithms which can be used to solve the transport and chemical equation sets.

2.3 Governing Equations of the One-Dimensional Model

FEHMN is a large complicated code. Therefore, it would be impractical to develop the reactive transport solution scheme for FEHMN without first examining various options on a simpler code. A finite difference code was constructed to examine various iterative solution strategies. A one-dimensional model was developed to mimic the reaction module of FEHMN while leaving out many of the other features of FEHMN which are not necessary in evaluating the performance of the reactive transport model. FEHMN can model non-isothermal, three-dimensional multi-phase flow. For simplicity, the test code models one-dimensional saturated transport. In addition, the code is only capable of modeling single phase chemical reactions, whereas FEHMN can model multi-species, sorption and precipitation reactions. The one-dimensional model is used to evaluate various solution schemes. The best scheme will then be incorporated into FEHMN.

In the model, the solute transport equation is solved for each individual species, i, present in the system. The one-dimensional solute transport equation describes the transport of the chemical species due to advection, dispersion, sources/sinks and is given by:

$$\frac{\partial C_i}{\partial t} = D_i \frac{\partial^2 C_i}{\partial x^2} - u \frac{\partial C_i}{\partial x} - \bar{S}_i \tag{1}$$

where C is the concentration, D is the hydrodynamic dispersion coefficient, u is the pore water velocity, t is the time, x is the spatial length scale and S is the source/sink term. The hydrodynamic dispersion coefficient is given by:

$$D = D^* + \alpha_L u \tag{2}$$

where D* is the molecular diffusion coefficient, and α_L is the dispersivity in the x direction. Chemical reactions are treated as sources and sinks in the formulation. Multiple reactions of the following form can be modeled:

$$a_1C_1 + a_2C_2 + \ldots + a_mC_m \underset{k_{rev}}{\overset{k_{for}}{\rightleftharpoons}} a_{m+1}C_{m+1} + a_{m+2}C_{m+2} + \ldots + a_nC_n \tag{3}$$

where the a's are the stoichiometric coefficients, k_{for} is the forward rate constant, k_{rev} is the reverse rate constant, m is the total number of reactants in the reaction and n is the total number of chemical species in the reaction. The reaction rate term for each chemical species in the above equation is given by the following kinetic formulation:

$$r_i = \pm\, a_i \left\{ k_{for} \prod_{j=1}^{j=m} \left[C_j\right]^{q(j)} - k_{rev} \prod_{j=m+1}^{j=n} \left[C_j\right]^{q(j)} \right\} \tag{4}$$

where r_i is defined as the loss/gain of species i per unit volume of porous media, and the exponent q(j) is the order of the reaction with respect to C_j. The subscript j loops over each chemical species which is reacting with species i. FEHMN uses this model to calculate the reaction rate term (Zyvoloski, 1995a). The reaction rate term given by (4) is added into the source/sink term, S, as follows:

$$S_i = \sum_{\text{all rxns}} r_i + \text{other sources/sinks(such as injection/extraction)} \tag{5}$$

where r_i is summed over all reactions containing species i.

The initial conditions of the transport problem are given by:

$$C_i(x, 0) = 0$$

The third type inlet inlet boundary condition allows for constant injection of each chemical species into the system. The variable $C_{i,feed}$ is the concentration injected at the inlet.

$$\left(uC_i - D_i \frac{\partial C_i}{\partial x} \right)_{x=0} = uC_{feed,i}$$

The exit boundary conditions at x = X is handled with the following Neumann condition:

$$\left(\frac{\partial C_i}{\partial x} \right)_{x=X} = 0$$

The Neumann condition allows the advective flux to leave the system, preventing a build up of mass within the domain.

Example

In the following example, chemical species A, B, and G undergo reaction as they are transported in the one-dimensional model. The one dimensional spatial domain is discretized into N spatial nodes. The species participate in the following chemical reaction:

$$\alpha A + \beta B \underset{k_{rev}}{\overset{k_{for}}{\rightleftharpoons}} \gamma G$$

where α, β and γ represent the stoichiometric coefficients. In this example it is assumed that the order of the reaction is 1st order with respect to species A, B and G. Therefore, q(j) in equation (4) is unity for each chemical species. The total number of chemical species in the system, M, is equal to three in this example. The rate terms for each species are given by the following expressions:

$$r_A = \alpha\left[k_{for}C_AC_B - k_{rev}C_G\right] \tag{6}$$

$$r_B = \beta\left[k_{for}C_AC_B - k_{rev}C_G\right] \tag{7}$$

$$r_G = \gamma\left[k_{rev}C_G - k_{for}C_AC_B\right] \tag{8}$$

In order to calculate $C_i(x,t)$, the model solves the solute transport equation at each node for each chemical species. The resulting equation set represents a set of coupled partial differential equations which fully describes the problem. The first step in numerically solving the problem is to finite difference the solute transport equation.

Equation (9) shows the finite differenced form of equation (1) for species A. The central difference approximation was used for the advection term. Equation (9) is written for an interior spatial node:

$$\frac{C_{A,p}^{k+1} - C_{A,p}^{k}}{\Delta t} = \lambda\left[\frac{D}{\Delta x^2}\left(C_{A,p+1}^{k+1} - 2C_{A,p}^{k+1} + C_{A,p-1}^{k+1}\right) - \frac{u}{2\Delta x}\left(C_{A,p+1}^{k+1} - C_{A,p-1}^{k+1}\right)\right. \tag{9}$$

$$\left. + r_A\left(C_{A,p}^{k+1}, C_{B,p}^{k+1}, C_{G,p}^{k+1}\right)\right] + (1-\lambda)\left[\frac{D}{\Delta x^2}\left(C_{A,p+1}^{k} - 2C_{A,p}^{k} + C_{A,p-1}^{k}\right)\right.$$

$$\left. - \frac{u}{2\Delta x}\left(C_{A,p+1}^{k} - C_{A,p-1}^{k}\right) + r_A\left(C_{A,p}^{k}, C_{B,p}^{k}, C_{G,p}^{k}\right)\right]$$

where λ is the implicitness weighting factor, the subscript p denotes the spatial node, the subscripts A,B & G denote the chemical species and k the time level. Note that the rate term, r, is left as a func-

tion of the chemical species in the system (A, B and G). Using standard finite difference notation, λ=0 is fully explicit, λ=1 is fully implicit, and λ=0.5 is Crank-Nicolson time differencing.

Equations of similar form to equation (9) are written for species B and G. The equations are written at each node and are adjusted accordingly to account for boundary conditions at the inlet and exit nodes.

The finite difference equation (9) involves the five unknowns, $C^{k+1}_{A,p-1}$, $C^{k+1}_{A,p}$, $C^{k+1}_{A,p+1}$, $C^{k+1}_{B,p}$, $C^{k+1}_{G,p}$, and is nonlinear due to the reaction rate terms given by equations (6), (7) and (8). Therefore, Newton's method is used to linearize the equation set. Newton's method solves a set of nonlinear equations by making use of a Taylor series expansion (e.g. Press et al. , 1986). In order to apply Newton's method, equation (9) is rewritten in residual form as:

$$f\left(C^{k+1}_{A,p-1}, C^{k+1}_{A,p}, C^{k+1}_{A,p+1}, C^{k+1}_{B,p}, C^{k+1}_{G,p}\right) = 0 \tag{10}$$

Applying Newton's method to equation (10) gives:

$$\frac{\partial f}{\partial C_{A,p-1}}\delta C_{A,p-1} + \frac{\partial f}{\partial C_{A,p}}\delta C_{A,p} + \frac{\partial f}{\partial C_{A,p+1}}\delta C_{A,p+1} + \frac{\partial f}{\partial C_{B,p}}\delta C_{B,p} + \frac{\partial f}{\partial C_{G,p}}\delta C_{G,p} \tag{11}$$

$$= - f\left(C^{k+1,m}_{A,p-1}, C^{k+1,m}_{A,p}, C^{k+1,m}_{A,p+1}, C^{k+1,m}_{B,p}, C^{k+1,m}_{G,p}\right)$$

where δC is defined by:

$$\delta C = C^{k+1,m+1} - C^{k+1,m} \tag{12}$$

where m represents the Newton iteration number.

After applying Newton's method to the full set of finite differenced solute transport equations at each node for each chemical species, the equation set takes on the matrix form:

$$[J]\delta C = b \tag{13}$$

where [J] is the Jacobian matrix and b is the vector of residuals. The Jacobian is comprised of the derivative terms on the left hand side of equation (11) and the b vector is made up of the function f, the right hand side of equation (11).

For the example reaction, the structure of equation set (13) is shown in Figure 1:

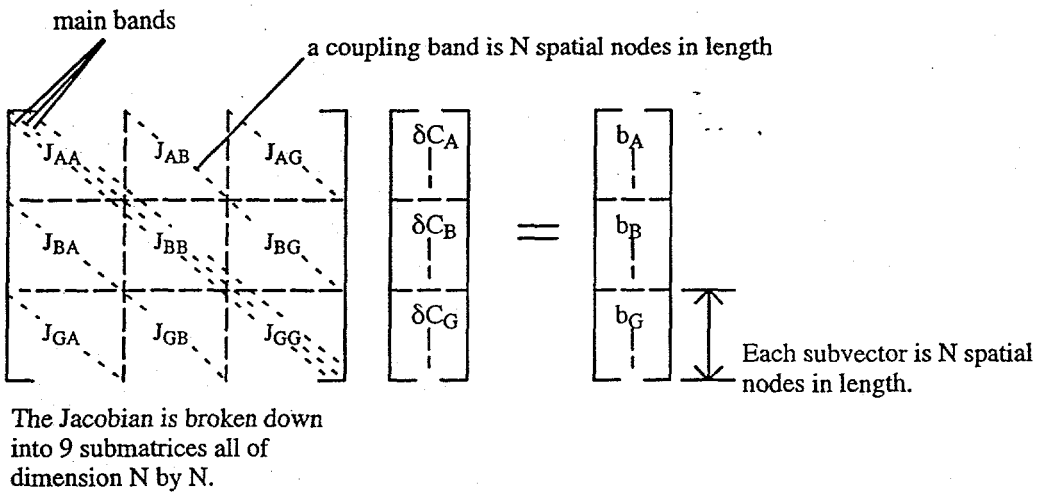

Figure 1: The structure of the equation set

The structure of equation (13) is obtained from applying Newton's method to the set of finite differenced solute transport equations. For example, the nonzero matrix elements for the submatrix J_{AA} are given below:

$J_{AA,p,p-1}$: $\lambda\Delta t\left(-\frac{D}{\Delta x^2}-\frac{u}{2\Delta x}\right)$ The subdiagonal element is obtained by differentiating equation (9)* with respect to: $C_{A,p-1}^{k+1}$

$J_{AA,p,p}$: $1+\lambda\Delta t\left[\frac{2D}{\Delta x^2}+\frac{\partial r_A}{\partial C_{A,p}^{k+1}}\right]$ The main diagonal element is obtained by differentiating equation (9)* with respect to: $C_{A,p}^{k+1}$

$J_{AA,p,p+1}$: $\lambda\Delta t\left(-\frac{D}{\Delta x^2}+\frac{u}{2\Delta x}\right)$ The superdiagonal element is obtained by differentiating equation (9)* with respect to: $C_{A,p+1}^{k+1}$

* equation (9) was multiplied through by Δt before the derivatives were taken.

In order to obtain the matrix elements for J_{BB} and J_{GG}, the solute transport equations for species B and G must be differentiated using the same procedure.

The coupling bands shown in Figure 1 represent the Jacobian cross derivative terms. These terms exist because the reaction rate for a particular species depends upon the concentration of other species. For example, the nonzero matrix elements of J_{AB} are given by:

$J_{AB,j,j}$: $\lambda \frac{\partial r_A}{\partial C_{B,p}^{k+1}} \Delta t$ This coupling band is obtained by differentiating equation (9) with respect to: $C_{B,p}^{k+1}$

The J_{AB} coupling band represents the dependence of the reaction rate of A on species B. Similarly, J_{BA} represents the dependence of the reaction rate of B on species A. The nonzero matrix elements of J_{BA} are given by:

$J_{BA,j,j}$: $\lambda \frac{\partial r_B}{\partial C_{A,p}^{k+1}} \Delta t$ This coupling band is obtained by differentiating the solute transport equation for species B (not shown) with respect to: $C_{A,p}^{k+1}$

The residual vector,b, contains all terms of the solute transport equation that are "known". Specifically, the terms with concentrations evaluated at the old Newton iteration, m, and old time level, k, make up the residual vector. The b vector for an interior node of species A is given by:

$$b = C_{A,p}^{k+1,m} - C_{A,p}^{k} - \lambda\Delta t\left[\frac{D}{\Delta x^2}\left(C_{A,p+1}^{k+1,m} - 2C_{A,p}^{k+1,m} + C_{A,p-1}^{k+1,m}\right)\right. \tag{14}$$

$$\left. - \frac{u}{2\Delta x}\left(C_{A,p+1}^{k+1,m} - C_{A,p-1}^{k+1,m}\right) + r_A\left(C_{A,p}^{k+1,m}, C_{B,p}^{k+1,m}, C_{G,p}^{k+1,m}\right)\right]$$

$$- (1-\lambda)\Delta t\left[\frac{D}{\Delta x^2}\left(C_{A,p+1}^{k} - 2C_{A,p}^{k} + C_{A,p-1}^{k}\right) - \frac{u}{2\Delta x^2}\left(C_{A,p+1}^{k} - C_{A,p-1}^{k}\right)\right.$$

$$\left. + r_A\left(C_{A,p}^{k}, C_{B,p}^{k}, C_{G,p}^{k}\right)\right] \quad =$$

Newton's method uses an iterative process to solve the system of equations. The iterative process converges as the new solution for concentration, $C^{k+1,m+1}$, approaches the previous solution, $C^{k+1,m}$. As $C^{k+1,m+1}$ approaches $C^{k+1,m}$, the residual vector approaches zero. The test code achieves convergence when the normalized residual, $|b_{norm}|$, is below a specified tolerance (i.e. 1×10^{-10}). The normalized residual is given by:

$$|b_{norm}| = \left\{\sum_{i=1}^{M}\sum_{p=1}^{N}(b_{i,p})^2\right\}^{\frac{1}{2}} \tag{15}$$

Therefore, $|b_{norm}|$ represents how accurately the entire equation set is being solved at each node for every species.

2.4 Various Solution Schemes

As mentioned in the previous section, Newton's method is used to linearize the equation set. Newton's method introduces an iterative scheme into the solution algorithm. Figure 2 shows the general framework under which several solution strategies are to be evaluated. Sections 2.4.1 – 2.4.3 will describe the various solution algorithms that can be used to solve equation (13). Three different methodologies will be examined to solve the chemical equation set shown in Figure 1. Each solution scheme will differ in how the cross derivative terms are treated in solving the equation set. Therefore, the schemes will vary in their CPU requirements and memory requirements. Chapter 3 will compare and contrast the various schemes in an effort to determine the best solution algorithm for the FEHMN reaction module.

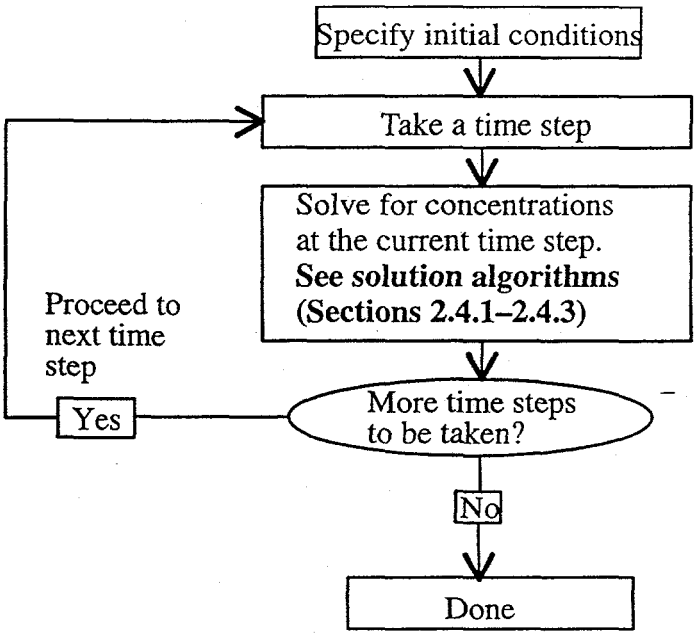

Figure 2: Basic algorithm for testing each solution algorithm

2.4.1 Fully Coupled Approach

The idea behind the Fully Coupled Approach (FCA) is to solve the entire equation set in one step. FCA has similarities to the Yeh and Tripathi (1989) Direct Substitution Approach in that both algorithms solve a set of coupled PDEs. However, they deal with an equilibrium formulation rather than the kinetic formulation developed in this thesis.

FCA solves a set of coupled PDEs simultaneously. Specifically, once all of the matrix elements in equation (13) are calculated, the system of equations can be solved by the linear equation solver, GZSOLVE (Zyvoloski and Robinson, 1995b). GZSOLVE solves the matrix equation set of the form of equation (13) using incomplete factorization and a Generalized Minimum Residual (GMRES) acceleration method.

The Fully Coupled Approach simply solves equation (13) without performing any iterations outside the linear equation solver. The entire Jacobian and vector of residuals are directly "fed" into the solver which computes the vector of δC for each species. In effect, the entire set of coupled partial differential equations is solved simultaneously. The equation set structure solved by FCA was shown in Figure 1. Figure 3 shows a detailed schematic of the solution algorithm.

Solving the entire matrix equation at once can be very computer intensive for a problem with a high number of chemical species or spatial nodes. In Chapter 3, the Fully Coupled Approach algorithm will be evaluated.

2.4.2 The Sequential Species Iteration Approach

The Sequential Species Iteration Approach (SSIA) attempts to circumvent the problem of solving the entire system of equations simultaneously in order to achieve better computational efficiency. Again, SSIA has similarities to Yeh and Tripathi's (1989) SIA algorithm, but is slightly different since they deal with an equilibrium formulation. The Yeh and Tripathi method requires iterating between their PDE solver and the chemical system which is described by algebraic equations. Their method cycles through each chemical component in the system. The SSIA in this thesis cycles through each chemical species in the system and solves a small subset of the full equation set.

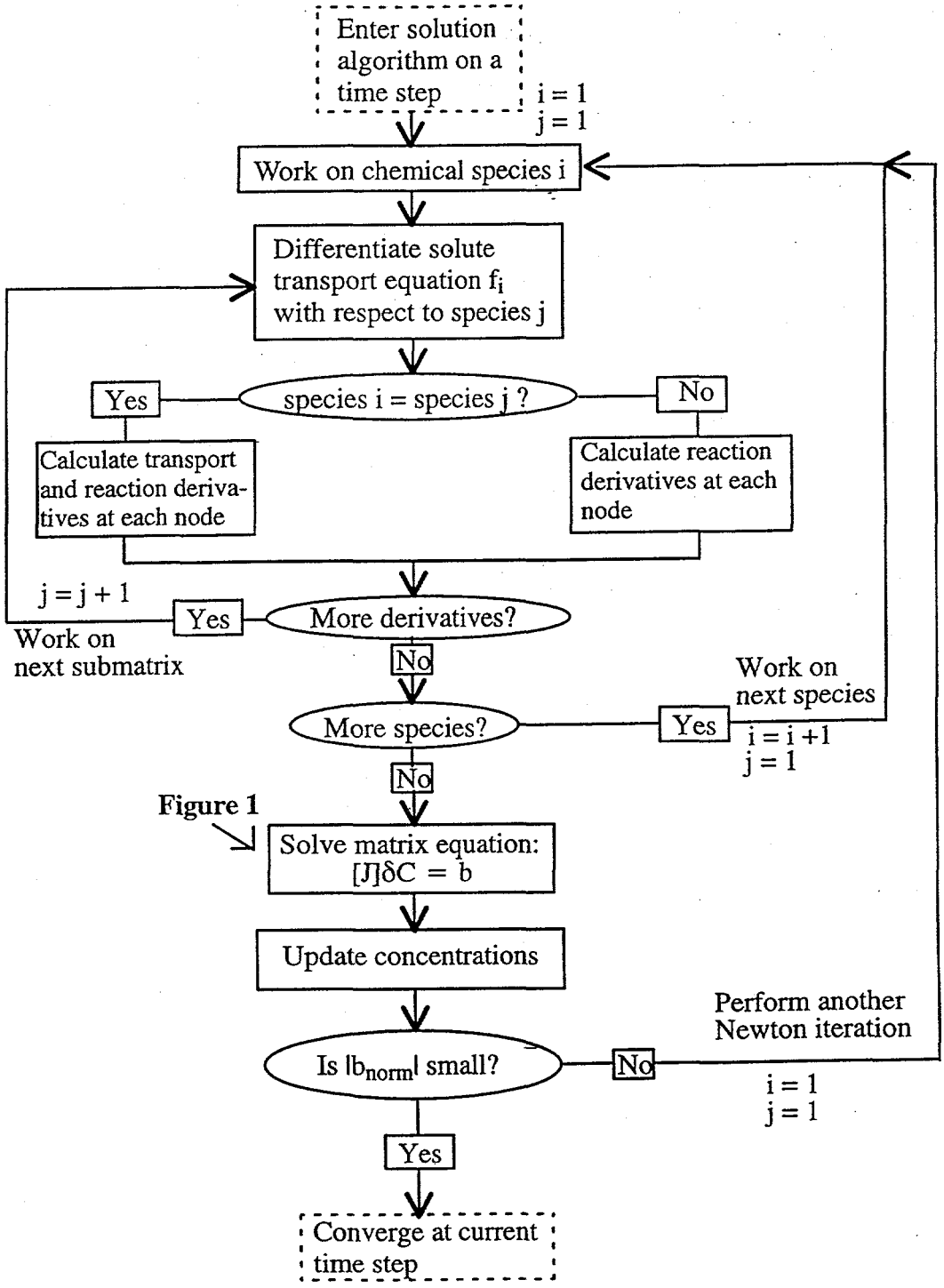

Figure 3: Fully Coupled Approach

Returning to the example, SSIA does not solve the entire equation set as shown by Figure 1. Instead the full set of equations is separated into an equation set for each chemical species. The reduced equation sets are then "fed" into to the linear equation solver GZSOLVE. The equations sets that result are shown in Figure 4. For this simple one-dimensional example, the reduced equation sets are tridiagonal and could be solved with a tridiagonal matrix solver. However to properly benchmark this solution algorithm in Chapter 3, GZSOLVE is used to solve the equation sets.

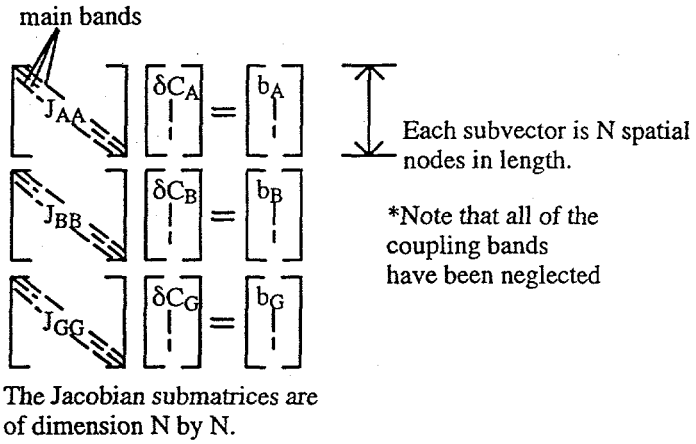

Figure 4: Sequentially solve for the concentration of each species by solving a reduced equation set for each species instead of the solving the full equation set shown in Figure 1

Figure 4 shows that SSIA neglects the Jacobian cross derivative terms given by the coupling bands shown in Figure 1. These coupling bands will be referred to as SSIA coupling bands in order to avoid confusion with the SNIA coupling bands which are discussed in the next section. Newton's method can still be used to solve each reduced equation set. For example, a Newton solution is performed on the reduced equation set for species A. The Newton solution converges when the normalized residual for species i, $|b_{norm}|_i$, is below a specified tolerance. The parameter $|b_{norm}|_i$ is given by:

$$|b_{norm}|_i = \left\{ \sum_{p=1}^{N} (b_{i,p})^2 \right\}^{\frac{1}{2}} \tag{16}$$

Once the Newton solution has converged, SSIA cycles through to solve a reduced equation set for species B and subsequently, species G. When solving for the concentration of species B, the previously computed solution for the C_A is used in evaluating the reaction term. Likewise, the previously computed solutions for C_A and C_B are used to evaluate the reaction term in the solution for species G. A sweep through the all the species comprises one outer iteration. After each outer iteration, the normalized residual $|b_{norm}|$ is checked for convergence (see equation (15)). If $|b_{norm}|$ does not meet the specified tolerance, the algorithm will perform an additional outer iteration. Figure 5 shows a schematic of the SSIA algorithm.

The reason the SSIA outer iteration results in convergence of the overall equation set can be explained by looking at the Gauss-Siedel Method (e.g. Vichnevetsky, 1981). Using simple matrix algebra, the equation set shown in Figure 1 can be written as:

$$J_{AA}\delta C_A + J_{AB}\delta C_B + J_{AG}\delta C_G = b_A$$
$$J_{BA}\delta C_A + J_{BB}\delta C_B + J_{BG}\delta C_G = b_B$$
$$J_{GA}\delta C_A + J_{GB}\delta C_B + J_{GG}\delta C_G = b_G$$

where J's are submatrices and the δC's and b's are subvectors. The Sequential Iteration Approach essentially uses the Gauss-Siedel Method as it cycles through each matrix equation. The iterative process used by SSIA is shown in Figure 6.

In Figure 6, "old" represents the values of δC at the previous iteration and "new" represents the current δC values. As shown above, SSIA converges on a Newton solution for a particular species before cycling through to the next species. The Newton solution converges as δC approaches zero. Therefore, the matrix equations written above simplify down to:

$$J_{AA}\delta C_A^{new} = b_A$$
$$J_{BB}\delta C_B^{new} = b_B$$
$$J_{GG}\delta C_G^{new} = b_G$$

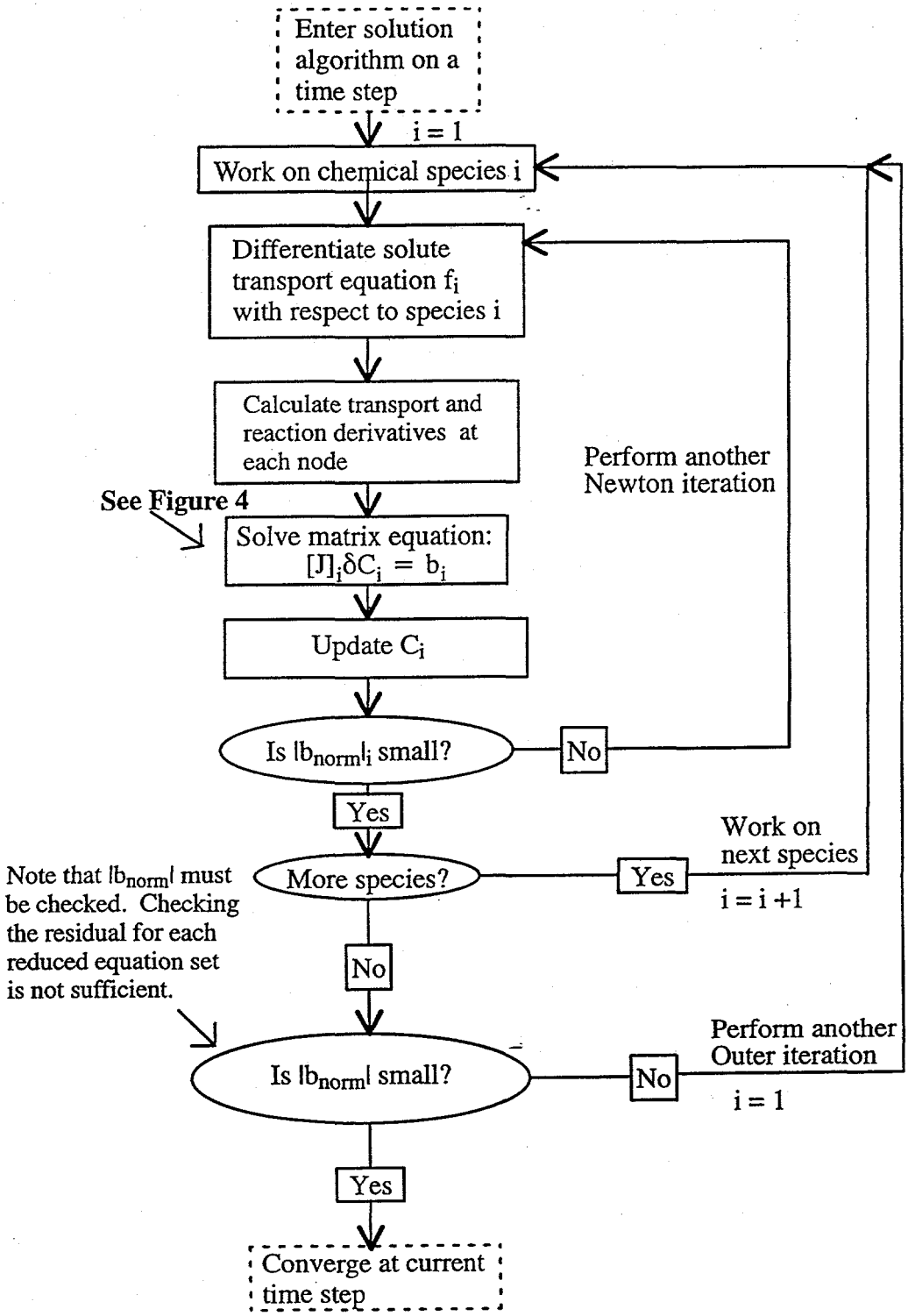

Figure 5: Sequential Species Iteration Approach

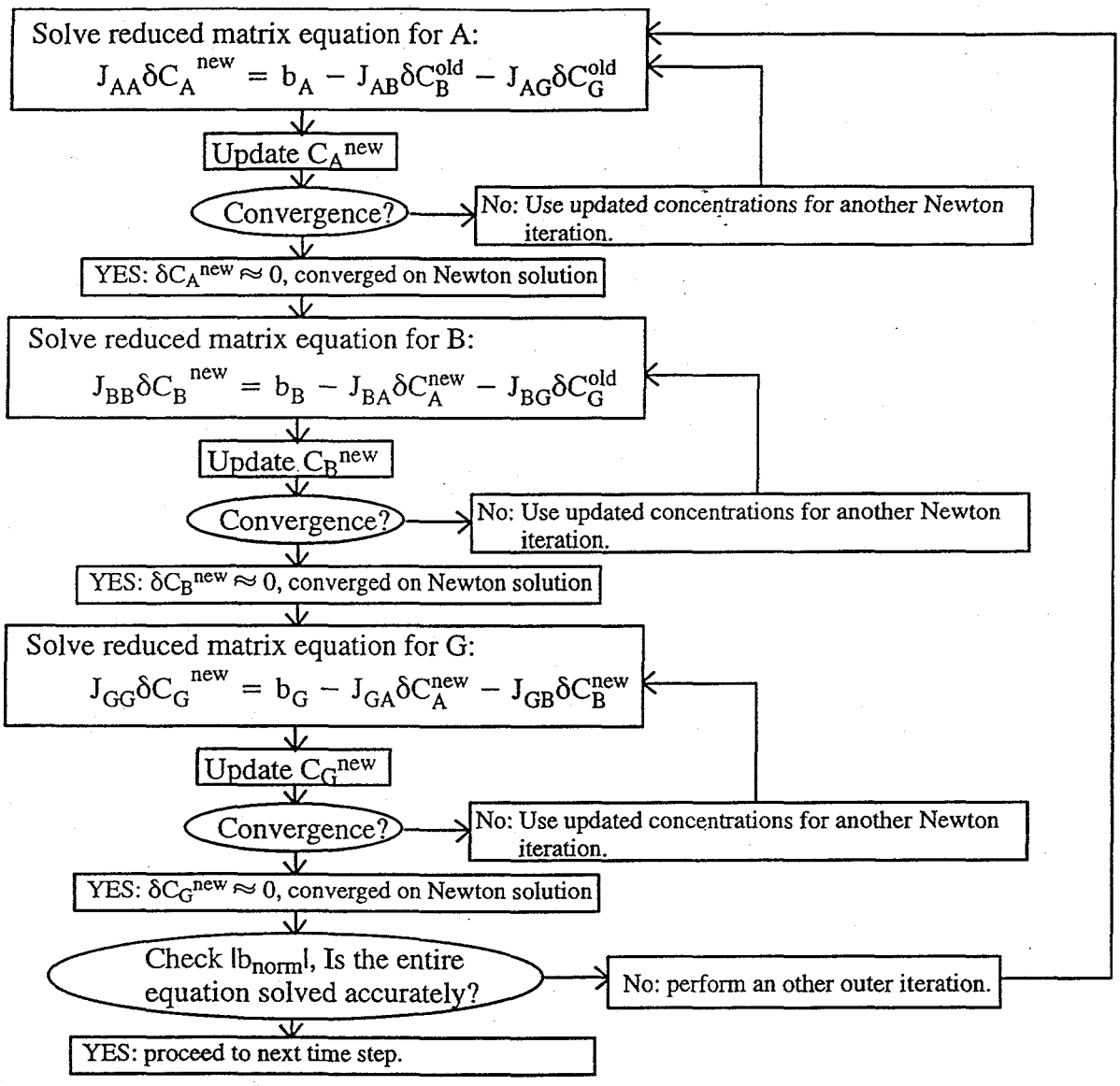

Figure 6: Gauss-Siedel iterative process used by SSIA.

Cycling through each species in this manner leads to convergence of the entire equation set just as the Gauss-Siedel Method leads to convergence.

The tradeoff between SSIA and FCA is clear. SSIA attempts to solve several reduced equation sets to cut down on the time spent in the linear equation solver in exchange for performing additional outer iterations. FCA requires no outer iterations but must send the full equation set into the solver. Chapter 3 will compare these solutions algorithms.

2.4.3 Sequential Nodes Iteration Approach

The Sequential Nodes Iteration Approach (SNIA), similarly to SSIA, attempts to avoid solving the entire system of equations simultaneously in order to attain better computational speed. SNIA cycles through each spatial node and solves a small subset of the full equation set. SNIA includes all of the derivatives with respect to node p but neglects derivatives from the neighboring nodes, p–1 and p+1. The derivatives neglected by SNIA will be called SNIA coupling bands.

In order to obtain the reduced equation set solved by SNIA, the equations are renumbered. The equation structure shown in Figure 1 is rearranged to obtain Figure 7. For simplicity, a five node problem is assumed to clearly show the equation structure.

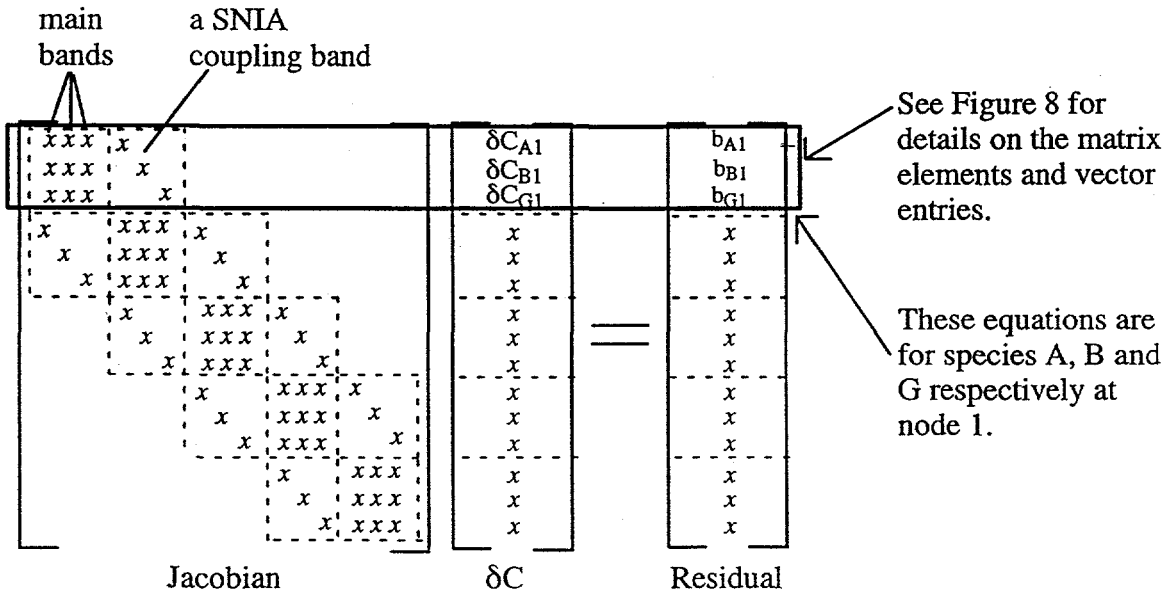

Figure 7: The structure of the equation set for SNIA

The entire equation set in Figure 7 can be rewritten in block matrix notation. An arbitrary node point p would have the following matrix notation:

$$J_{p-1}\delta C_{p-1} + J_p\delta C_p + J_{p+1}\delta C_{p+1} = b_p$$

where the dimensions of the J matrices, δC and b vectors are equal to the number of species. Figure 8 shows the structure for J_p and J_{p+1} for the three species example.

$$\underbrace{\begin{bmatrix} \frac{\partial f_A}{\partial C_{A,p}} & \frac{\partial f_A}{\partial C_{B,p}} & \frac{\partial f_A}{\partial C_{G,p}} \\ \frac{\partial f_B}{\partial C_{A,p}} & \frac{\partial f_B}{\partial C_{B,p}} & \frac{\partial f_B}{\partial C_{G,p}} \\ \frac{\partial f_G}{\partial C_{A,p}} & \frac{\partial f_G}{\partial C_{B,p}} & \frac{\partial f_G}{\partial C_{G,p}} \end{bmatrix}}_{J_p} \underbrace{\begin{bmatrix} \delta C_{A,p} \\ \delta C_{B,p} \\ \delta C_{G,p} \end{bmatrix}}_{\delta C_p} = \underbrace{\begin{bmatrix} b_{A,p} \\ b_{B,p} \\ b_{G,p} \end{bmatrix}}_{b_p}$$

main bands

Equation set solved by Reaction Approach

$$\underbrace{\begin{bmatrix} \frac{\partial f_A}{\partial C_{A,p+1}} & & \\ & \frac{\partial f_B}{\partial C_{B,p+1}} & \\ & & \frac{\partial f_G}{\partial C_{G,p+1}} \end{bmatrix}}_{J_{p+1}}$$

An example coupling band. Note that the coupling bands are neglected by SNIA.

Figure 8: Cycle through each node solving reduced equation sets instead of solving the full equation set shown in Figure 7

Again, the Gauss–Siedel approach is used to develop the general algorithm shown in Figure 9. The SNIA coupling bands are neglected when solving each reduced equation set. Similarly to SSIA, an outer iteration is performed to correct for neglecting the coupling bands. The Sequential Nodes Iteration Approach is compared to SSIA and FCA in Chapter 3.

2.4.4 Summary of the Three Solution Algorithms

All three solution algorithms solve equation (13). Both SSIA and SNIA send a small subset of the full equation set into the linear equation solver thereby decreasing the time spent in the solver. However, in order obtain reduced equation sets, terms in the full equation set must be neglected. Therefore, an outer iteration is necessary for these algorithms to ensure that the entire equation set is being solved accurately. SSIA and SNIA neglect different terms and will behave differently depending on the simulation. FCA simply solves the full equation set simultaneously. Since SSIA and

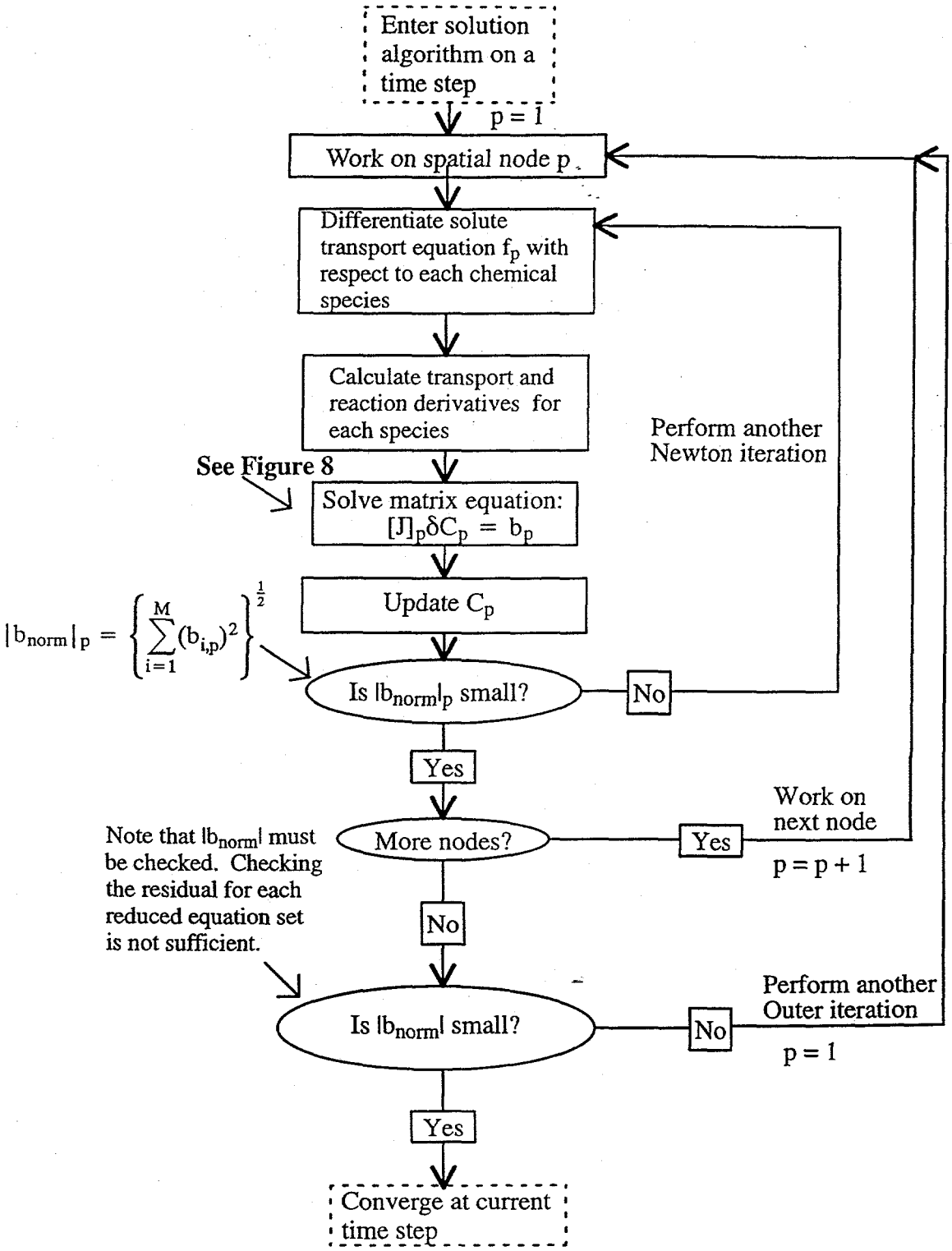

Figure 9: Sequential Nodes Iteration Approach

SNIA neglect terms, these algorithms may not converge under all conditions or may require many outer iterations for convergence. On the other hand, FCA should converge under the same general conditions for which Newton's method converges. The memory requirements for the algorithms are also quite different. FCA is much more memory intensive than SSIA or SNIA since it includes all of the terms in the Jacobian. These algorithms will be tested and evaluated in Chapter 3.

3. EVALUATION OF THE SOLUTION SCHEMES USING A ONE-DIMENSIONAL MODEL

3.1 Overview

The solution methods proposed in Chapter 2 are tested and evaluated in this chapter. Each method will be shown to have certain advantages and disadvantages. Therefore, two mixed algorithms are constructed which attempt to take advantage of each method by combining the FCA, SSIA, and SNIA techniques. The Chapter concludes by proving that the SSIA-FCA algorithm is the best scheme for FEHMN.

3.2 Testing the Numerical Accuracy of the Solution Schemes

3.2.1 Nonreactive Transport Problem

In order confirm that the transport portion of each solution algorithm was working properly, the algorithms were compared with an analytical solution. The analytical solution for one-dimensional solute transport with the 3rd type inlet boundary condition and Neumann exit boundary condition is given by (Javandel et al., 1984):

$$\frac{C(x,t)}{C_{feed}} = \frac{1}{2}\operatorname{erfc}\left(\frac{x-ut}{2\sqrt{Dt}}\right) + \sqrt{\frac{u^2t}{\pi D}}\exp\left[-\frac{(x-ut)^2}{4Dt}\right] \tag{17}$$

$$-\frac{1}{2}\left(1+\frac{ux}{D}+\frac{u^2t}{D}\right)\exp\left(\frac{ux}{D}\right)\operatorname{erfc}\left(\frac{x+ut}{2\sqrt{Dt}}\right)$$

where u is the pore water velocity, D is the hydrodynamic dispersion coefficient, t is the time, x is the position, and C is the concentration. The initial conditions and boundary conditions for this problem are given in Section 2.3. Table 1 shows the parameters used to test the numerical algorithms. The Courant and grid Peclet numbers were chosen to guarantee numerical accuracy.

Table 1: Parameters for one-dimensional nonreactive transport problem

u, the pore water velocity	0.005 m/day
D, the dispersion coefficient	2.5×10^{-4} m^2/day
Δt , time step	1 day
Δx, the mesh spacing	0.05 m
Grid Peclet No., $u\Delta x/D$	1
Courant No., $u\Delta t/\Delta x$	0.1
Simulation Time	100 days
Reactor Length	1 m
C_{feed}	1 mole/L

The analytical solution and the numerical solutions are compared in Figure 10. As expected, the numerical solutions from FCA, SSIA, and SNIA are nearly identical to the analytical solution. For this test case, FCA and SSIA solve the same system of equations since only one chemical species is simulated. SNIA solves a reduced equations set for each spatial node to obtain the solution. However, each algorithm uses $|b_{norm}|$ to check for convergence. Therefore, numerical accuracy of each algorithm is the same. Except for some roundoff error, the numerical solutions were nearly identical and are shown in Figure 10.

Since this transport problem was run for a single conservative chemical species, the FCA and SSIA numerical algorithms solve a tridiagonal matrix equation. A direct tridiagonal matrix solver based upon the Thomas algorithm (Pinder and Gray, 1977) was used to confirm that GZSOLVE was working properly. The tridiagonal solver and GZSOLVE produced identical results.

3.2.2 Transport Problem with First-Order Decay

The reaction:

$$A \xrightarrow{k_{for}} \text{Products}$$

is incorporated into the transport problem discussed in Section 3.2.1 . For this reaction, the rate law given by equation (4) simplifies to:

$$r_A = -\frac{\partial C_A}{\partial t} = k_{for} C_A \tag{18}$$

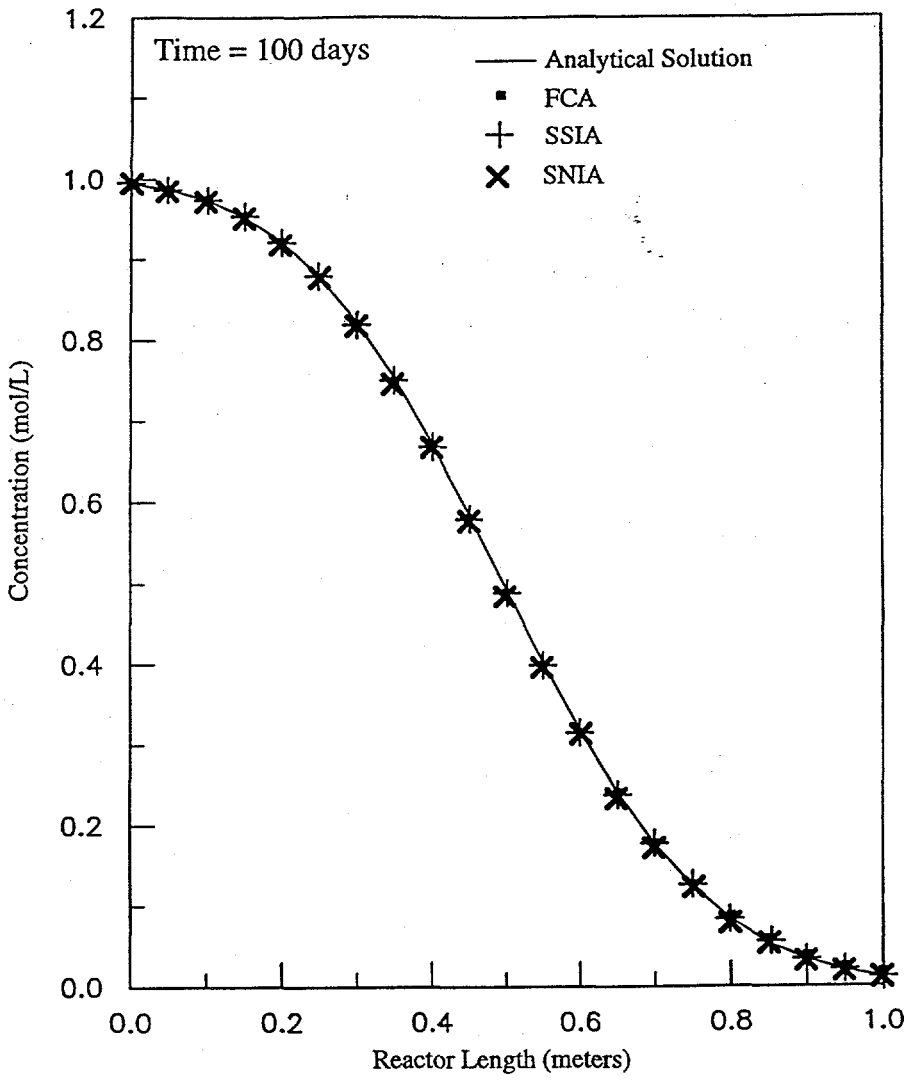

Figure 10: Nonreactive transport problem

The analytical solution for one-dimensional solute transport with first-order decay is given by (Javendal et al., 1984):

$$\frac{C(x,t)}{C_{feed}} = \frac{u}{u+U}\exp\left[\frac{x(u-U)}{2D}\right]\operatorname{erfc}\left[\frac{x-Ut}{2\sqrt{Dt}}\right] \tag{19}$$

$$+\frac{u}{u-U}\exp\left[\frac{x(u+U)}{2D}\right]\operatorname{erfc}\left[\frac{x+Ut}{2\sqrt{Dt}}\right]$$

$$+\frac{u^2}{2Dk_{for}}\exp\left[\frac{ux}{D}-k_{for}t\right]\operatorname{erfc}\left[\frac{x+ut}{2\sqrt{Dt}}\right]$$

where $U = \sqrt{u^2 + 4Dk_{for}}$. Again, the initial conditions and boundary conditions are given in Section 2.3. For this simulation, the parameters shown in Table 2 are used.

Table 2: Parameters for one-dimensional transport problem with decay

u, the pore water velocity	0.005 m/day
D, the dispersion coefficient	2.5 x 10^{-4} m^2/day
Δt , time step	1 day
Δx, the mesh spacing	0.05 m
Simulation Time	100 days
Reactor Length	1 m
C_{feed}	1 mole/L
k_{for}, decay constant	0.005 day^{-1}

Figure 11 shows that the numerical solutions closely match the analytical solution.

3.2.3 Verification of Newton's Method

The test problems shown in Sections 3.2.1 and 3.2.2 result in a set of linear finite difference equations. Recall from Chapter 2 that only the reaction rate term can cause the finite difference form of the solute transport equation to become nonlinear. For linear problems, Newton's method converges after one iteration. However, chemical reactions of order greater than one result in nonlinear rate laws, and for these cases, the Jacobian will contain terms which are dependent on concentration. Since the concentrations in the Jacobian matrix must be evaluated at the previous Newton iteration, Newton's method requires more than one iteration to solve the equation set. Since FCA, SSIA, and SNIA all employ Newton's method, a second order reaction was simulated to check the Newton-Raphson iterative scheme. The reaction:

$$A \xrightarrow{k_{for}} \text{Products}$$

is again used. However, the kinetics of the reaction is second order and so the rate law is given by:

$$r_A = -\frac{\partial C_A}{\partial t} = k_{for} C_A^{\,2} \tag{20}$$

where the rate constant, k_{for}, has units of day^{-2}. All parameters used in this simulation are identical to those given in Table 2. An analytical solution which accounts for dispersion was not found for

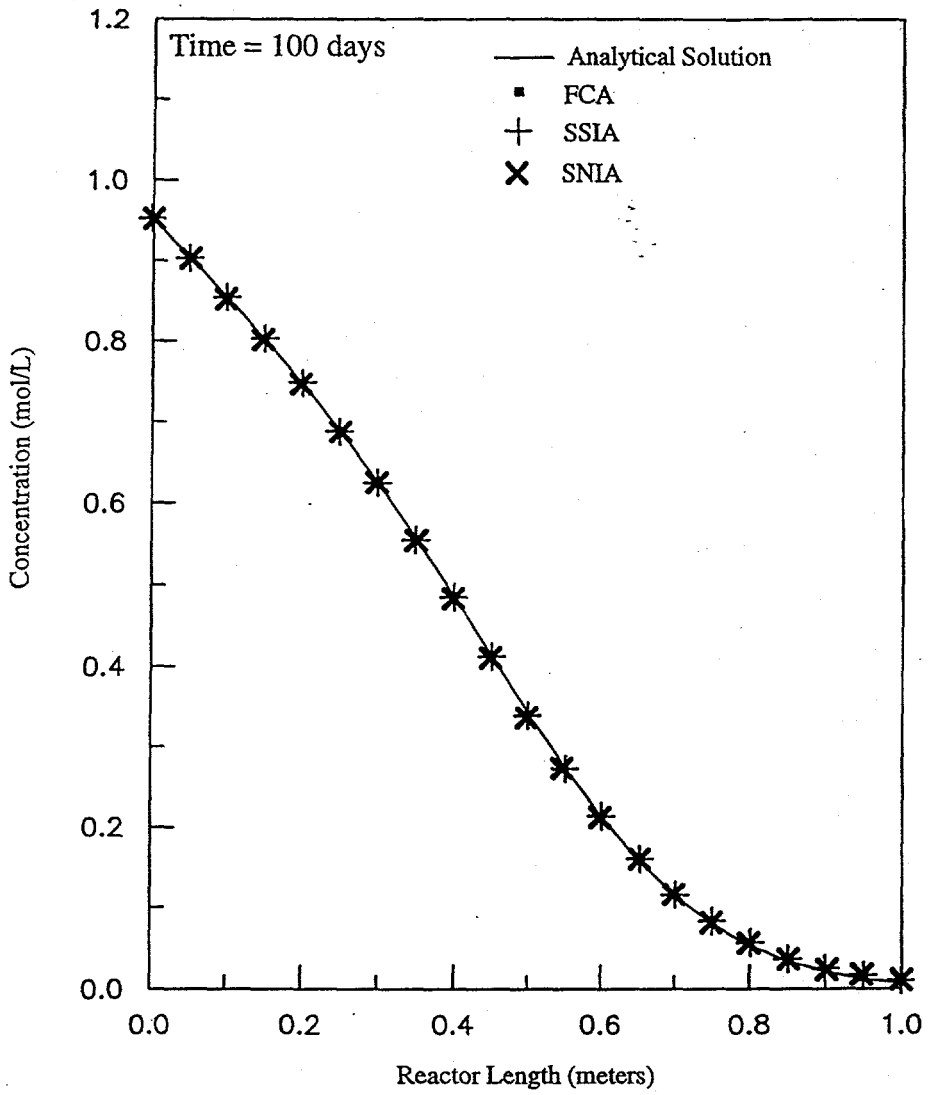

Figure 11: Transport problem with first order decay

this test problem. However, the steady state concentration at the exit can be calculated for a case that assumes no dispersion. Separating variables and integrating equation (20) yields:

$$\frac{1}{C_{A,exit}} - \frac{1}{C_{A0}} = k_{for}\tau \tag{21}$$

where τ is the mean residence time of the solute and is equal to L/u=200 days. Solving equation (21) for C_A gives:

$$C_{A,exit} = \frac{C_{A0}}{C_{A0}k_{for}\tau + 1} \tag{22}$$

With $C_{A0} = 1$, $k_{for} = 0.005$ /day, C_A should equal 0.5 moles/liters at steady state. The simulations were run out to 600 days to ensure that the system reached steady state. The numerical solution algorithms reached a steady state concentration of 0.51 at the exit. As expected, FCA, SSIA, and SNIA took an average of 3 to 4 Newton iterations per time step to converge due to the nonlinearity of the problem.

3.3 Benchmarking of the Solution Strategies

The problems in Sections 3.2.1–3.2.3 confirm the numerical accuracy of the solution algorithms for one chemical species undergoing transport and reaction. For multiple chemical species undergoing transport and reaction among one another, the solution strategies employ different iterative schemes. Each strategy will still provide a numerically accurate solution. However, the computer time required for convergence will be dependent on the solution algorithm and the particular problem.

Each solution algorithm varies in its computational and memory requirements for several reasons. Each solution algorithm sends different equation sets into the solver. FCA sends the full equation set into solver, whereas SSIA and SNIA send reduced equation sets. Both SSIA and SNIA neglect certain terms to achieve the reduced equation sets and therefore require an outer iteration to ensure the entire equation set is solved accurately. Therefore, the time spent in the solver per iteration is no longer the same and the number of calls to the equation solver will be different for each strategy. In addition, the time required to formulate the coefficients to send into the solver will also be different. FCA requires the calculation of all of the Jacobian derivative terms, whereas SNIA and SSIA do not have to calculate some Jacobian cross derivative terms.

In this section, a benchmarking study is performed to evaluate the solution strategies. The test problems have been chosen to highlight the advantages and disadvantages of each solution algorithm. Section 3.4 will describe the construction of two mixed algorithms which attempt to incorporate the advantages of each method by combining the FCA, SSIA, and SNIA techniques. The solution algorithms were tested on a Sun Sparc 20 Workstation. The CPU times were obtained by using

the UNIX command GPROF. In order to obtain CPU times, 10,000 node test problems were used in the benchmarking tests. A 10,000 node problem allowed the time spent in each solution algorithm to be "significant." The GPROF routine gave CPU times that were accurate to within 10% for these 10,000 node problems. It should be noted that for problems containing less than 1000 nodes, the GPROF routine provided times with errors up to 25%. The inaccuracy was due to the minimal time spent in the solution algorithm for the 1000 node simulations.

In order to simulate these 10,000 node problems, the time step, the pore water velocity, and hydrodynamic dispersion coefficients were adjusted accordingly to obtain a grid Peclet number of 1 and a Courant number of 0.1. The transport parameters used in the following simulations are given in Table 3. The test problems discussed in 3.2.1–3.2.3 were rerun with these new parameters.

Table 3: Parameters for 10,000 node benchmarking studies

u, pore water velocity	0.01 m/day
D, the dispersion coefficient	1.0×10^{-6} m^2/day
Δt, time step	0.001 days
Δx, the mesh spacing	0.0001 m
Grid Peclet No., $u\Delta x/D$	1
Courant No., $u\Delta t/\Delta x$	0.1
L, the reactor length	1 m
Simulation Time	1 day

3.3.1 Transport of Multiple Conservative Species

In this section, the transport problem described in Section 3.2.1 is run with multiple conservative species transporting simultaneously. This example will be used to study the relationship between the computational cost of each strategy and the number of species in the simulation.

Table 4 shows the relationship between the number of conservative species simulated and the CPU time per time step. It should be noted that each algorithm required only one Newton iteration per time step to achieve convergence.

Table 4: Performance of the algorithms for conservative transport problem

Number of species	FCA	SSIA		SNIA	
	CPU time per time step (seconds)	# Outer Iterations	CPU time per time step (seconds)	# Outer Iterations	CPU time per time step (seconds)
1	1.1	1	1.1	3	0.8
2	3.5	1	2.4	3	2.8
3	11.6	1	3.9	4	9.6
4	14.9	1	5.6	4	21.6
6	67.5	1	8.8	4	70.0
8	296.3	1	12.0	4	135.4

These trials were designed to show the extreme case in which SSIA outperforms FCA and SNIA. The SSIA coupling bands are nonexistent for this test problem, SSIA converges after performing one outer iteration. Recall that the approximation made by SSIA is that the reaction cross derivative terms are neglected. Since there is no reaction in these trials, these derivatives are equal to zero. Since SSIA solves reduced equation sets and does not have to perform any additional outer iterations, SSIA runs faster than FCA. For this problem the SNIA coupling bands are significant, therefore SNIA requires several outer iterations for convergence. Therefore, SSIA runs faster than SNIA for this problem.

The trends shown in Table 4 can be explained by examining the equation sets solved by each algorithm (Figure 12). FCA is slower than SSIA because it sends a larger problem to the linear equation solver. For example, when simulating three species, FCA must solve one large equation set of dimension 3N by 3N. SSIA solves three reduced equation sets of dimension N by N. It is clear that the FCA equation set is nine times larger than each of the three reduced systems solved by SSIA. For this same three species case, SNIA solves N reduced equation sets of dimension three by three. However, Table 4 shows that SNIA requires additional outer iterations to achieve convergence for this problem. Therefore, even though SNIA sends reduced equation sets to the solver, the additional outer iterations result in slow convergence compared to SSIA. The structure of the equation sets solved by FCA, SSIA and SNIA for a problem with three species and five spatial nodes (N=5) is

shown in Figure 12. A more detailed of explanation of these matrix structures can be found in Chapter 2.

From this first benchmarking study, it is clear that the number of additional outer iterations will be a major factor in determining whether SSIA and SNIA will outperform FCA. As seen from the flowcharts in Chapter 2, an outer iteration returns to the beginning of the solution algorithm with new guesses for the concentration vector. All the calculations in the algorithm are carried out again. In effect, the solution algorithm is called again for every additional outer iteration.

Another major factor in performance will be the solver type used by the algorithms. FCA and SSIA both use GZSOLVE (Zyvoloski, 1995b) which utilizes the GMRES algorithm (Barrett et al., 1994; Dongarra et al., 1991) to solve the banded equation sets. SNIA uses a direct solver to solve the small, dense equation sets. The direct solver employs LU Decomposition followed by back substitution to solve each equation set (e.g. Press et al., 1992). For a problem with many species and many nodes, the different solvers could have a significant effect on the performance of the algorithms for simulations with a large number of nodes and chemical species.

Plotting the results of Table 4 produces some trends which effectively explain the behavior of the solution algorithms. Figure 13 shows a plot of CPU time / time step versus the number of conservative species in the simulation.

For this problem, SSIA's time for convergence increases linearly with the number of species. The SSIA reduced equation sets are the same size whether one or more species are simulated. Therefore, the increase in overall CPU time is simply due to the number of times the solver is called. For, example, the solver is call once per outer iteration for the one species case, whereas, the solver is called three times per outer iteration for the three species case.

The convergence time behavior for SNIA is more complex. SNIA's convergence time increases at a much greater rate as the number of species increases. The reduced equation sets solved by SNIA increase in dimension as the number of species increase. The direct solver which solves the reduced equation sets uses LU decomposition followed by back substitution. For this procedure, approxi-

Full equation set solved by FCA

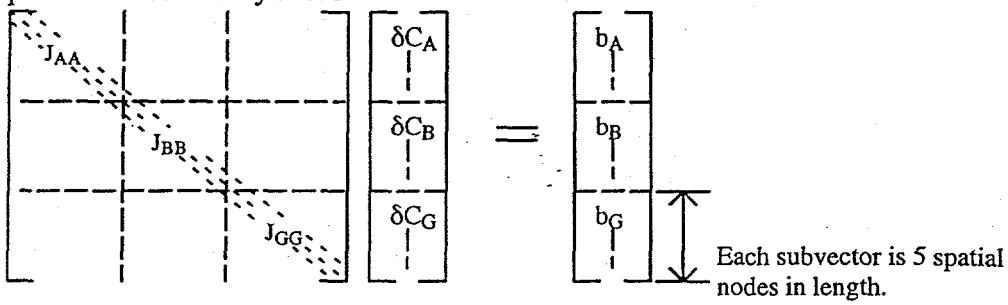

Reduced equations sets solved by SSIA

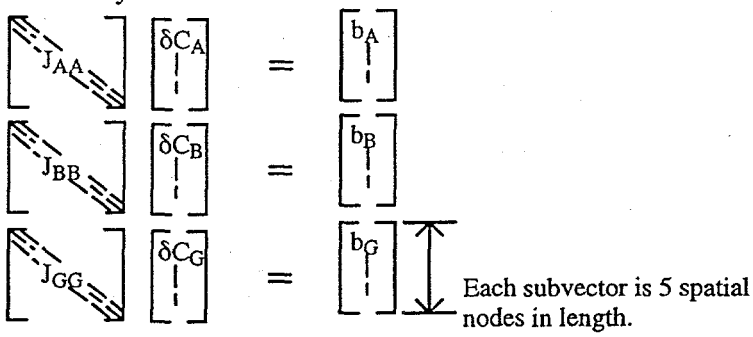

Reduced equations sets solved by SNIA

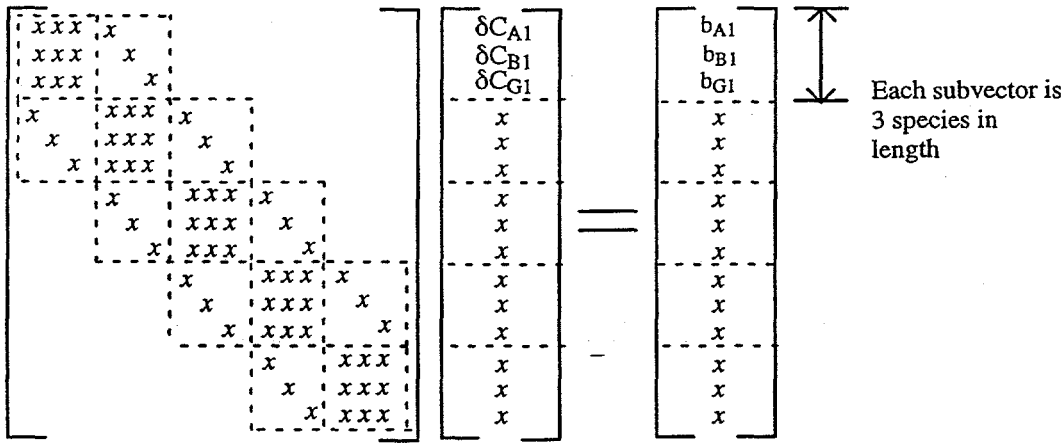

Figure 12: Comparison of the equation sets for three conservative species undergoing transport (assume five node problem)

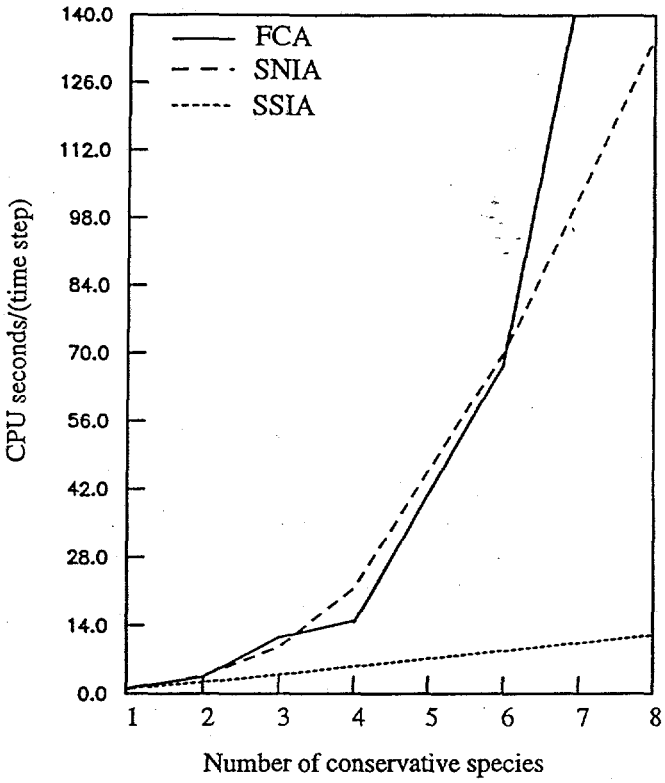

Figure 13: Benchmarking test of nonreactive species

mately $N^3/3$ operations are necessary to solve each reduced equation set (Press et al., 1986). The CPU time required to solve the equation set is directly proportional to the number of operations. Therefore, the overall time for convergence for SNIA greatly increases with the number of species. In fact, the CPU time per outer iteration increases by an approximate factor of N^3 for SNIA. For example, if the number of chemical species is doubled, the CPU time per outer iteration approximately increases by a factor of 8.

The FCA curve shows that the time for convergence for FCA increases exponentially with the number of species. Although FCA has no real upper limit on the number of species being modeled, solving for number species simultaneously will be very computationally intensive.

This test problem was used to examine the extreme case in which no coupling exists between any of the chemical species and was therefore ideal for the SSIA algorithm. FCA and SNIA clearly become increasingly inefficient as the number species in the simulation increases, whereas, SSIA's convergence time per time step increases linearly. This example was used to study the relationship

between the computational cost of each strategy and the number species in the simulation. Based on this analysis, one should never solve for the transport of multiple conservative species using any of these algorithms because the most cost effective approach would be to solve for each species independently. However, the real purpose of these algorithms is to simulate the transport of chemical species which interact with one another. The behavior of the solution strategies for multiple reacting species will be shown in the next section.

3.3.2 Transport of Multiple Reacting Species

In this section, the three reaction strategies are used to simulate reversible reactions in which the transporting species interact with one another. Therefore, the SSIA coupling bands become significant in these problems.

The first reaction to be simulated is given below.

$$A \underset{k_{rev}}{\overset{k_{for}}{\rightleftharpoons}} B$$

The rate law of the reaction is given by:

$$r_A = -r_B = k_{for}C_A - k_{rev}C_B \tag{23}$$

Species A and B transport from the inlet to the outlet of the reactor. Both species start with concentrations of zero within the reactor. Species A is injected into the inlet node with a concentration of 1 *M*. As A enters the reactor it reacts to form species B according the reaction given above. The forward and reverse rate constants are chosen to be equal for each simulation. If the rate constants are high enough to simulate equilibrium conditions, the concentration of A and B will be equal to each other at every spatial node. At steady state, the concentration of species A and B should equal 0.5 *M*.

For this reaction, the SSIA coupling bands (returning to Chapter 2 notation) are given by:

$J_{AB,j,j=} \lambda k_{rev}\Delta t$ and $J_{BA,j,j=} \lambda k_{for}\Delta t$

Examining these coupling bands, it is clear that as the kinetics of the reaction increase, the coupling bands increase in value. Therefore, one would expect the efficiency of the SSIA algorithm to decrease as the kinetics of the reaction increases.

Table 5 compares the performance of the three algorithms for various rate constants. It is clear that kinetic rate constants do not affect the time for convergence for SNIA and FCA. However, SSIA takes more outer iterations as the kinetics of the reaction increases. Therefore, the time for convergence for SSIA is greatly affected.

Table 5: Performance of the algorithms over a range of kinetic rate constants

Rate Constants $k_{for}=k_{rev}$ (day^{-1})	FCA	SSIA		SNIA	
	CPU time per time step (seconds)	# Outer Iterations	CPU time per time step (seconds)	# Outer Iterations	CPU time per time step (seconds)
1	3.6	1	2.4	3	2.7
$1x10^1$	3.5	2	4.6	3	2.9
$1x10^2$	3.7	3	7.2	3	2.8
$1x10^3$	3.6	7	16.8	3	2.9
$1x10^4$	3.5	37	85.1	3	2.9
$1x10^5$	3.6	120	312	3	2.8
$1x10^6$	3.6	–	no convergence	3	2.9

Figure 14 shows these trends graphically. Table 5 and Figure 14 indicate that the kinetics of the reaction has no effect on FCA and SNIA. There is no effect because these methods include all of the reaction cross derivatives when solving the equation set. On the other hand, the SSIA coupling bands become increasingly important as the rate constants increase. Therefore, SSIA's approximation of neglecting the coupling bands becomes worse as the rate constants increase in value. For SSIA, the time spent in the solver per outer iteration is not dependent on the kinetics of the reaction. However, the number of outer iterations greatly increases for fast kinetic reactions. Therefore, the amount of time for convergence greatly increases with the kinetics of the reaction.

This test problems brings into question SSIA's ability to model an equilibrium reaction. Table 5 shows that kinetic constants higher than 100 day^{-1} result in relatively slow convergence for SSIA. However, if kinetic constants 100 day^{-1} are sufficiently fast enough to simulate local equilibrium

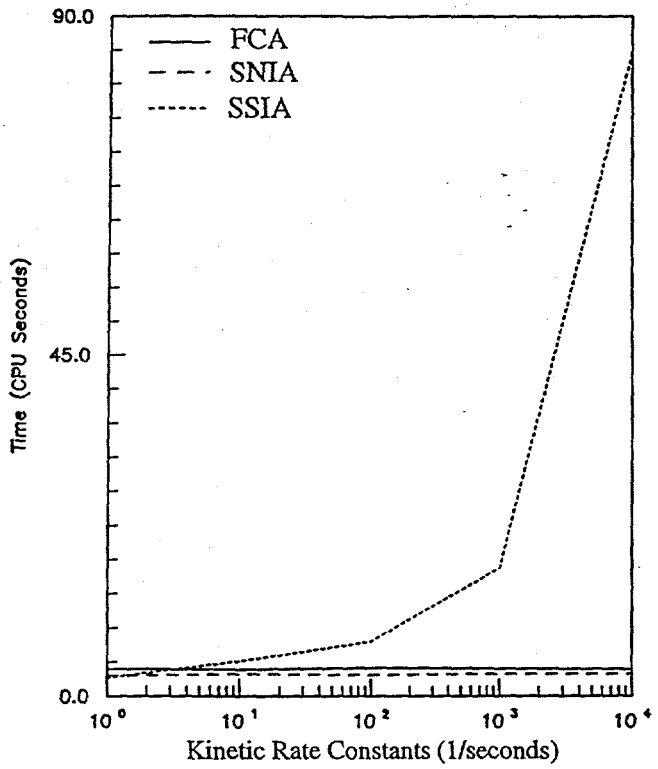

Figure 14: Benchmarking test of reacting species

for this problem, SSIA would still be an acceptable scheme to model both equilibrium and kinetic reactions. For this reaction, Valocchi (1985) found that the local equilibrium assumption is valid when:

$$k_{rev}\frac{\Delta x}{u} \geq 100 \qquad (24)$$

where the dimensionless quantity, $k_{rev}\Delta x/u$, is a dimensionless rate parameter also known as the Damköhler number. For this simulation, u = 0.01 meters/day and $\Delta x = 0.0001$ meters. Therefore, k_{rev} should be greater than 10,000 day^{-1} for local equilibrium conditions to be simulated at each spatial node. Table 5 shows that for a k_{rev} = 10,000 day^{-1}, SSIA requires 312 outer iterations to converge. Upon convergence, equilibrium conditions are simulated at each spatial node. However, SSIA is clearly an impractical solution technique for simulating equilibrium reactions and is only an efficient algorithm for simulating slow kinetic reactions.

3.3.3 The effect of varying the Courant Number and Grid Peclet Number

Unlike SSIA which neglects coupling bands which contain reaction terms, SNIA neglects coupling bands which describe the advective and dispersive transport between a node and it's neighbors. Therefore, the number of SNIA outer iterations should be sensitive to transport parameters rather than chemical kinetic parameters. For the one-dimensional case, transport parameters such as the Courant number ($u\Delta t/\Delta x$) and grid Peclet number ($u\Delta x/D$) are the primary factors which control the number of outer iterations necessary for SNIA to achieve convergence.

The nonreactive transport problem shown in Section 3.3.1 was rerun. Two sets of simulations were run in which Δx was kept constant. In the first set, the Courant number was varied by adjusting the pore water velocity. The grid Peclet number was kept constant by adjusting the hydrodynamic dispersion coefficient. In the second set, the grid Peclet number was varied while keeping the Courant number constant. The "rules of thumb" to guarantee an accurate numerical solution for one-dimensional transport require that the Courant number be less than 1 and the grid Peclet number less than 2 (Pinder and Gray, 1977). Therefore, the parameters in the tables were kept within these limits. Table 6 shows the first set of trials and Table 7 shows the second set.

Table 6: Performance of the algorithms over a range of Courant numbers (grid Peclet No. = 1)

Courant No.	FCA	SSIA		SNIA	
	CPU time per time step (seconds)	# Outer Iterations	CPU time per time step (seconds)	# Outer Iterations	CPU time per time step (seconds)
0.001	15.1	1	5.6	1	4.9
0.01	14.0	1	5.8	2	10.8
0.1	14.8	1	5.6	4	20.6
0.5	14.4	1	5.8	7	35.7
1	14.7	1	5.6	11	58.3

Table 7: Performance of the algorithms over a range of grid Peclet numbers (Courant No. = 0.1)

Grid Peclet No.	FCA	SSIA		SNIA	
	CPU time per time step (seconds)	# Outer Iterations	CPU time per time step (seconds)	# Outer Iterations	CPU time per time step (seconds)
0.1	14.8	1	5.6	11	57.2
1	14.7	1	5.6	4	20.6
2	14.4	1	5.6	2	11.2

As expected, FCA is not sensitive to changes in the Courant number and grid Peclet number as long as Δx is kept constant. Since this is a conservative transport problem, no conclusions can be drawn from the performance on SSIA. Recall that SSIA requires only one outer iteration to converge for conservative transport problems. SNIA requires additional outer iterations for convergence as the Courant number increases and as the grid Peclet number decreases. Higher Courant numbers result in a solute front which moves faster from node to node. The SNIA coupling bands become more significant as the solute front speed increases. The grid Peclet number controls the spreading of the front. Low grid Peclet numbers signify a more disperse solute front. The solute front will spread faster throughout the domain for a lower grid Peclet number, again making the SNIA coupling bands more significant.

The limits on the grid Peclet number and Courant number bring into question SNIA's flexibility. SNIA is very sensitive to these transport parameters. For these one-dimensional simulations, it has been shown that SNIA performs efficiently if the grid Peclet number and Courant number are chosen carefully. However, SNIA has not been examined for two or three dimensional problems. Since FEHMN is a finite element code capable modeling three dimensional geometries, the main bands shown in Figure 1 would contain 27 bands for the three-dimensional case rather than 3 bands for the one-dimensional case. Therefore, SNIA would neglect 26 coupling bands for a three-dimensional simulation rather than the 2 coupling bands neglected in the one-dimensional case. Restrictions on the Courant number and grid Peclet number will most certainly be more stringent for two and three dimensional problems.

Incorporating SNIA into FEHMN would simply not be practical. FEHMN is capable of using three-dimensional unstructured grids and variable time stepping. Therefore, the Courant and grid Peclet numbers are not easily controlled over the entire domain or the over the entire simulation time for an FEHMN simulation. SNIA simply does not have the necessary robustness to be able to model a wide variety of FEHMN reactive transport problems.

3.4 Combinations of FCA/SSIA and SSIA/SNIA

The benchmarking tests showed that each solution algorithm has certain advantages and disadvantages. FCA's performance was independent of the transport or reaction parameters of the problem. However, FCA has a practical limit of modeling four chemical species simultaneously. Simulations with more than four chemical species require a large amount of memory and CPU time. Specifically, a Sparc 20 Workstation is not capable of modeling more than four species simultaneously for simulations with more than one thousand nodes. SSIA is extremely efficient for simulating multi-species, slow kinetic reactions but cannot simulate fast kinetic or equilibrium reactions. SNIA is better than FCA and SSIA for a problem with relatively slow transport and fast reactions. However, SNIA is extremely sensitive to the grid Peclet number and Courant number. This section describes the construction of two mixed algorithms which attempt to take advantage of each method by combining the FCA, SSIA, and SNIA techniques. In particular, combinations of SSIA-SNIA and FCA-SSIA were constructed.

3.4.1 SSIA-SNIA

SSIA and SNIA attempt to solve several reduced equation sets to cut down on the time spent in the linear equation solver in exchange for performing additional outer iterations. Both algorithms neglect coupling bands in order to solve the reduced equation sets, SSIA neglecting the reaction coupling among species at a given node and SNIA neglecting the transport coupling between adjacent nodes. SSIA-SNIA alternates between solving the SNIA and SSIA equation sets. The goal of SSIA-SNIA is to allow for SSIA to accurately describe the transport processes and for SNIA to accurately solve for the reaction processes. In doing so, the objective is to reduce the number of outer iterations necessary for convergence while still only solving reduced equation sets. Combining the

two algorithms is quite straightforward in that the same outer iteration loop can be used to check for overall convergence equation set. The schematic of SSIA and SNIA can be merged to generate the schematic for SSIA-SNIA (Figure 15).

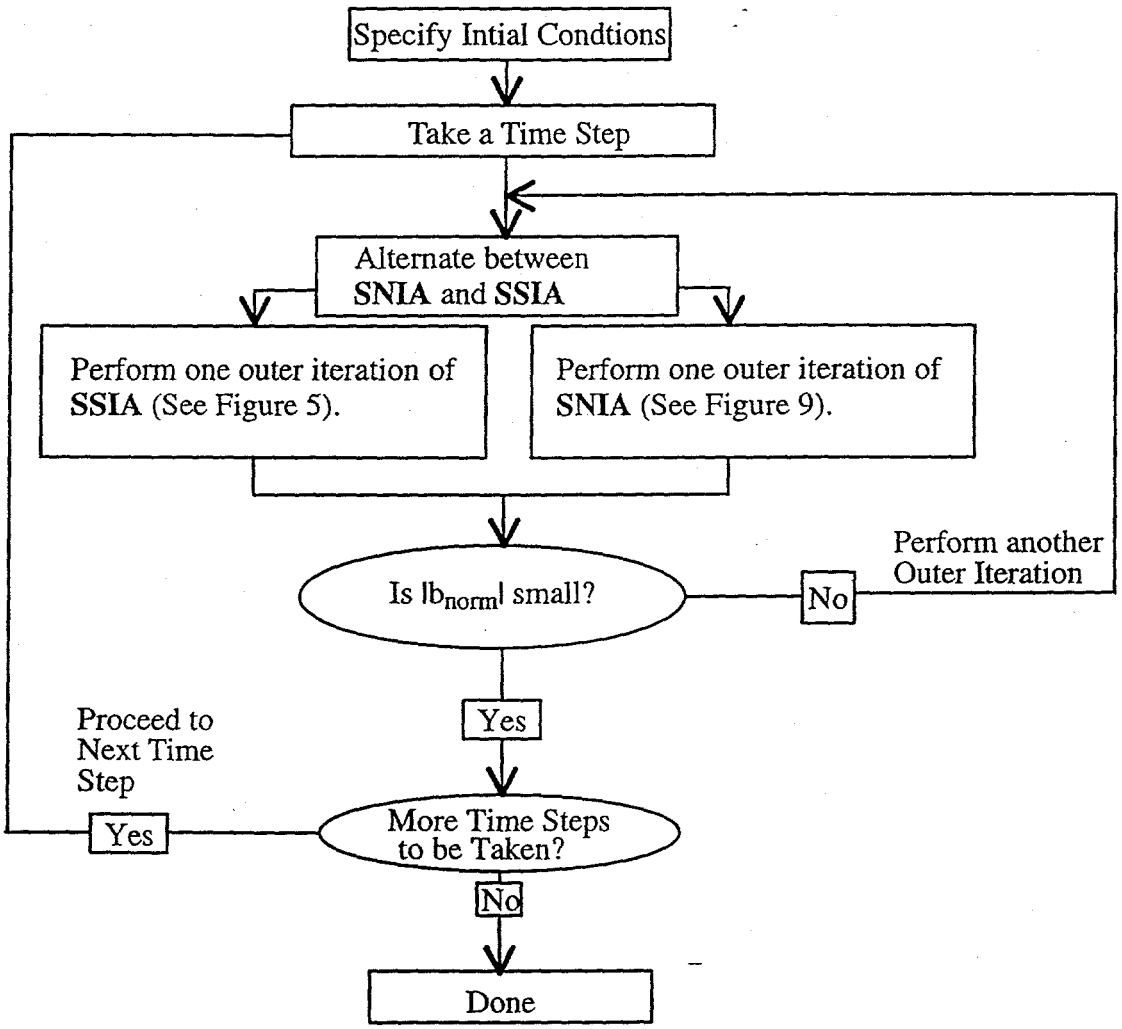

Figure 15: Combination of SSIA and SNIA

The reactive transport problem discussed in Section 3.3.2 is also a good test for the SSIA-SNIA algorithm. Recall that as the kinetics of the reaction increases SSIA begins to take additional outer iterations for convergence (see Table 5). SNIA was not affected by the kinetics of the reaction but only by the Courant and Grid Peclet numbers. For this problem the Courant number was 0.1 and the Grid Peclet Number was 1. The problem was rerun to study the performance of SSIA-SNIA.

Table 8 shows that combining the two algorithms results in an overall performance which is between the performance of SSIA and SNIA. The SSIA-SNIA algorithm never outperforms SNIA

for this example. At higher kinetics, the SSIA iterations hinder the SNIA iterations from converging upon a solution. The purpose of SSIA-SNIA was to achieve convergence with fewer outer iterations than SSIA or SNIA. Unfortunately, alternating methods does not achieve this goal. Therefore, the SSIA-SNIA method is not an effective scheme for FEHMN.

Table 8: Evaluation of the mixed SSIA-SNIA algorithm over a range of kinetic rate constants

Rate Constants $k_{for}=k_{rev}$ (day^{-1})	SSIA		SNIA		SSIA-SNIA	
	# Outer Iterations	CPU time per time step (seconds)	# Outer Iterations	CPU time per time step (seconds)	# Outer Iterations	CPU time per time step (seconds)
1	1	2.4	3	2.7	1	2.7
$1x10^2$	3	7.2	3	2.8	3	5.7
$1x10^3$	7	16.8	3	2.9	5	8.9
$1x10^4$	37	85.1	3	2.9	6	9.6
$1x10^6$	–	no convergence	3	2.9	6	9.6

3.4.2 FCA-SSIA

FCA-SSIA was designed to take advantage of the computationally efficient properties of FCA and SSIA. The mixed algorithm allows the user the place highly coupled species into groupings. For example, all species in an equilibrium reaction are strongly coupled to one another and should be placed in a grouping. In FCA-SSIA, all species in a particular grouping are solved by the FCA method. Since each grouping is not strongly coupled to the other groupings, an outer loop using the SSIA method is used to solve the entire equation set by sequentially looping through each grouping. For FCA-SSIA to work properly, the user must choose groupings which are not strongly coupled to one another. Figure 16 shows the basic schematic of the FCA-SSIA algorithm.

The performance of the FCA-SSIA algorithm can be shown by studying the following set of reversible reactions in series:

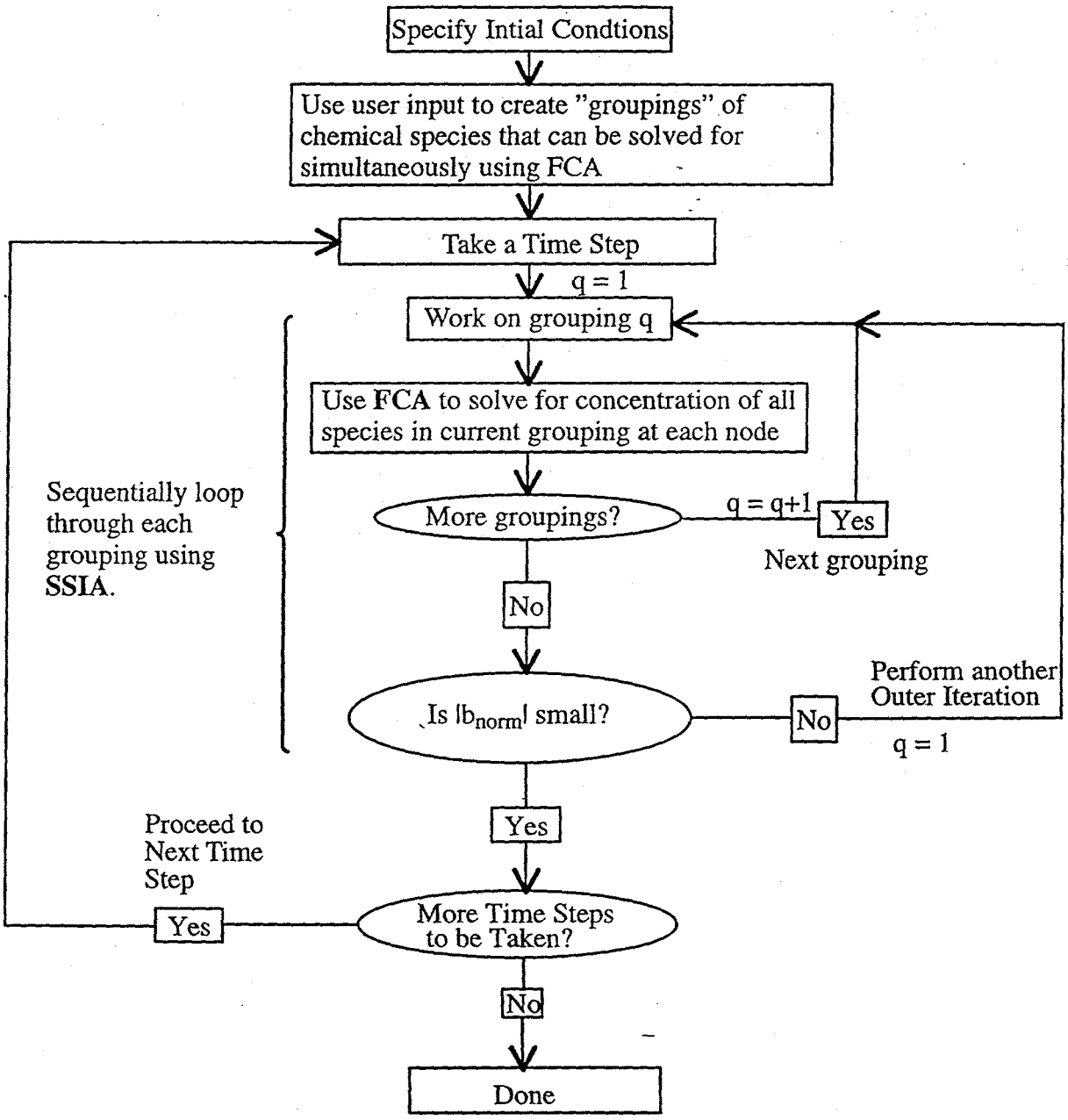

Figure 16: Combination of FCA and SSIA

Reaction 1: $A \underset{k_{rev_1}}{\overset{k_{for_1}}{\rightleftharpoons}} B;$

Reaction 2: $B \underset{k_{rev_2}}{\overset{k_{for_2}}{\rightleftharpoons}} C$

Reaction 3: $C \underset{k_{rev_3}}{\overset{k_{for_3}}{\rightleftharpoons}} D;$

Reaction 4: $D \underset{k_{rev_4}}{\overset{k_{for_4}}{\rightleftharpoons}} E;$

In this example, reactions 1, 3 and 4 are equilibrium reactions and reaction 2 is a kinetic reaction. Since reaction 2 is kinetically limited, it is the rate limiting step in the reaction sequence. The equilibrium reactions are simulated by using rate constants that are high enough to achieve local equilibrium throughout the domain. Recall that a kinetic formulation has been chosen to model both equilibrium and kinetic reactions. Each reaction is of the same form as the reaction shown in Section 3.3.2. Therefore, forward and reverse rate constants greater than 1×10^4 day^{-1} will result in equilibrium conditions. For this set of simulations, the rate constants for reaction 2 are varied to study the behavior of the FCA-SSIA algorithm (the rate constants for reactions 1, 3 and 4 are kept constant at 10,000 day^{-1} to ensure equilibrium conditions for this reaction).

In this test problem, FCA-SSIA will be compared to the FCA algorithm. SSIA cannot be used in the comparison since reactions 1, 3 and 4 are equilibrium reactions which cannot be handled by SSIA. To use the FCA-SSIA algorithm, the user must place the strongly coupled chemical species into groupings. Since reaction 2 is the rate limiting step of the reaction sequence, the two logical groupings for this problem are: A-B, and C-D-E. The kinetic parameters for reaction 2 will control the number of outer iterations required by FCA-SSIA to attain convergence. Table 9 shows the compares the performance of FCA-SSIA against FCA for this reaction sequence.

Table 9: Evaluation of the mixed FCA-SSIA algorithm over a range of kinetic rate constants

Rate Constants $k_{for2}=k_{rev2}$ (day^{-1})	FCA-SSIA		FCA
	# Outer Iterations	CPU time per time step (seconds)	CPU time per time step (seconds)
$1x10^{-3}$	1	37.3	52.3
$1x10^{-2}$	1	37.3	50.5
$1x10^{-1}$	3	102.6	55.2
$1x10^{0}$	5	169.0	53.7
$1x10^{1}$	17	632.4	55.5
$1x10^{2}$	137	4986.8	57.3

This problem illustrates that FCA-SSIA groupings take advantage of the properties of FCA and SSIA. FCA-SSIA outperforms FCA for kinetic rate constants lower than $1x10^{-2}$ day^{-1}. For these trials, the groupings are weakly coupled. However, as the kinetic constants are increased, the grouping become strongly coupled and FCA-SSIA requires additional outer iterations making it inefficient. It is clear that if the chemical species in the system can be placed into groupings which are weakly coupled to one another, then the FCA-SSIA algorithm will be much more efficient than the FCA algorithm. If no weakly coupled groupings can be found, FCA-SSIA can still be used to solve for all species simultaneously by simply placing all the species together into one grouping. Under these conditions, FCA-SSIA reduces down to the FCA algorithm.

The FCA-SSIA algorithm is better than either the FCA or the SSIA algorithm. In the worst of circumstances FCA-SSIA will reduce down to the FCA algorithm. In many circumstances in which appropriate groupings can be found, FCA-SSIA will out perform the FCA algorithm.

3.4.3 The Most Efficient Algorithm for FEHMN

Except for FCA-SSIA, each of the algorithms described in the preceding sections have major limitations which make them inappropriate algorithms for the FEHMN reactive transport model. In summary, the major limitations to these schemes are:

1. SSIA cannot model equilibrium reactions.
2. SNIA is too sensitive to the grid Peclet number and the Courant number.

3. SSIA-SNIA proved to be less efficient than SSIA or SNIA.
4. FCA-SSIA can always be reduced down to FCA.

FCA-SSIA proved to be a flexible algorithm since it is capable of modeling mixed kinetic-equilibrium problems. In addition, FCA-SSIA has no theoretical upper limit on the number of species which can be modeled. However, FCA-SSIA does have a major practical limitation. The major limitation of FCA-SSIA is that numerous strongly coupled species (i.e. numerous equilibrium reactions) cannot be modeled simultaneously since the SSIA portion of the algorithm cannot be used to simplify the problem. For these problems, the FCA portion of the algorithm must solve the entire transport and chemical system simultaneously resulting in computationally inefficient behavior. However, this scenario should rarely occur since FEHMN will be used to model relatively small chemical systems (i.e. less than 10 species). The only way to avoid this computationally inefficient behavior would be to completely restructure FEHMN so that a mixed kinetic-equilibrium formulation would be used rather than fully kinetic formulation.

The FCA-SSIA algorithm should be adequate for the FEHMN reactive transport model. The chemical processes that are to be studied by FEHMN will be very specific. Information from large geochemical codes will be distilled down to 10 or fewer species which can then be modeled by FEHMN. The reactions modeled by FEHMN will be used to refine transport calculations which assumed an equivalent K_d to simulate retardation effects. Yeh and Tripathi (1991) showed that it may be inappropriate to use an equivalent K_d to simulate retardation effects due to nonlinear effects caused by the chemical equations. Therefore, simplifying assumptions using an equivalent K_d should be supported by performing more rigorous chemical transport calculations. The FCA-SSIA algorithm should be sufficient for these small chemical simulations (e.g. less than 10 species) coupled to large scale heat and flow simulations (10,000 spatial node problems).

4. MODIFICATION AND VERIFICATION OF THE FEHMN REACTIVE TRANSPORT MODEL

4.1 Overview

In this chapter, the FCA-SSIA algorithm will be incorporated into FEHMN. In addition, a technique will be developed to allow the user to simulate an equilibrium reaction by entering the equilibrium constant for the reaction. This method will prevent the user from having to manually adjust the kinetic rate constants for each problem in which equilibrium conditions are to be simulated. The last sections of this chapter consider verification of the FEHMN reactive transport model.

4.2 Incorporating FCA-SSIA into FEHMN

The one-dimensional transport codes discussed in Chapter 3 were developed to mimic the reaction module of FEHMN while leaving out many of the other features which were not necessary in evaluating the performance of the reactive transport model. The first version of the FEHMN reaction module used the SSIA algorithm. Chapter 3 showed that the SSIA algorithm cannot model equilibrium reactions. After evaluating the algorithms in Chapter 3, the FCA-SSIA algorithm was shown to be the best solution scheme for FEHMN.

Incorporating the FCA-SSIA algorithm to FEHMN is a straightforward procedure. Figure 17 shows a very general schematic of how the FEHMN reactive transport model utilizes the FEHMN flow solution. Figure 18 shows the schematic for the FEHMN reactive transport model after FCA-SSIA algorithm has been incorporated.

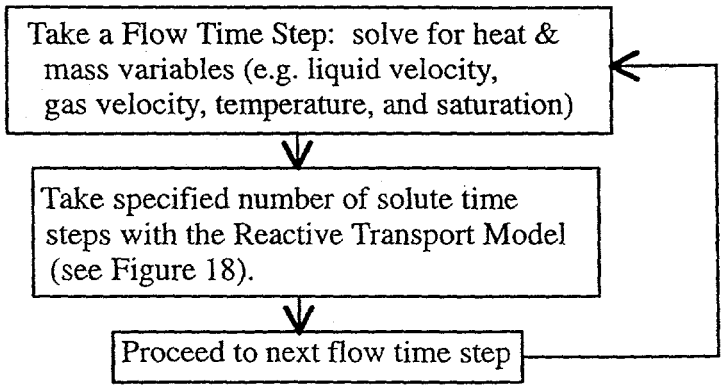

Figure 17: Schematic of the flow and transport models.

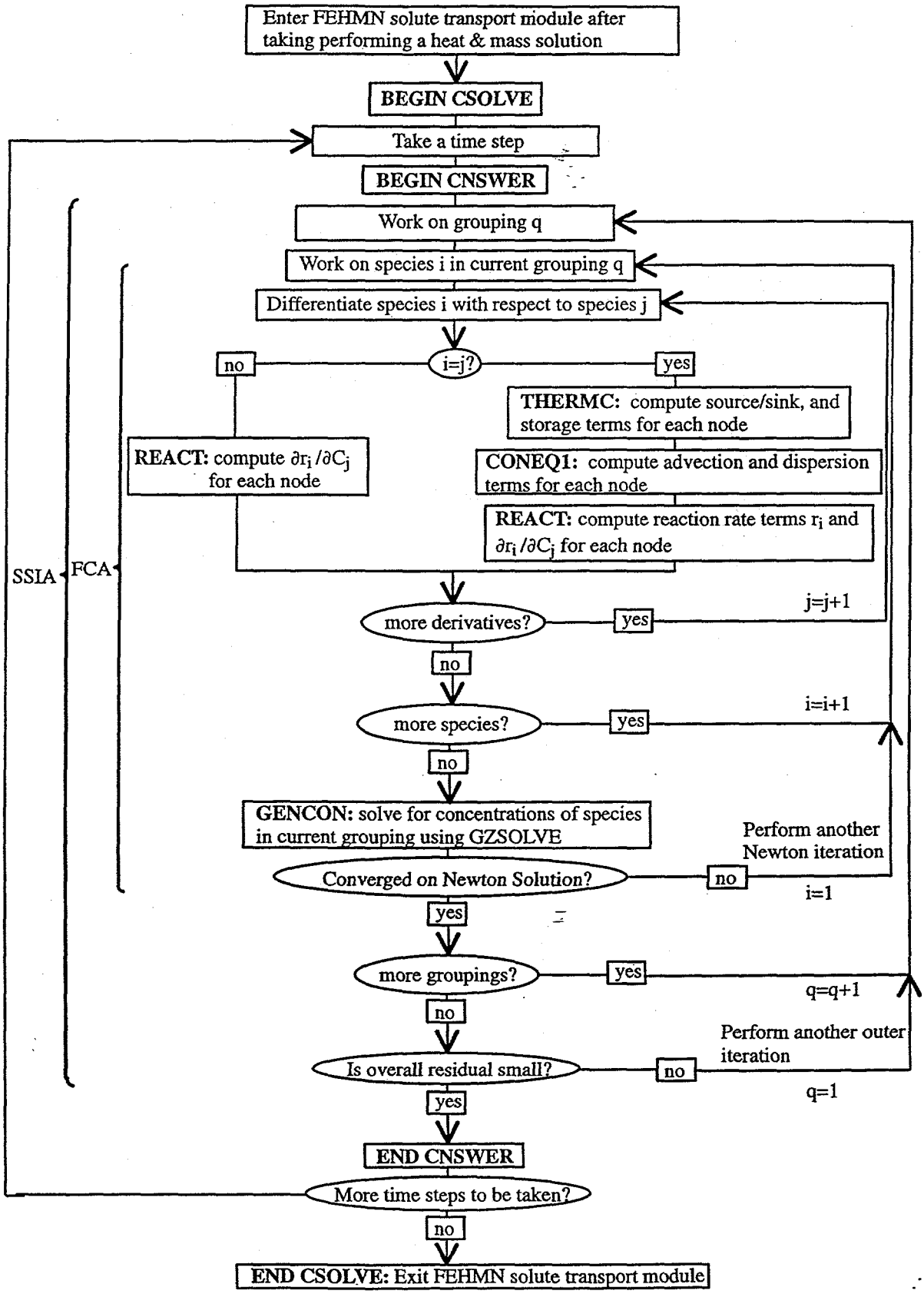

Figure 18: The FEHMN solute transport module

4.3 Simulating Equilibrium Reactions with a Kinetic Formulation

Some of the geochemical reactions required in the FEHMN simulations of Yucca Mountain are often modeled with the local equilibrium assumption because the transport time scale is slower than the reaction time scale. Since FEHMN uses a fully kinetic formulation, an automatic method was developed to select kinetic rate constants high enough to simulate equilibrium reactions. With this technique, the user enters equilibrium coefficients and the code calculates the appropriate kinetic rate constants to model equilibrium conditions.

The method uses the kinetic view of equilibrium in order to simulate an equilibrium reaction. FEHMN can model reactions of the general form:

$$a_1C_1 + a_2C_2 + \ldots + a_mC_m \underset{k_{rev}}{\overset{k_{for}}{\rightleftharpoons}} a_{m+1}C_{m+1} + a_{m+2}C_{m+2} + \ldots + a_nC_n \tag{25}$$

The rate of disappearance of C_1 by the forward reaction is:

$$r_{C_1,\text{forward}} = -a_i\left\{k_{for}\prod_{j=1}^{j=m}\left[C_j\right]^{q(j)}\right\} \tag{26}$$

and the rate of formation of C_1 by the reverse reaction is:

$$r_{C_1,\text{reverse}} = a_i\left\{k_{rev}\prod_{j=m+1}^{j=n}\left[C_j\right]^{q(j)}\right\} \tag{27}$$

At equilibrium there is no net formation of C_1, hence:

$$r_{C_1,\text{forward}} + r_{C_1,\text{reverse}} = 0 \tag{28}$$

Equations (26)-(28) can be used to develop an equation which can be used to check for equilibrium conditions. For simplicity two ratios can be defined:

$$\frac{k_{for}}{k_{rev}} = K_{eq}$$

$$Q = \frac{\prod_{j=m+1}^{j=n}\left[C_j\right]^{q(j)}}{\prod_{j=1}^{j=m}\left[C_j\right]^{q(j)}}$$

When the system is in equilibrium, $Q = K_{eq}$. Similarly, if $Q \neq K_{eq}$, the system is not in equilibrium (Levenspiel, 1972).

When a user specifies an equilibrium reaction in FEHMN, the reaction should be at equilibrium at every node in the domain at each time step. For each equilibrium reaction in the system, the following expression is used to check for equilibrium conditions at each time step for node point p:

$$\max(\gamma_{rxn})_p < \gamma_{tol}$$
$$\text{where} \quad \gamma_{rxn} = 1 - \frac{Q}{K_{eq}} \tag{29}$$

The variable γ_{tol} is a specified tolerance (e.g. 1.0×10^{-4}). As Q approaches K_{eq}, the reaction approaches equilibrium and $\max(\gamma_{rxn})_p$ approaches zero. If equation (29) is not satisfied within the specified tolerance, the following relationships can be used to estimate the increased rate constants necessary for equilibrium conditions:

$$k_{for,new} = \left(1 - \frac{Q}{K_{eq}}\right) \frac{k_{for,old}}{rate\_factor} \tag{30}$$

The variable rate_factor is an acceleration parameter entered by the user which controls the increase in the rate constants. A value of rate_factor of 1×10^{-3} was found to result in equilibrium conditions for most problems. The adjusted forward rate constant, $k_{for,new}$ is used to calculate the reverse rate constant, $k_{rev,new}$ using equation (31).

$$k_{rev,new} = \frac{k_{for,new}}{K_{eq}} \tag{31}$$

The adjusted rate constants given by equations (30) and (31) estimate the increase in the rate constants required to achieve equilibrium. However, these equations do not necessarily guarantee equilibrium. Therefore, an equilibrium iteration is introduced into FEHMN. For each equilibrium reaction, FEHMN reads in a temperature dependent equilibrium constant. Since FEHMN simulations of Yucca Mountain geochemical transport are often nonisothermal, the equilibrium constant can vary spatially by over an order of magnitude. FEHMN calculates k_{for} and k_{rev} such that $k_{for}/k_{rev} = K_{eq}$ at all locations. In the subroutine REACT, equation (29) is used to flag nodes for which the kinetic constants do not meet the equilibrium criteria throughout the domain. Before taking another

time step, the subroutine CSOLVE checks the equilibrium flag for each equilibrium reaction to determine whether the rate constants must be increased in order to achieve equilibrium conditions. If the rate constants require adjustment, FEHMN again solves the equation set with the adjusted rate constants. This sequence comprises an FEHMN equilibrium iteration.

Redoing all of the calculations starting with CSOLVE is very computer intensive. However, equilibrium iterations are often only necessary for the first few time steps. For the first time step, the rate constants are started at values which are usually high enough to guarantee equilibrium for many problems. At each new time step, the rate constants from the previous time steps are used. Equation (29) is again used to flag nodes for which the kinetic constants do not meet the equilibrium criteria throughout the domain. For many FEHMN simulations, the rate constants are adjusted at the first time step and these rate constants are usually high enough to maintain equilibrium conditions for the rest of the simulation. For these simulations, very few equilibrium iterations are necessary. However simulations exist in which transport and flow time scales are time variant requiring equilibrium iterations at many time steps throughout the simulation.

4.4 Verification of the FEHMN Reactive Transport Model

FEHMN has been thoroughly tested against analytical solutions and against other well-documented porous flow codes. These verification runs are documented in the V&V Report (Dash, 1995b) for the FEHMN Application and the V&V Plan and Procedures for the FEHMN Application (Dash, 1995a). After the new reactive transport was added to FEHMN, these verification runs were rerun to confirm that FEHMN was still working properly after the numerous code revisions. The verification runs presented in this section were used check the new reactive features of FEHMN. First, the test problems used to validate the one-dimensional algorithms of Chapter 3 were used to check that the FCA-SSIA algorithm was properly incorporated into FEHMN. As expected, the FEHMN reactive transport model behaved similarly to the FCA-SSIA algorithm for these test problems. These test problems are not presented in this thesis to prevent unnecessary repetition. The next three sections will confirm that FEHMN is working properly for more complicated and realistic reaction sequences.

4.4.1 Kinetic Nonlinear Adsorption and the Langmuir Isotherm

The Langmuir isotherm commonly used to model adsorption data from a column experiment or tracer test. By definition, an isotherm assumes that the adsorbed phase concentration is in equilibrium with the aqueous phase concentration. Frequently column studies are kinetically limited because the aqueous concentration and the adsorbent concentration do not have time to reach equilibrium over the duration of the study. For these cases, a kinetic Langmuir model (bilinear adsorption model) is often used to model data (Fetter, 1993).

In this test problem, a nonlinear kinetic Langmuir adsorption reaction is introduced into a one-dimensional transport simulation. The kinetic Langmuir model should reduce down to the Langmuir isotherm if the kinetics of the reaction are much faster than the time scale of transport. The kinetic Langmuir model can be incorporated into the FEHMN reactive transport model. In addition, FEHMN has a special option for modeling the Langmuir isotherm. These models will be compared for kinetic rate constants with different magnitudes.

The following reaction is modeled:

$$C_1 + \text{sorbent} \underset{k_{rev}}{\overset{k_{for}}{\rightleftharpoons}} S_1$$

The rate law is given by:

$$\frac{\partial C_1}{\partial t} = k_{for} C_1 (S_{max} - S_1) - k_{rev} S_1 \qquad (32)$$

where S_1 is the adsorbed concentration, C_1 is the aqueous phase concentration, S_{max} is the maximum possible adsorbed concentration. This example introduces a solid-aqueous phase reaction. All solid phase concentrations in FEHMN are expressed in moles per kilogram of rock and aqueous phase concentrations are in moles per kilogram of water. Equation (32) simplifies to the Langmuir isotherm for fast reaction kinetics (Fetter, 1993). As $k_{for} \rightarrow \infty$ and $k_{rev} \rightarrow \infty$, the Langmuir isotherm results and the dissolved phase can be related to the adsorbed phase by the simple expression:

$$(S_1)_{eq} = \frac{K_{eq} S_{max} C_1}{1 + K_{eq} C_1} \tag{33}$$

where $K_{eq} = k_{for}/k_{rev}$ and $(S_1)_{eq}$ is the equilibrium concentration of the adsorbed phase. The kinetic formulation is compared to the Langmuir isotherm for different values of k_{for} and k_{rev}. To make a valid comparison, the Langmuir isotherm parameters must be related to the rate constants. FEHMN requires two input parameters to model a Langmuir isotherm. The parameters, a_1 and a_2, fit into the model as follows:

$$(S_1)_{eq} = \frac{a_1 C_1}{1 + a_2 C_1} \tag{34}$$

where $a_1 = k_{for} * S_{max}/k_{rev}$ and $a_2 = k_{for}/k_{rev}$. Table 10 shows the parameters used that are shared by the kinetic and equilibrium simulations.

Table 10: Parameters common to the kinetic and equilibrium Langmuir model simulations

reactor length	1 m
reactor cross sectional area	1 m^2
ϱ_f, fluid density	1000 kg/m^3
ϱ_b, bulk rock density	2500 kg/m^3
θ, porosity	0.3
u, pore water velocity	0.075 m/s
α_L, dispersivity	0.033 m
Δt , maximum time step	0.1 s
Δx, mesh spacing	0.005 m
simulation time	100 s
mean residence time, τ	13.3 s
C_{1i}, inlet concentration	1.0 mole/kg H_2O

A S_{max} of 0.12 mole/ kg rock was chosen for the kinetic simulations. Three kinetic simulations were carried out with rate constants of varying magnitudes while fixing the ratio between the rate constants. Table 11 shows the parameters used in the four trials.

Table 11: Kinetic and equilibrium parameters

Trial	Reaction	Parameters
1	equilibrium	$a_1 = 0.12$ kg H_2O/kg rock , $a_2 = 1$ kg H_2O/ mole
2	kinetic	$k_{for} = 1x10^{-6}$ kg H_2O/(mole*s), $k_{rev} = 1x10^{-6}$ s^{-1}
3	kinetic	$k_{for} = 1x10^{-5}$ kg H_2O/(mole*s), $k_{rev} = 1x10^{-5}$ s^{-1}
4	kinetic	$k_{for} = 1x10^{-4}$ kg H_2O/(mole*s), $k_{rev} = 1x10^{-4}$ s^{-1}

As expected, as the magnitude of the kinetic rate constants increase, the kinetic Langmuir model approaches the Langmuir isotherm. The breakthrough curves of the exit concentration are shown in Figure 19.

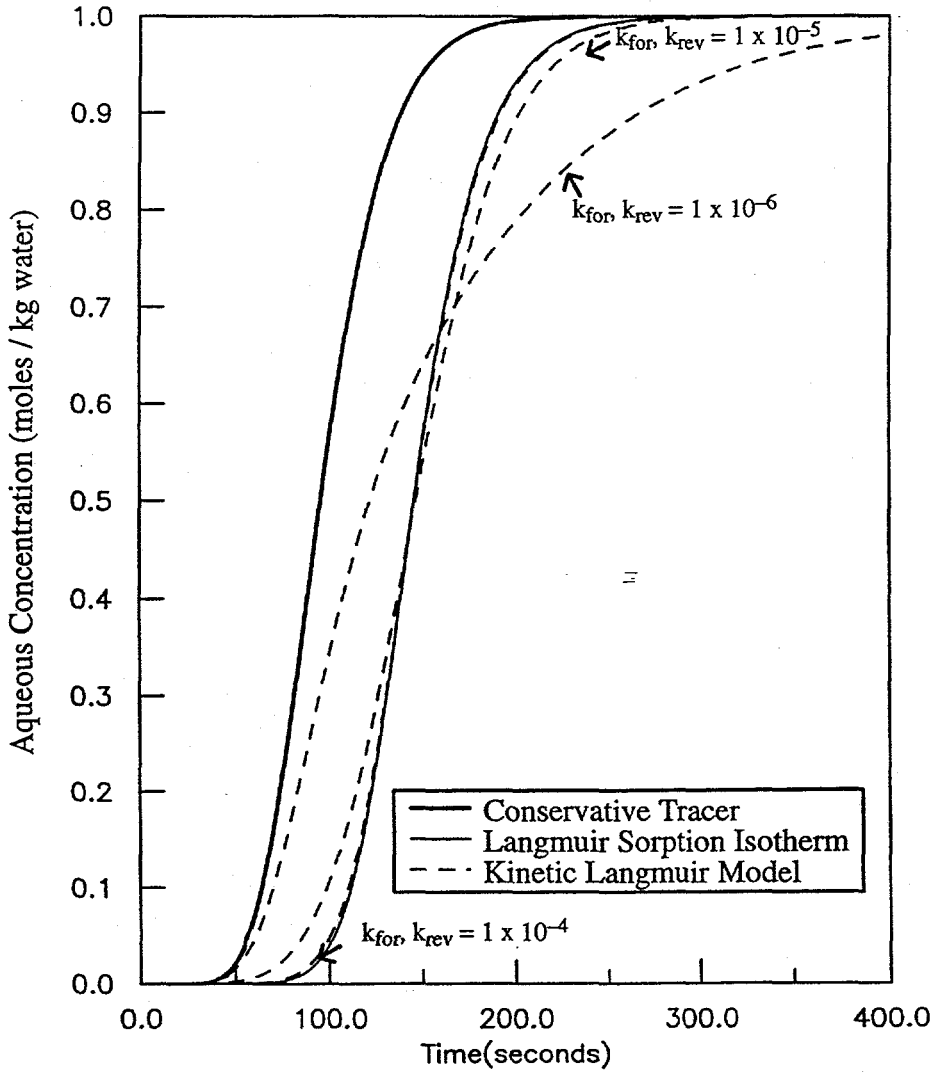

Figure 19: Comparison of kinetic and equilibrium Langmuir models

This test problem confirms that FEHMN correctly models a nonlinear adsorption reaction. The next problem will examine a more complicated reaction sequence to prove that the FEHMN reactive transport model is working properly for multiple kinetic and equilibrium reactions.

4.4.2 Multiple Complexation, Kinetic Adsorption and Surface Exchange Reactions

This example shows a real scenario for which the FEHMN reactive transport model can be used to gain insight into a complex problem. Over the past 40 years soils and groundwaters at DOE facilities have been contaminated by complex mixtures of radioactive, inorganic and organic chemical wastes. Cobalt, as ^{60}Co, is an important radioactive contaminant found migrating in the subsurface at several DOE facilities. The migration of ^{60}Co has been greater than anticipated due to complexation of divalent cobalt with organic ligands such as EDTA. EDTA is a decontaminating agent also found in the subsurface at these DOE facilities. Experimental studies have shown that the complexation of EDTA with cobalt greatly increases the mobility of the cobalt. Specifically, complexed cobalt does not adsorb as much as free metal cobalt thereby allowing for greater migration of the toxic metal. The subsurface chemistry of these DOE sites is complex making prediction of contaminant migration difficult (Szecsody et al., 1994).

At Pacific Northwest Laboratories, several column experiments on CoEDTA transport through iron-oxide coded sand have been performed. Valocchi et al. (1994) have developed a two-dimensional multicomponent reactive transport code, PDREACT, which has been used to model the physical and chemical processes of the column experiments. The most important reactions targeted for initial study were:

$$Co(aq) + EDTA(aq) \rightleftharpoons CoEDTA(aq) \quad ; Keq_1 = 1x10^{18} \text{ kg/mole}$$

$$Fe(aq) + EDTA(aq) \rightleftharpoons FeEDTA(aq) \quad ; Keq_2 = 6.31x10^{24} \text{ kg/mole}$$

$$Co(aq) \underset{k_{rev_3}}{\overset{k_{for_3}}{\rightleftharpoons}} \overline{Co(s)} \quad ; k_{for3} = 2.7x10^{-4}\ s^{-1},\ k_{rev3} = 5.48x10^{-5}\ s^{-1}$$

$$CoEDTA(aq) \underset{k_{rev_4}}{\overset{k_{for_4}}{\rightleftharpoons}} \overline{CoEDTA(s)} \quad ; k_{for4} = 2.7x10^{-4}\ s^{-1},\ k_{rev3} = 5.21x10^{-4}\ s^{-1}$$

$$\text{FeEDTA(aq)} \underset{k_{rev_5}}{\overset{k_{for_5}}{\rightleftharpoons}} \overline{\text{FeEDTA(s)}} \qquad ; k_{for5} = 2.7\text{x}10^{-4}\ s^{-1},\ k_{rev5} = 6.5\text{x}10^{-4}\ s^{-1}$$

$$\overline{\text{CoEDTA(s)}} + \text{Fe(OH)}_3\text{(s)} \xrightarrow{k_{for_6}} \overline{\text{Co(s)}} + \overline{\text{FeEDTA(s)}} \qquad ; k_{for6} = 1.3125\ \text{mole/(kg*s)}$$

In the reactive system, EDTA(aq) complexes with both Fe(aq) and Co(aq). Each of the aqueous components also adsorb to the iron oxide sand which fills the column. A kinetic linear model was chosen to model the adsorption. An irreversible surface exchange reaction between the solid species in the system also takes place as the contaminants migrate through the column. All of these reactions coupled to the transport result in complex nonlinear behavior which cannot be accurately modeled with a simple effective K_d.

PDREACT was thoroughly tested and matched against experimental data for this reactive system. Specifically, PDREACT showed reasonable agreement with the experimentally determined breakthrough curve. The agreement was only possible if the sorption kinetics were kinetically controlled and if the surface exchange reaction proceeds at a much faster rate than that estimated experimentally at Pacific Northwest Laboratory. These column experiments are an example of when the local equilibrium assumption cannot be assumed for all of the reactions. The FEHMN reactive transport model is also capable modeling this reactive transport problem. Since this simulation contains eight species ($Fe(OH)_3$(s) exists in abundance and is not modeled), the species must be grouped to obtain optimum computational efficiency. Many possible sets of group are possible to obtain efficient convergence. However, the best set of groups for this problem is given by:

Group 1: Co(aq), EDTA(aq), CoEDTA(aq)

Group 2: Fe(aq), EDTA(aq), FeEDTA(aq)

Group 3: $\overline{\text{Co(s)}}$

Group 4: $\overline{\text{CoEDTA(s)}}$

Group 5: $\overline{\text{FeEDTA(s)}}$

In this example, the species in the first two equilibrium reactions are placed in groups 1 and 2 since these species are strongly coupled to one another. Groups 3, 4 and 5 simply contain the remaining

species in the simulation since all species must be present in at least one group. This set of groups results in efficient convergence since the strongly coupled species are grouped together and the groups are weakly coupled to one another. Specifically, FEHMN took an average of 2-3 outer iterations per time step and only required 8 equilibrium iterations at the first time step for this simulation.

The comparison of the two codes provides a check of FEHMN's reactive transport model for a complicated realistic system. FEHMN and PDREACT solve the reactive transport problem using completely different methods. FEHMN uses a fully kinetic formulation to model relatively small chemical systems. FEHMN is intended for large scale simulations in which coupled processes such as heat, unsaturated and saturated flow, and geochemical processes are important. On the other hand, PDREACT contains a mixed kinetic-equilibrium formulation. PDREACT was developed to model complex chemical problems under isothermal and saturated flow conditions.

The key assumption made by PDREACT which is not made by FEHMN is that chemical systems in porous media can be represented accurately by assuming that all aqueous-phase reactions go to equilibrium, while all solid-phase reactions are kinetically controlled. This assumption is commonly made in reactive transport codes and is widely accepted to be valid (Lasaga and Steefel, 1994). FEHMN does not make this assumption for practical reasons. Specifically, it would have required major software restructuring to introduce a mixed kinetic-equilibrium formulation into FEHMN (see discussion in Section 2.2 for further discussion on the choice of formulation). In summary, the different approaches taken in the codes are a result of the different applications for which they are to be used.

A one-dimensional FEHMN simulation was constructed to match the results obtained by PDREACT. The simulation involved a pulse containing a mixture of ^{60}Co, Fe, and EDTA which was injected for 76 hours. The parameters used by both FEHMN and PDREACT are provided in Table 12.

Table 12: FEHMN parameters used in PDREACT comparison problem

reactor length	10 m
reactor cross sectional area	1 m^2
ϱ_f, fluid density	1000 kg/m^3
ϱ_b, bulk rock density	1500 kg/m^3
θ, porosity	0.4
u, pore water velocity	1 m/hr
α_L, dispersivity	0.05 m
Δt , maximum time step	0.1 hr
Δx, mesh spacing	0.1 m
simulation time	150 hr
Co inlet concentration	3.1623×10^{-5} moles/kg H_2O
Fe inlet concentration	1×10^{-10} moles/kg H_2O
EDTA inlet concentration	3.1623×10^{-5} moles/kg H_2O

Figure 20 shows the time history of both the aqueous and solid species concentrations at the exit of the column. FEHMN and PDREACT produce nearly identical results. Both codes accurately model the complex chemistry that takes place in this reactive system. The aqueous species time history plot shows that Co(aq) and EDTA(aq) complex to form CoEDTA(aq). Although Fe(aq) is injected into the column at an extremely low concentration, FeEDTA(aq) shows up at significant concentrations due to the surface exchange reaction and the desorption of $\overline{\text{FeEDTA(s)}}$ to FeEDTA(aq). Co(aq) is retarded by the complex chemistry but begins to build as the simulation progresses showing that the Co(aq) is effectively mobilized.

Figure 20 shows that the solid species all display complex behavior also. The surface exchange reaction results in $\overline{\text{Co(s)}}$ adsorbing in significant quantities. $\overline{\text{Co(s)}}$ then desorbs resulting in the mobile aqueous cobalt, Co(aq). In summary, the EDTA is shown to greatly increase the mobility of Co(aq), CoEDTA(aq) and FeEDTA(aq). The increase mobility could not be accurately predicted without accounting for the complex chemistry which takes place in the column.

The fact that both codes produce nearly identical results for this problem is a very promising result. This result proves that the fully kinetic formulation used by FEHMN reduces down to the mixed equilibrium-kinetic formulation used by PDREACT for a complicated chemical system.

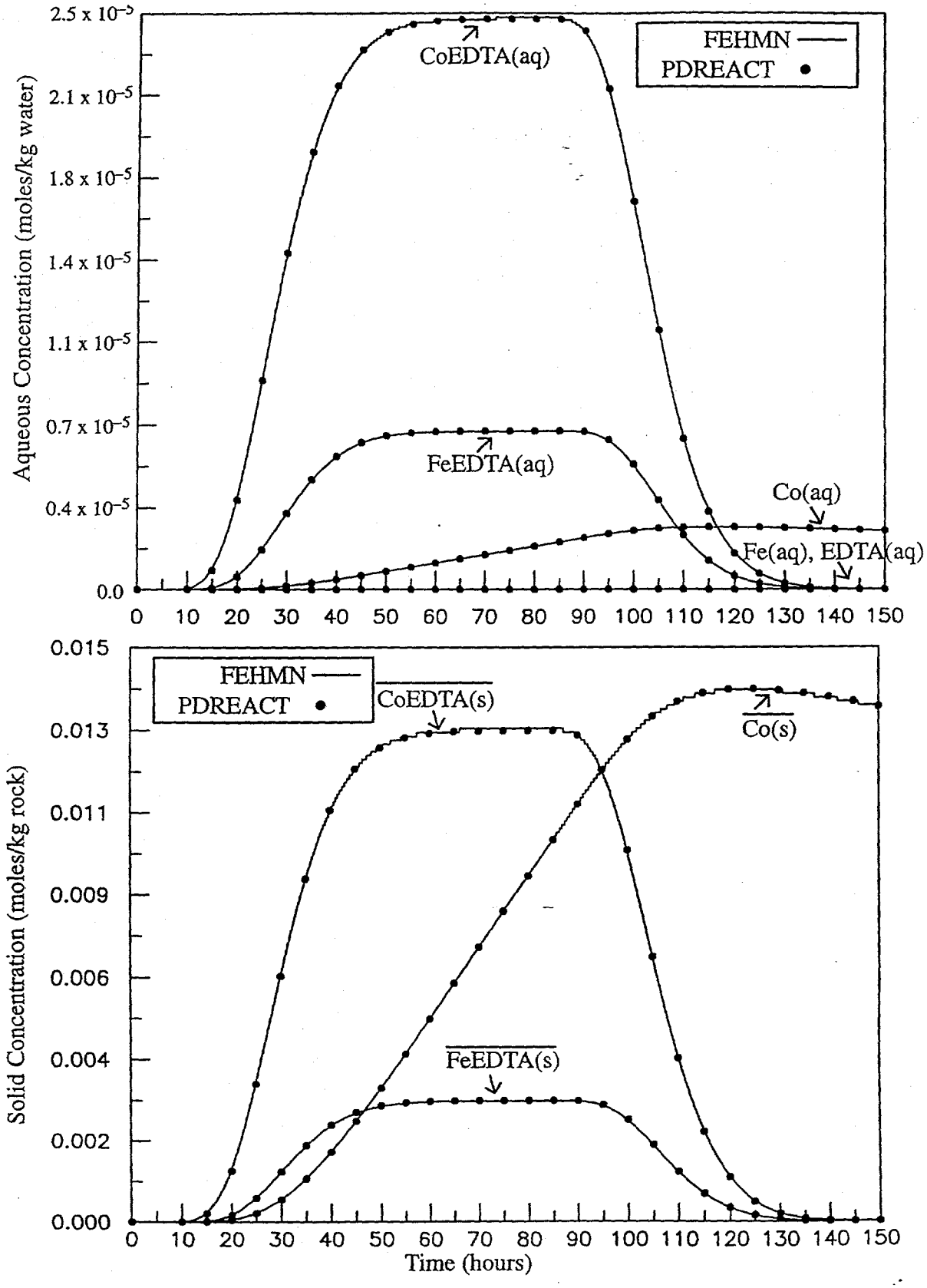

Figure 20: Time history of species at column outlet (x=10 m)

4.4.3 Sharp Dissolution Front

The analytical solution for the movement of a sharp moving, equilibrium mineral front has been used to verify numerical simulations of precipitation-dissolution reactions in the past (e.g. Engesgaard, 1991, Schweich and Sardin, 1985, Walsh et al., 1984). In this example, the analytical solution is used to check FEHMN's ability to model a precipitation-dissolution reaction. The analytical solution neglects dispersion and is given by:

$$u_{mineral} = \frac{u\Delta C_{aq}}{\Delta C_{aq} + \frac{\varrho_b}{\theta}\Delta C_{solid}} \tag{35}$$

where u is the pore water velocity, u_m is the velocity of the mineral front, ϱ_b is the bulk rock density, θ is the porosity, ΔC_s is the change in solid concentration across the front and ΔC_{aq} is the change in aqueous concentration across the front. Figure 21 illustrates the mineral front described by the analytical solution. Referring to the figure, concentrations to the right of the front represent locations in the column where mineral is still present, whereas concentrations preceding the front represent locations in the column where the mineral has dissolved away.

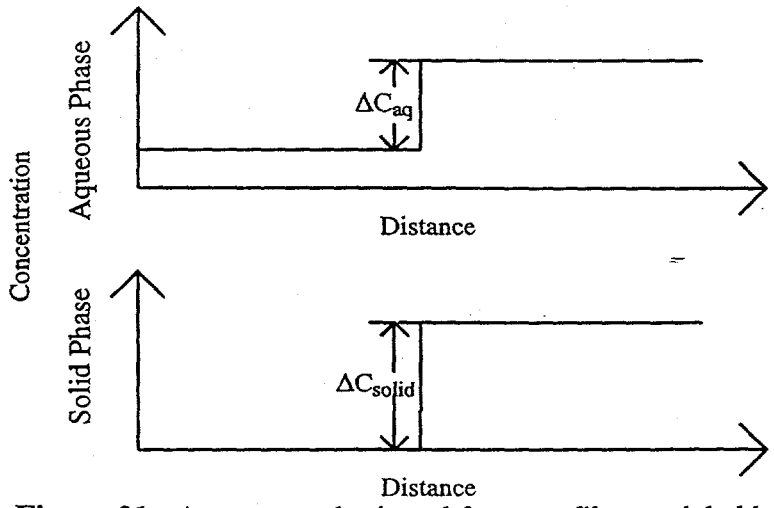

Figure 21: Aqueous and mineral front profiles modeled by the analytical solution

A one dimensional numerical simulation was constructed to simulate the dissolution of calcite ($CaCO_3(s)$). In this example, Ca^{2+}, CO_3^{2-} and $CaCO_3$ are the only species in the system. The column initially is in equilibrium with calcite. Inlet concentrations were $[Ca^{2+}] = [CO_3^{2-}] = 0$ moles/

kg water. A FEHMN simulation was configured in which the dispersivity was set to a very low value. The parameters used in the simulation are shown in Table 13.

Table 13: FEHMN parameters used to model dissolution front

reactor length	0.50 m
reactor cross sectional area	1 m^2
ϱ_f, fluid density	1000 kg/m^3
ϱ_b, bulk rock density	1800 kg/m^3
θ, porosity	0.32
u, pore water velocity	9.37×10^{-6} m/s
α_L, dispersivity	0.001 m
Δt , maximum time step	100 s
Δx, mesh spacing	1.151×10^{-3} m
simulation time	1×10^5 s
Ca^{2+} initial concentration	6.26×10^{-5} moles/kg H_2O
CO_3^{2-} initial concentration	6.26×10^{-5} moles/kg H_2O
$CaCO_3$ initial concentration	2×10^{-5} moles/kg rock
Ca^{2+} inlet concentration	0.0 moles/kg H_2O
CO_3^{2-} inlet concentration	0.0 moles/kg H_2O

Figure 22 shows that the analytical solution and FEHMN compare closely in predicting the location of the mineral front. FEHMN's numerical solutions exhibit a very slight spreading of the

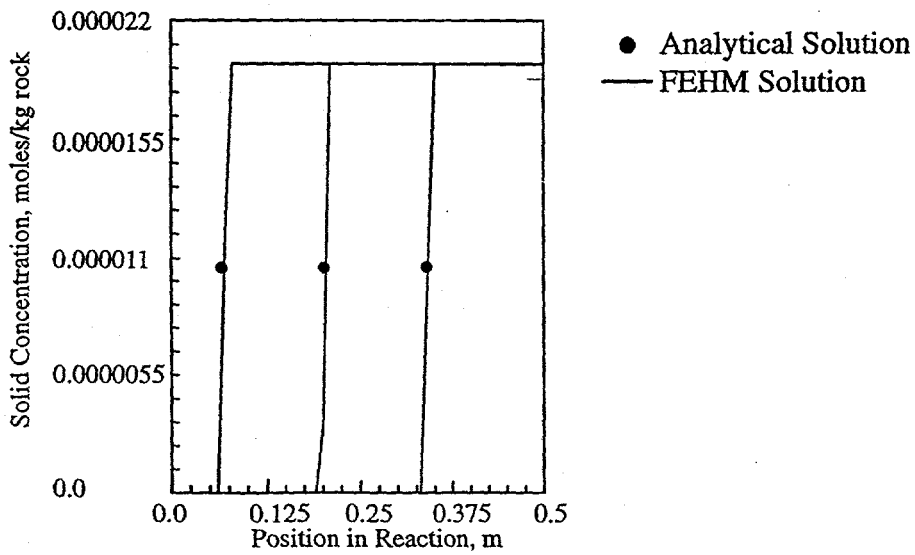

Figure 22: Comparison of FEHMN and the analytical solution for the position of the dissolved mineral front

front due to the small, but nonnegligible dispersivity. Nonetheless, the position of the front agrees with the predicted value with a maximum error of 2.4%.

4.5 Summary

The test problems presented in this Chapter ensure that the solution algorithm of FEHMN is capable of modeling multiple kinetic and equilibrium reactions for one-dimensional saturated flow problems. Additional reactive test problems are documented in the V&V Report for the FEHMN Application (Dash, 1995b) and the V&V Plan and Procedures for the FEHMN Application (Dash, 1995a). Although numerous verification tests have been conducted, FEHMN is simply too complex for complete and unambiguous verification and validation. However, the reactive transport model appears to be working properly over a wide variety of problems. Therefore, the next logical step is to begin using the enhanced reaction capabilities of FEHMN to refine the Los Alamos National Laboratory's site scale model of the Yucca Mountain Site. In Chapter 5, LANL's site scale model of Yucca Mountain is used to model unsaturated zone ^{14}C transport at Yucca Mountain.

5. APPLICATION OF THE FEHMN REACTION MODEL TO TRANSPORT STUDIES AT YUCCA MOUNTAIN

5.1 Overview

Scientists at Los Alamos National Laboratory (LANL) have been developing hydrologic flow and transport models of the Yucca Mountain site using FEHMN. The FEHMN solute transport model has been used to conduct simulations of the transport of environmental isotopes to provide data to calibrate the hydrologic flow models. Simulations of ^{14}C and ^{36}Cl transport have already been conducted with LANL. Transport studies for these species have been carried out using a simple half life model to simulate decay. However, more complex chemical interactions with ^{14}C and ^{36}Cl have not yet been examined. The enhancements of the FEHMN reactive transport model now make it possible to include more complicated reaction sequences into the transport models for ^{14}C and ^{36}Cl. By treating the chemical system more rigorously, more representative predictions of transport should be possible. In addition, the equivalent K_d approach of modeling solute transport used in previous transport studies can be buttressed by these more rigorous calculations.

A good introductory application for the reactive transport model is to model the significant reactions which influence the transport of ^{14}C at Yucca Mountain. The following sections will detail the steps taken to develop a chemical model for ^{14}C. Sections 5.2.1–5.2.3 develop and verify that the multiphase carbonate chemistry is working properly in FEHMN for a batch system. Next, Section 5.3.1 models one-dimensional transport of $CO_2(g)$ in an unsaturated column to examine the effect of temperature and pH on $CO_2(g)$ retardation. The chapter concludes with Sections 5.3.2-5.3.3 which discuss the incorporation of the ^{14}C chemical equations into LANL's site scale model.

5.2 Carbonate Chemistry Batch Simulations

To simulate the most basic reactions in the carbonate system, the FEHMN reaction module is given the following reactions:

$$CO_2(g) \rightleftharpoons CO_2(aq); \qquad K_H(T)$$
$$H_2CO_3^* \rightleftharpoons H^+ + HCO_3^-; \qquad K_{a,1}(T)$$
$$HCO_3^- \rightleftharpoons H^+ + CO_3^{2-}; \qquad K_{a,2}(T)$$

where K_H, $K_{a,1}$ and $K_{a,2}$ are functions of temperature. These polynomial functions were obtained from Plummer et al. (1982) and can be directly incorporated into FEHMN. In the above reactions, the equilibrium between aqueous and vapor carbon dioxide is given by Henry's law. In addition, H_2CO_3 and $CO_2(aq)$ are combined into a hypothetical species $H_2CO_3^*$ to represent the sum of H_2CO_3 and $CO_2(aq)$. This is a common technique since H_2CO_3 and $CO_2(aq)$ are difficult to distinguish between in analytical procedures (Snoeyink and Jenkins, 1980). The equilibrium reactions for these reactions are given by:

$$K_H(T) = \frac{[CO_2(aq)]}{[CO_2(g)]} \tag{36}$$

$$K_{a,1}(T) = \frac{[H^+][HCO_3^-]}{[H_2CO_3^*]} \tag{37}$$

$$K_{a,2}(T) = \frac{[CO_3^{2-}][H^+]}{[HCO_3]} \tag{38}$$

More complexity can be added to the reaction sequence if other chemical reactions are to be considered. For example, Section 5.2.3 includes the calcite dissolution reaction into the model.

A common assumption in ^{14}C studies is to assume that the concentrations of ^{14}C are proportional to those of ^{12}C (Ross et al., 1992). Therefore, equations (36)–(38) hold for ^{14}C. In addition, activity coefficients are assumed to be unity for these simulations. This assumption holds for solutions with low ionic strength. Ionic strength data of Yucca Mountain groundwater is necessary to check this assumption. For these preliminary studies, the assumption will be made for convenience.

5.2.1 Carbonate System Chemistry in a Closed System

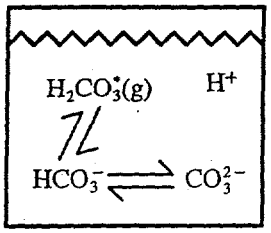

Figure 23: Conceptual model of carbonate chemistry in a closed system

Before any work began on incorporating the ^{14}C transport into the site scale model, several tests on FEHMN's carbonate chemistry calculations need to be performed. In this section, we verify that the aqueous carbonate species are partitioning correctly for a given C_{T,CO_3} at a fixed pH in a closed system (Figure 23). C_{T,CO_3} is is defined by equation (39).

$$C_{T,CO_3} = [H_2CO_3^*] + [HCO_3^-] + [CO_3^-] \tag{39}$$

By fixing C_{T,CO_3}, the constraint that the system be in equilibrium with a partial pressure of carbon dioxide has been removed. Therefore, equation (36) is not necessary in this simulation. By eliminating this equation, the problem is reduced to a one phase batch simulation and $H_2CO_3^*$ can be treated as a nonvolatile diprotic acid. This reaction sequence contains three chemical equations (37)-(39) and four chemical species (H^+, $H_2CO_3^*$, HCO_3^- and CO_3^{2-}). Fixing the pH fully constrains the chemical system.

In order to check the partitioning of the aqueous carbonate species, a simple four node problem with no flow or transport was formulated. Equations (37) and (38) were entered into the reaction module of FEHMN as equilibrium reactions. The simulation started with initial concentrations of $[H_2CO_3^*]=10^{-5}\,M$,$[HCO_3^-]=0\,M$ and $[CO_3^{2-}]=0\,M$. FEHMN then calculates the equilibrium concentrations of each species. The concentrations of the carbonate species for a $[C_{T,CO_3}] = 10^{-5}$ at 25 °C for a closed system are documented by Snoeyink and Jenkins (1980). Table 14 shows that the FEHMN results are identical to those presented by Snoeyink and Jenkins. The simulation results were also checked by back substituting the species concentrations into equations (37) and (38) con-

firming that these equations were satisfied. This simulation confirmed that the aqueous carbonate species are partitioning correctly.

Table 14: Comparison of FEHMN and Snoeyink & Jenkins for a closed carbonate system

pH=5.7	$H_2CO_3^*$	HCO_3^-	CO_3^{2-}
Snoeyink & Jenkins	$10^{-5.1}$	$10^{-5.7}$	$10^{-10.4}$
FEHMN	$10^{-5.1}$	$10^{-5.7}$	$10^{-10.4}$

pH=7.6	$H_2CO_3^*$	HCO_3^-	CO_3^{2-}
Snoeyink & Jenkins	$10^{-6.4}$	10^{-5}	$10^{-7.6}$
FEHMN	$10^{-6.4}$	10^{-5}	$10^{-7.6}$

pH=9.0	$H_2CO_3^*$	HCO_3^-	CO_3^{2-}
Snoeyink & Jenkins	$10^{-7.6}$	10^{-5}	$10^{-6.3}$
FEHMN	$10^{-7.6}$	10^{-5}	$10^{-6.3}$

5.2.2 Carbonate System Chemistry in an Open System

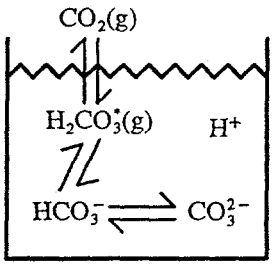

Figure 24: Conceptual model of carbonate chemistry in an open system

The next logical step is to simulate carbonate system chemistry in an air-water system (Figure 24). The two phase model capability for FEHMN is necessary for this simulation. Equation (36) is used along with equations (37) and (38) to model an open system. Equation (36) is used to control the concentration of CO_2(aq) in equilibrium with CO_2(g). One additional variable, CO_2(g), is added to the system but equation (36) is also added. Therefore, the problem is again fully constrained by fixing pH and the concentration CO_2(g). Fixing the concentration CO_2(g) is equivalent to fixing the partial pressure of CO_2 which is an accurate assumption in an open system. As in the previous example, a simple four node problem with no flow and transport was constructed.

Light et al. (1989) define the gas-liquid distribution coefficient for inorganic carbon to be:

$$K_D = \frac{[H_2CO_3^*] + [HCO_3^-] + [CO_3^{2-}]}{[CO_{2(g)}]} \quad (40)$$

At a pH of 7 and a temperature of 50 °C, they report a $K_D = 3$ m^3 air/m^3 water. FEHMN should obtain this same distribution coefficient under these conditions. To simulate this problem with FEHMN, a fixed concentration of $CO_2(g)$ is input along with a fixed H^+ concentration of $1x10^{-7}$ moles/ kg water. The FEHMN reaction module then calculates the appropriate equilibrium concentrations. The concentrations of each species are output by FEHMN. Substituting the FEHMN species concentrations into equation (40) results in a K_D of 3.1, proving that FEHMN is properly simulating this air-water system.

5.2.3 Carbonate System Chemistry in an Open Batch System with Calcite

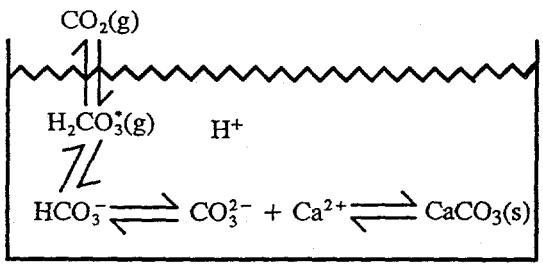

Figure 25: Conceptual model of an open system in equilibrium with calcite

Minerals play an important role in controlling pH and alkalinity in most geochemical systems. Calcite is present in Yucca Mountain core samples from the unsaturated zone. In addition, calcite precipitation-dissolution kinetics are fast relative to the groundwater flow suggesting that equilibrium saturation with calcite is a reasonable assumption in the unsaturated zone of Yucca Mountain (Ross, 1992, Meijer, 1993). In this simulation, FEHMN will be used to model and open system in equilibrium with calcite (Figure 25). In order to simulate saturation with respect to calcite, the solubility product expression for calcite must be included in the reaction sequence. The expression is given by:

$$CaCO_3(s) \rightleftharpoons Ca^{2+} + CO_3^{2-}; \qquad K_{sp}(T)$$

This reaction results in the following solubility product:

$$K_{sp}(T) = [Ca^{2+}][CO_3^{2-}] \quad (41)$$

Adding equation (41) to the reaction sequence introduces Ca^{2+} as a variable. It should be noted that solid species dissolution is a zero order process, solid species activity is unity, and that $CaCO_3$ is not an additional variable in the system. Therefore, fixing the partial pressure of $CO_2(g)$ and the pH would appear to constrain the chemical system with five equations and five unknowns. However, equation (39) no longer holds for the chemical system. The total amount of carbonate in the system is now affected by the presence of calcite. Therefore, one more constraint must be added to the system. The electroneutrality expression can be used to fully constrain the chemical system. The expression is given by:

$$2[Ca^{2+}] + [H^+] = [HCO_3^-] + 2[CO_3^{2-}] + [OH^-] \quad (42)$$

For the range of partial pressure of $CO_2(g)$ found in groundwater, equation (42) simplifies to:

$$2[Ca^{2+}] \approx [HCO_3^-] \quad (43)$$

since all the other species exist at low concentrations.

In these simulations, for a fixed concentration of $CO_2(g)$ (equivalent to a fixed partial pressure of CO_2) , FEHMN calculates the pH of the system along with the concentrations of each species in equilibrium with calcite. MINTEQ2A (Allison, 1991) , a well known batch geochemical equilibrium code, was used verify that the FEHMN simulated this chemical system properly. MINTEQA2 is capable of modeling activity corrections unlike FEHMN. Therefore, the ionic strength for the MINTEQA2 simulations was held at zero. In addition, the exact same equilibrium coefficients were used in both codes. Therefore, both codes should produce nearly identical results.

Figure 26 shows simulated dissolved species concentrations as a function of the partial pressure of carbon dioxide. MINTEQA2 was run for the two partial pressure values indicated in Figure 26. As seen in Figure 26 and Table 15, FEHMN and MINTEQA2 produced nearly identical results. The slight discrepancies are most likely due to numerical errors. FEHMN uses a fully kinetic formulation with high rate constants to simulate the equilibrium behavior, whereas, MINTEQA2 is strictly

an equilibrium code. This problem shows that FEHMN correctly models the geochemistry of the system when a mineral is present.

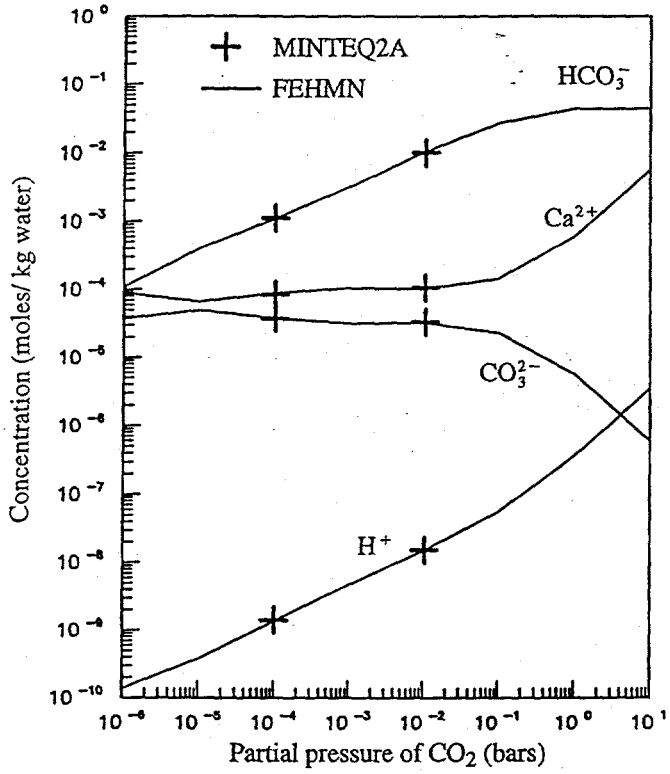

Figure 26: Simulated FEHMN and MINTEQ2A concentrations in equilibrium with calcite as a function of the partial pressure of carbon dioxide

Table 15: Comparison of FEHMN and MINTEQA2 for an open system in equilibrium with calcite

partial pressure $CO_2(g) = 10^{-2}$ bars	$H_2CO_3^*$ (molality)	HCO_3^- (molality)	CO_3^{2-} (molality)	Ca^{2+} (molality)	pH
MINTEQA2	3.32×10^{-4}	2.76×10^{-3}	2.42×10^{-6}	1.38×10^{-3}	7.27
FEHMN	3.32×10^{-4}	2.76×10^{-3}	2.41×10^{-6}	1.38×10^{-3}	7.27
MINTEQA2	3.32×10^{-6}	5.87×10^{-4}	1.09×10^{-5}	3.07×10^{-4}	8.60
FEHMN	3.32×10^{-6}	5.87×10^{-4}	1.09×10^{-5}	3.07×10^{-4}	8.60

FEHMN can now be used to check the assumption that the Yucca Mountain groundwater is in equilibrium with calcite. The partial pressure of $CO_2(g)$ was measured in gas samples at intervals to a depth of 1200 feet in Yucca Mountain (Yang, 1994). A characteristic value from these measurements is 0.0011 bars. FEHMN indicates that the pH of a water in equilibrium with calcite at this partial pressure is about 8.0. Measurements of unsaturated zone water near Rainier Mesa (near Yucca Mountain) yield pH values between 7 and 8 (Ross, 1992). Benson et al.(1983) found pH values

between 7 and 8.0 in the Yucca Mountain area. Values of pH below 8 indicate that either the water is not in equilibrium with calcite throughout the mountain or the partial pressure of carbon dioxide must vary from about 0.5 to 00075 bars throughout the mountain. Another possible explanation for the range of pH values could be due to measurement errors.

At this time the calcite reaction cannot be used to gain additional insight about the carbonate chemistry at Yucca Mountain since the spatial distributions of calcite and other minerals are not known. Therefore, for these preliminary studies, the chemical properties are assumed homogeneous. The calicte reaction could still be included, making the assumption that the Yucca Mountain groundwater is in equilibrium with calcite throughout the mountain. The partial pressure of $CO_2(g)$ could then be varied in each simulation to obtain a characteristic pH. However, since spatial distributions are not known, the pH of the simulations can be simply fixed numerically to a characteristic value instead of using the calcite reaction to buffer the pH. This will reduce the number of species from six to four thereby reducing the computational effort required to solve the problem.

For the preliminary runs discussed in the next section, equations (36)–(38) will be used to simulate the carbonate chemistry. Therefore, the simulations that will be conducted in this thesis are not more chemically sophisticated than those that use an equivalent K_d (equation (40)). It is clear that that an equivalent K_d approach is the computationally better option if only equations (36)–(38) are necessary to accurately model the carbonate chemistry at Yucca Mountain. However, an equivalent K_d model cannot be further refined as more geochemical information becomes available. In the future more information on the mineral assemblage will allow for spatial distributions of various minerals to be incorporated into the site scale model. In addition, aqueous phase chemical reactions other than equations (36)–(38) may also be shown to be important in describing carbonate chemistry at Yucca Mountain. As additional experimental data becomes available, more chemically sophisticated models for the carbonate chemistry at Yucca Mountain can be simulated using the FEHMN reactive transport model. Equations (36)–(38) can be thought of as the "base" reactions for the carbonate model. These "base" reactions will serve to confirm that the reactive transport model is working properly when used in conjunction with the site scale model.

5.3 Carbonate Chemistry Transport Simulations

The previous simulations tested the carbonate chemistry in a batch system. Section 5.3.1 will test the carbonate chemistry by simulating $CO_2(g)$ transport in a one-dimensional unsaturated column. Sections 5.3.2-5.3.3 will discuss the ^{14}C transport simulations with the Los Alamos National Laboratory site scale model.

5.3.1 One Dimensional $CO_2(g)$ Transport Simulations

The next set of tests will study $CO_2(g)$ transport in a one dimensional transport simulation. It is assumed that a constant concentration of $CO_2(g)$ is injected with the incoming air into the unsaturated column. The air is mobile and the water is stagnant in these simulations. Therefore, as $CO_2(g)$ dissolves in the water, it will be retarded by the immobile water. The amount of $CO_2(g)$ that can dissolve in water is governed by equations (36)-(38), and therefore these chemical equations describe $CO_2(g)$ retardation for this problem. It is clear from the chemical equations that the $[H^+]$ concentration is a factor in the amount of $CO_2(g)$ retardation. Also, these reactions are controlled by the temperature dependent equilibrium constants. Therefore, the amount of retardation is also dependent on temperature. In these simulations, the effect of pH and temperature on $CO_2(g)$ transport will be studied. The parameters used in the one dimensional simulations are given in Table 16.

Table 16: Parameters for the one-dimensional $CO_2(g)$ transport simulations

reactor length	1 m
ϱ_f, fluid density	1000 kg/m^3
θ, porosity	0.3
s, liquid saturation	0.2
u, pore air velocity	0.01 m/day
α_L, dispersivity	0.033 m
Δt , maximum time step	2 days
Δx, mesh spacing	0.05 m
simulation time	1000 days
C_i, inlet concentration	1.0 mole CO2(g) /kg air

In order to analyze these simulations, it is useful to define an effective retardation factor given by:

$$R = 1 + K_d\left[\frac{s}{1 - s}\right] \tag{44}$$

where s is the liquid saturation, R is the effective retardation factor and K_d is the gas-liquid distribution coefficient defined in equation (40). For this chemical system, the effective retardation factor can be used to check that FEHMN is correctly modeling the full chemical system.

Figure 27 shows that carbon retardation increases with pH. As pH increases, equations (35)-(37) produce more bicarbonate and carbonate allowing for more $CO_2(g)$ to be dissolved into the immobile water. The controlling reaction for $CO_2(g)$ retardation is equation (37). As the pH increases above $K_{a,1}$ ($K_{a,1} \approx 10^{-6.3}$ at 25 °C), the retardation increases significantly. The previous section showed that Yucca Mountain pH can vary between 7 and 8.0. Therefore, the retardation of $CO_2(g)$ is very sensitive to pH over the pH range of interest to the Yucca Mountain project.

As expected, the results of these simulations with the full chemical system matched the simulations with the effective retardation factor for all of the cases. Figure 27 shows that the effective retardation factor given in equation (44) matches the full chemical model for the pH=8.0 case. The additional cases were not shown on Figure 27 to prevent cluttering of the graph.

Figure 28 shows that temperature also affects $CO_2(g)$ retardation. $CO_2(g)$ retardation decreases with temperature as consequence of the temperature dependent equilibrium constants. For the ^{14}C environmental isotope transport calculations that will be performed in the next section, the temperature gradient only varies from 18-28 °C. Therefore, the effects on retardation due to temperature will appear to be minimal for these environmental isotope transport calculations. However, the next sections will show that temperature effects are an important factor in the two dimensional Yucca Mountain hydrological flow model. Temperature and pressure gradients are the driving forces for air movement throughout the unsaturated zone.

5.3.2 Background on ^{14}C Transport Studies

Prior to above ground nuclear testing in 1953, ^{14}C in the atmosphere was produced solely from nitrogen transmutation caused by the bombardment of cosmic rays (Freeze and Cherry, 1979). Any ^{14}C in the atmosphere is quickly oxidized to form carbon dioxide and thereby enters the carbonate

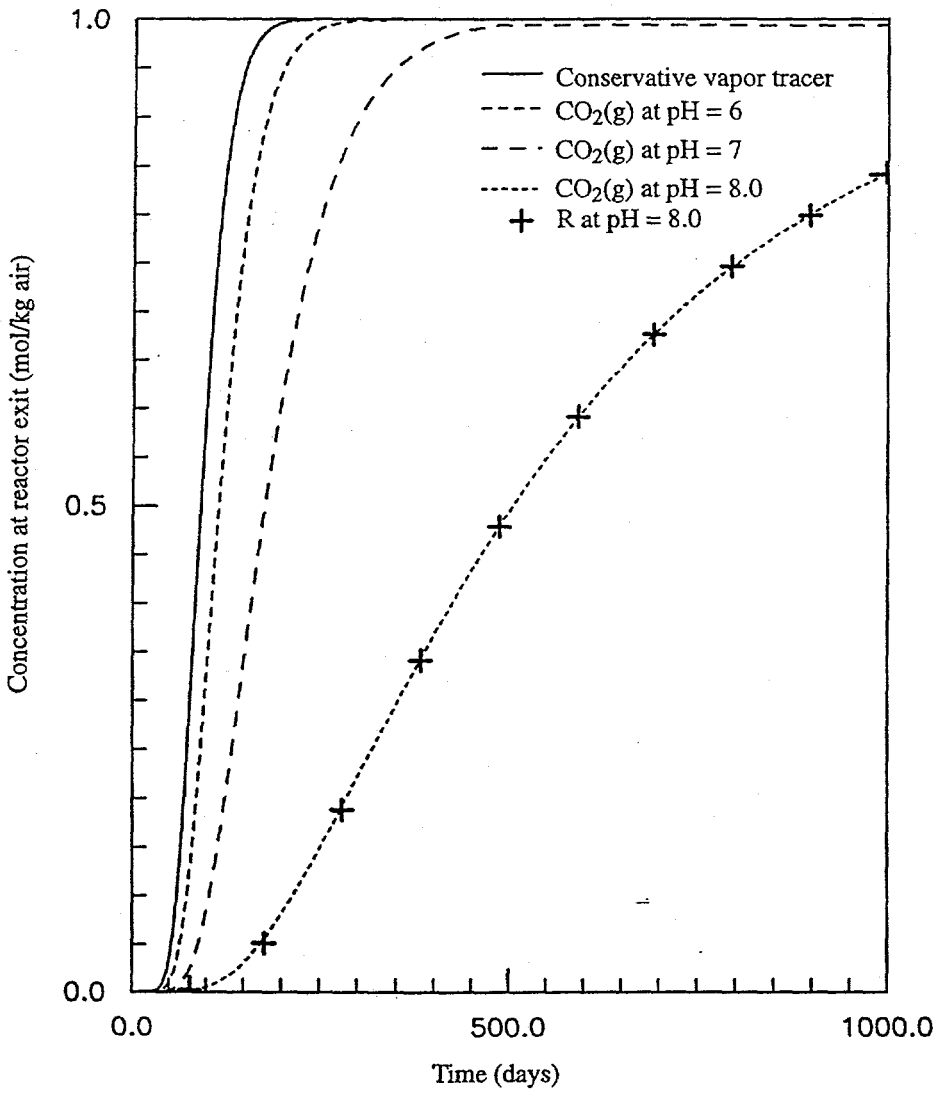

Figure 27: The effect of pH on $^{14}CO_2$(g) retardation (for these simulations, temperature = 25°C and liquid saturation = 0.2)

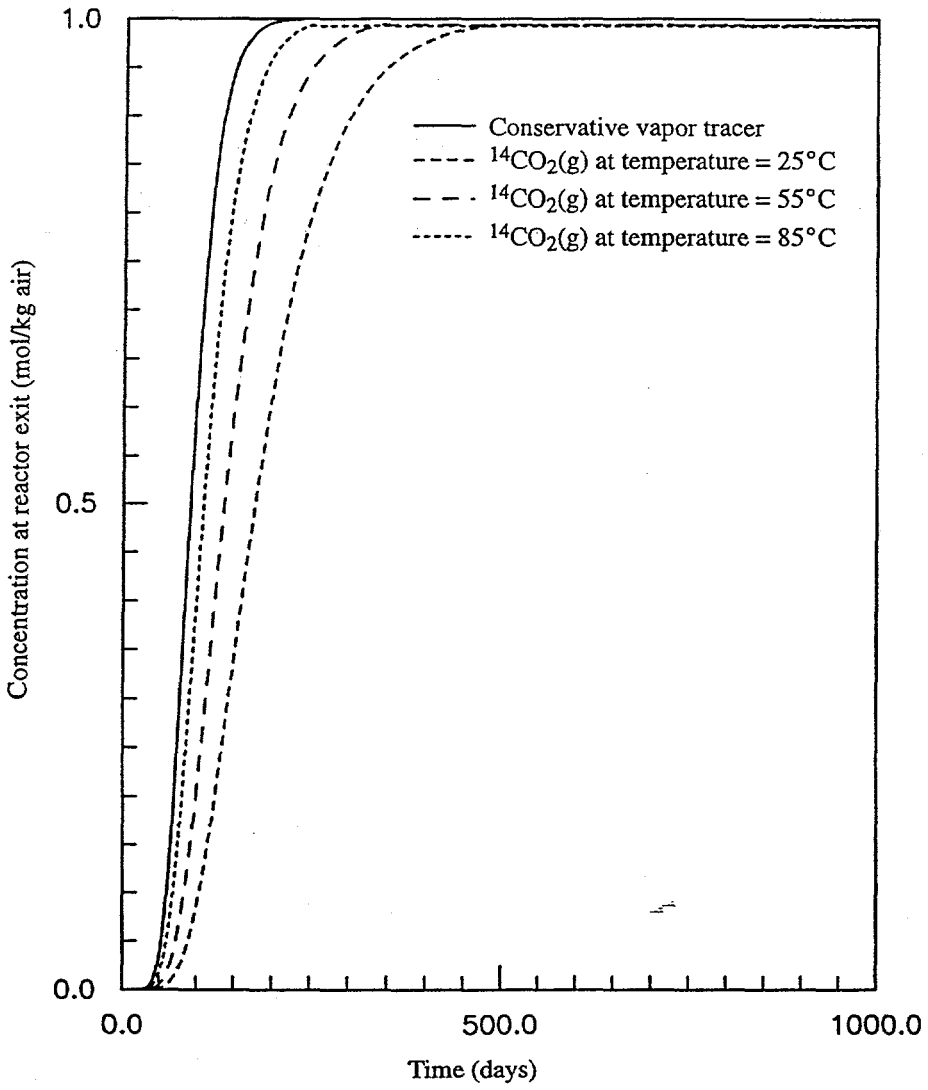

Figure 28: The effect of temperature on $^{14}CO_2$(g) breakthrough curves (for these simulations, pH=7 and liquid saturation = 0.2)

system. ^{14}C is radioactive and decays with a half life of 5730 years (CRC, 1981). Two types of ^{14}C transport are of interest to the Yucca Mountain Mountain Project: natural ^{14}C background studies and ^{14}C repository breach simulations. The study conducted in this thesis will only be concerned with conducting studies on natural ^{14}C background concentrations.

Natural ^{14}C background concentrations can in principal be used to date infiltrating groundwater at different depths throughout the mountain since the only source of ^{14}C is from the surface of the mountain. The half life of 5730 years, allows for apparent ages between $\sim$1,000 to 40,000 years to be measured accurately. Apparent groundwater ages should provide insight on the hydrologic flow and the time scales of transport at Yucca Mountain. In the unsaturated zone, gas phase transport of ^{14}C could greatly affect the concentration of ^{14}C present in the water, thereby affecting the ^{14}C apparent age.

The initial focus of the ^{14}C studies is to aid in calibrating the hydrological flow model of the site. ^{14}C, ^{36}Cl, and tritium data have been collected from numerous boreholes at Yucca Mountain. These radioisotopes are being used in attempts to identify the travel time of precipitating water from the ground surface to points where the measurements are taken. Since the surface is the only source of the radioisotopes, the radiometric analysis yields the apparent ages of the water. Apparent ages of sampled water based on ^{36}Cl analysis are about two orders of magnitude older than the ^{14}C apparent ages (Liu et al., 1995). One possible explanation for the discrepancy between ^{14}C and ^{36}Cl ages is that they transport via different mechanisms. ^{14}C transports in both the vapor and aqueous phase, whereas, ^{36}Cl travels solely in the aqueous phase. Thus one hypothesis is that ^{14}C travels more quickly in the gas phase than in the aqueous phase and gives water samples a younger age signature via partitioning of CO_2 from the gas to the aqueous phase.

To examine the possibility of ^{14}C transport in the gas phase, we take a hypothetical case in which the vapor and liquid fluxes are about equal in magnitude. The transport velocity of the vapor solute would be greater than the liquid velocity by a factor of:

$$\frac{\varrho_l s_l}{\varrho_v s_v} \tag{45}$$

where ϱ_l is the liquid density, s_l is the liquid saturation, ϱ_v is the vapor density and s_v is the vapor saturation. Under most conditions the ratio between the densities is the major factor in determining the difference between the vapor and liquid velocities. Specifically, the ratio of liquid density to vapor density is approximately a factor of 1000, whereas , the ratio of saturations is typically closer to unity. Therefore, under typical unsaturated zone conditions, the gas velocity is about three orders of magnitude faster than the liquid velocity. Therefore, the ^{36}Cl ages may be more representative of the groundwater age, whereas, ^{14}C ages may reflect the transport time of a species that partitions between the air and water in the unsaturated zone of the mountain. In order to study this hypothesis, FEHMN will be used to model two-dimensional, multi-phase, temperature dependent ^{14}C transport.

Transport studies of ^{14}C that have already been conducted within the Yucca Mountain Project take an "equivalent K_d" approach to simulate the partitioning of ^{14}C between the liquid and vapor phases (Ross, 1992). The equivalent K_d is a function of pH and temperature and is often obtained from using equilibrium geochemical codes to simulate the complex chemistry (equation (40)). In addition ^{14}C retardation is a strong function of saturation (equation (44)). This approach does not directly couple the chemistry to the heat and unsaturated flow problem but rather applies average time-invariant values of pH, temperature and saturation throughout the simulation. The enhancements to FEHMN now make it possible to simulate the carbonate system reactions directly. The chemistry calculations can be directly coupled to the thermohydrologic calculations. More representative predictions of ^{14}C transport should be possible due to the more rigorous treatment of the chemical and physical system (Robinson, 1995).

5.3.3 Two Dimensional ^{14}C Transport Simulations with LANL's Site Scale Model

The previous sections confirmed that the carbonate system chemistry is being simulated correctly by the FEHMN reactive transport model. The carbonate chemistry can now be incorporated with confidence into LANL's site scale model. The primary goal of this investigation is to examine the hypothesis that gas phase transport of ^{14}C is an important process at Yucca Mountain. The effect

of fracture permeability, pH, and diffusion on ^{14}C ages and retardation will be studied. These parameters were chosen because: 1) they can significantly affect ^{14}C transport 2) they are not known with a great deal of accuracy.

A typical simulation consists of a two step process. First FEHMN is used to establish a steady state hydrologic flow field across a two dimensional cross section of the mountain. The second step is to conduct the ^{14}C transport simulation using the steady state flow field. An East-West cross section taken from the three dimensional site scale model was used for these simulations. This cross section represents an area that cuts through the repository horizon and was generated from Sandia's CALMA Model (Robinson, 1995). The cross section shown in Figure 29 is discretized into an approximately 1000 node unstructured grid which distinguishes between 11 stratigraphic units. The landform is composed of alternating layers of interbedded and welded tuffs that have been uplifted, tilted, fractured and faulted (Liu et al., 1995). The units labeled with "w" are welded tuffs and the units labeled with "n" are nonwelded tuffs. Further details on the stratigraphy used in these simulations can be found in Three-Dimensional Model of Reference Thermal/Mechanical and Hydrological Stratigraphy at Yucca Mountain (Ortiz et al., 1985).

5.3.3.1 The FEHMN Hydrological Flow Model

Model Description

The flow field is solved by FEHMN using coupled flow and energy transport equations. The processes which are simulated include: two phase (water and air/water vapor) flow, heat and mass transfer with pressure and temperature dependent fluid and gas properties. The document, Model and Methods Summary for the FEHMN Application, details these processes (Zyvoloski et al., 1995). A great deal of work has gone into constructing LANL's site scale model. The purpose of this thesis is not to discuss the intricacies of the model but to discuss the chemical transport modeling. Therefore, only a brief summary of the assumptions and processes simulated by the flow model will be discussed. Sources for more information will be provided which discuss each individual process in greater detail.

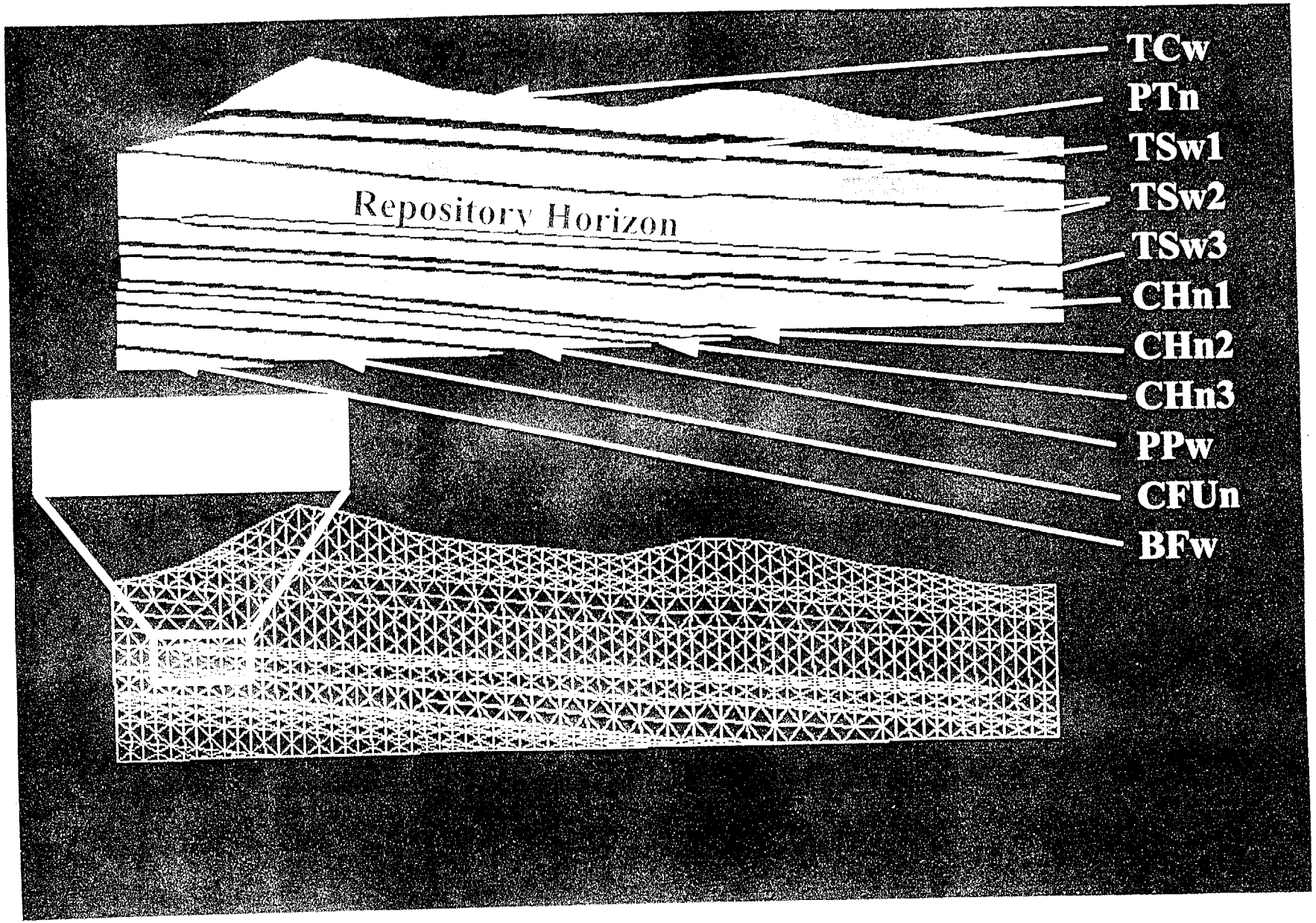

Figure 29: The Yucca Mountain stratigraphy and the site scale model finite element mesh

The ^{14}C simulations use LANL's Equivalent Continuum Model (ECM) instead of LANL's more complex Dual Permeability Model (DPM). The ECM uses a weighted average between fracture and matrix permeability to calculate the saturated permeability, whereas, the DPM models both fracture and rock matrix permeabilities separately. The ECM assumes local thermodynamic equilibrium between the rock matrix and fractures. Specifically, the rock and fractures are in capillary pressure equilibrium. Where applicable, the model provides a major simplification in modeling fluid and heat flow in fractured porous media. The literature has indicated that gas flow tends to transport primarily through fractures and that advective and diffusive transport between the fractures and the matrix is rapid enough to use the ECM for these ^{14}C simulations (Pruess et al., 1990).

Unsaturated zone flow is modeled through the use of relative permeabilities. Relative permeability can be thought of as an "effective" unsaturated zone permeability and is defined as:

$$k_l = r_l k_{sat} \tag{46}$$

where k_l is the relative permeability, and k_{sat} is the saturated permeability. The variable r_l results from the van Genuchten equations and is used to calculate the relative permeability as a function saturation (van Genuchten, 1980). Measurements for the van Genuchten relative permeability as a function of stratigraphy were obtained and were used in LANL's Equivalent Continuum Model.

The temperature boundary conditions as well as the permeability and porosity of the geological units were obtained from Total-System Performance Assessment for Yucca Mountain-SNL Second Iteration (Wilson et al., 1993). The temperature along the water table (bottom boundary) is set to 27 °C and the surface temperature was set using equations which account for topographic effects and the surface air temperature. Further details are given by Wilson et al. (1993). FEHMN is then used to calculate a steady state temperature field throughout the cross section. The permeability and porosity are highly variable among the geologic units. The general trend is that the nonwelded tuffs have higher matrix permeabilities and porosities but lower fracture permeabilities and porosities than the welded tuffs.

The pressure boundary conditions were obtained from Numerical Studies of Rock-Gas Flow in Yucca Mountain (Ross, 1992). The water table and the left and right boundaries are no flow boundaries for the gas and liquid flow. The gas pressure at the top boundary is set using equations derived by Ross et al. (1992). The equations use linear variation as a function of elevation and the ideal gas law to solve for pressure as a function of elevation. The temperature and pressure gradients are the predominant factors in driving the gas flow through the mountain.

Establishing a pseudo-steady state flow field

The FEHMN transport simulations conducted in this thesis use a steady state flow field. A two step process is used to obtain the pseudo-steady state flow field necessary for the ^{14}C transport simulations. First, FEHMN performs an isothermal flow simulation with constant infiltration to obtain a saturation field representative of the Yucca Mountain cross section. In the second step, the infiltration is turned off and the temperature and pressure boundary conditions are imposed on the flow field. Recall that the goal of these simulations was to study the effect of gas flow on ^{14}C transport, therefore the water flow (infiltration) is turned off. This second step is used to achieve a steady state temperature and gas velocity field. It should be noted that the saturation field never attains steady state once the gas flow begins. The gas flow acts to slowly dry out the mountain and slowly changes the saturation field obtained from the first step. However, this is a very slow process and the saturation field can be considered in pseudo-steady state condition. The flow field can now be used to conduct the ^{14}C transport studies.

The key assumptions made to obtain the steady state flow field are:

1. The water infiltration rate is assumed to be equal to the rate of evaporation (no infiltration, no evaporation). Specifically, the capillary forces at each spatial location are balanced by the gravitational forces.
2. The boundary conditions are not time variant. Daily and seasonal changes in temperature or barometric pressure are not taken into account.

Figure 30 shows the saturation, temperature, and velocity flow fields from an example simulation. The saturation field clearly reflects the parameters in the various geologic units. Most notably, the nonwelded tuff units such as the PTn and and CHn's (Figure 29) are much lower in saturation than the welded tuffs. This is an expected trend since the matrix permeabilities of the nonwelded units are much higher than the welded tuff. These high matrix permeabilities allow the PTn and CHn to transmit more water flow but less gas flow than the other units. Since only gas flows in these simulations, the nonwelded tuffs act as barriers to transport. The stratigraphic effects of the PTn can also be seen in the gas velocity field. The velocity field indicates that gas flow enters the valleys and exits out of the peaks due the pressure and temperature gradients which form due to the elevation change. The PTn acts as a barrier to the gas flow. The velocity field appears to be conceptually correct and corresponds well to the velocity fields given in Numerical Studies of Rock-Gas Flow in Yucca Mountain (Ross, 1992). The temperature gradient is straightforward in that it varies linearly with elevation with the exception of the topographic effects near the mountain surface. The steady state conditions of the hydrological flow model are next used to simulate ^{14}C transport.

5.3.3.2 The FEHMN Reactive Transport Model

Model Description

After establishing the steady state flow field, FEHMN is used to conduct the ^{14}C transport studies. FEHMN's Reactive Transport Model is used to perform a sensitivity analysis to determine the effect of fracture permeability, pH, and CO_2 molecular diffusion coefficient on ^{14}C retardation and ^{14}C age distributions. These preliminary calculations will be used to refine the gas flow in the hydrological model.

The steady state flow field is used to model ^{14}C transport and decay. Equations (36)–(38) are used to define the ^{14}C chemical system. Each species with ^{14}C ($H_2^{14}CO_3(aq)$, $H^{14}CO_3^-(aq)$, $^{14}CO_3^{2-}(aq)$, $^{14}CO_2(g)$) decays with a half life of 5730 years. A normalized concentration of $^{14}CO_2(g)$ is injected with the gas flow entering from the surface of the mountain. Since the only source of ^{14}C is from the surface, the amount of ^{14}C that has decayed at each spatial location in the

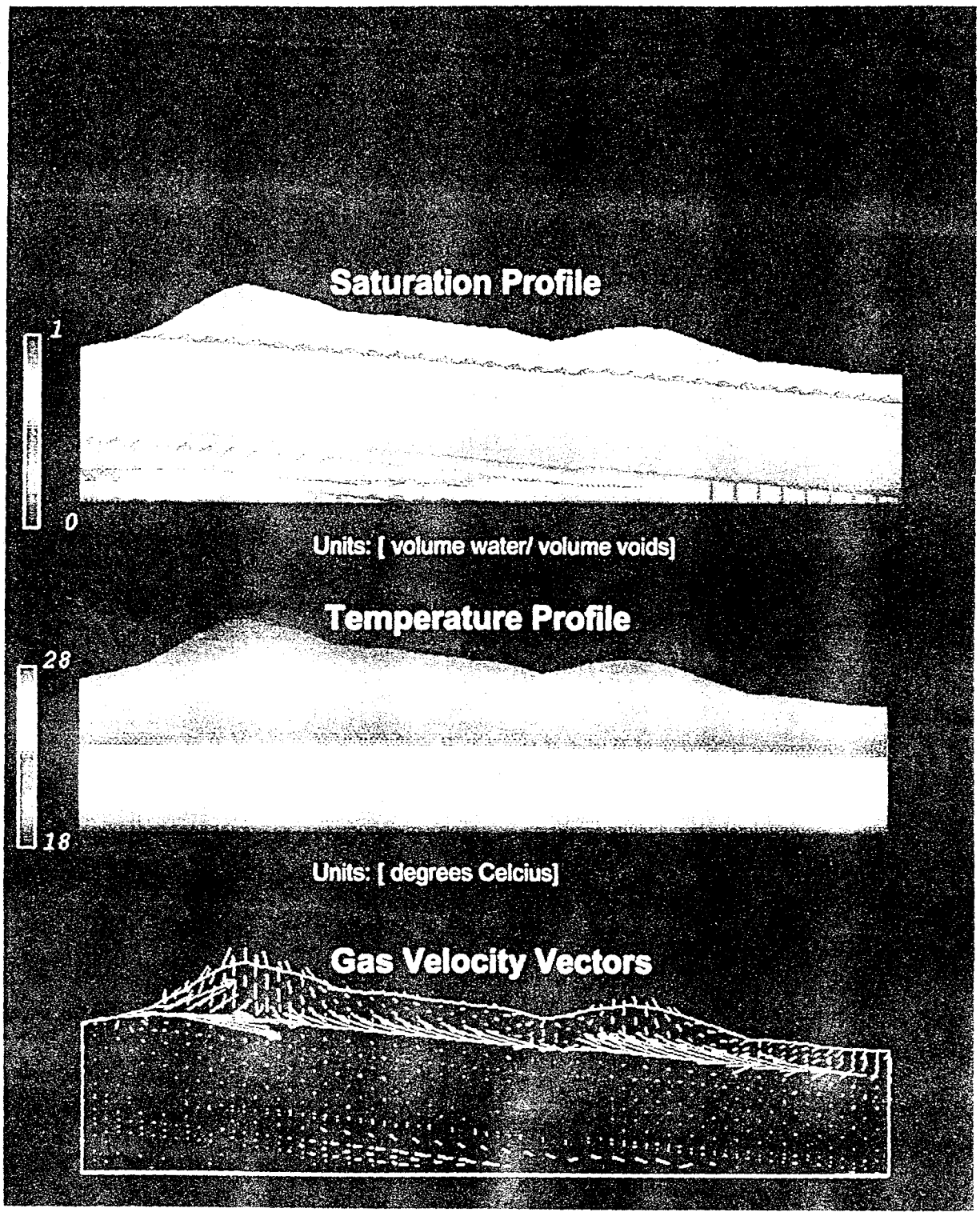

Figure 30: Steady state conditions from a PFLOTRAN hydrologic flow mode used as initial conditions for the PFLOTRAN reactive transport model.

mesh can be used to calculate the ^{14}C age. Specifically, the ^{14}C age can be calculated by (Freeze and Cherry, 1979):

$$\text{age} = -\frac{T}{\ln(0.5)}\log\left(\frac{A_i}{A_o}\right) \tag{47}$$

where age is the ^{14}C apparent age in years, T is the half life of ^{14}C (5730 years), A_i is the concentration of ^{14}C at a spatial location and A_o is the surface concentration of ^{14}C.

In these simulations, the pH, $CO_2(g)$ dispersion and the fracture permeability will be varied to determine their effect on ^{14}C retardation. The pH is an important factor for the reasons discussed in Section 5.3.1. Specifically, the pH of the solution determines the amount of $CO_2(g)$ that can dissolve into the immobile water. A reasonable pH range for Yucca Mountain is from 7 to 8 (Ross et al., 1992; Benson et al.,1983). Since water is stagnant in these simulations, molecular diffusion is the only mechanism that can transport ^{14}C into regions where there is no gas flow. The free molecular diffusion coefficient of $CO_2(g)$ into air is $1.39\text{x}10^{-5}$ m^2/s (CRC, 1981). A diffusion coefficient between $1\text{x}10^{-5}$ m^2/s to $1\text{x}10^{-6}$ m^2/s will be used in the sensitivity analysis to account for tortuosity effects that occur in porous media. The fracture permeability in the relative permeability model is a difficult parameter to determine experimentally. The fracture permeability varies a great deal between stratigraphic units. A characteristic set of high and low fracture permeabilities will be used in the sensitivity analysis. Specifically, the high set will contain fracture permeabilities that are one order of magnitude higher than the low permeabilities for each stratigraphic unit.

Example ^{14}C Transport Simulation

The results of a typical ^{14}C transport run can be postprocessed to obtain ^{14}C air-liquid distribution coefficients (K_d), retardation factors and ages as a function of spatial position (Figure 31). The simulation results shown in Figure 31 use a pH of 8, a $CO_2(g)$ diffusion coefficient of $1\text{x}10^{-5}$ m^2/s, and a characteristic set of fracture permeabilities.

The K_d values vary from 79 to 87 m^3 air/ m^3 water. Recall from equation (40), that K_d is a function of pH and temperature. Since pH is constant spatially in the simulation, the variation in K_d is due solely to the temperature field.

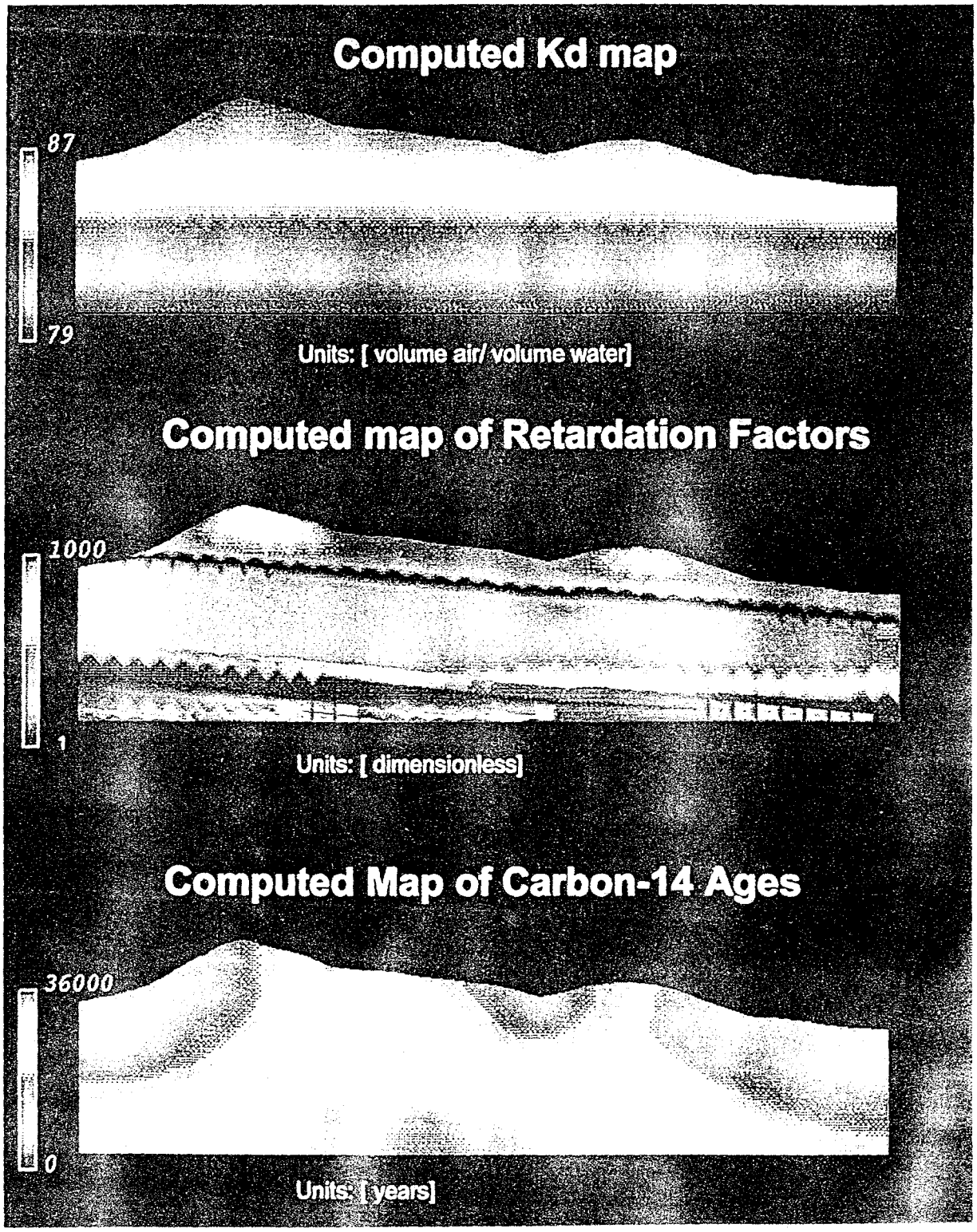

Figure 31: Example output for a ^{14}C transport simulation

The map of effective retardation factors is a function of saturation and K_d (recall K_d is a function of temperature and pH). Equation (44) illustrates that the retardation factor is much more sensitive to saturation than K_d for the range of K_d and saturation in this simulation. Therefore, the map of retardation factors greatly reflects the saturation profile shown in Figure 30. Low saturation regions exhibit little $CO_2(g)$ retardation since there is not enough water to retard the $CO_2(g)$. Regions with an extremely large retardation factor due to large saturations represent locations with very little gas flow. Any gas which does enter these locations is tied up by the large amount of water in these regions.

The map of ^{14}C ages reflects the $CO_2(g)$ velocity field. Young ^{14}C ages result at locations close to where fresh ^{14}C in the form of $CO_2(g)$ enters from the surface. The oldest ^{14}C ages result in areas where ^{14}C can only transport via diffusion (e.g. locations with little or no gas flow). At a pH of 8.0, the age ranges from 0 to 36000 years.

5.3.3.3 ^{14}C Transport Simulations: Sensitivity Analysis

In this section, the pH, $CO_2(g)$ dispersion and the fracture permeability will be varied to determine their effect on ^{14}C retardation. In each simulation, one parameter will be varied while holding the other parameters constant in order to isolate the processes which control ^{14}C retardation.

pH sensitivity

The first set of simulations was constructed to determine the effect of pH on ^{14}C retardation. Simulations of pH = 7, 7.5 and 8 were run. These pH values reflect measurements taken at Yucca Mountain. A molecular diffusion coefficient of $1x10^{-5}$ m^2/s and the set of high fracture permeabilities were used in the simulations. Figure 32 shows that as pH increases, the $CO_2(g)$ retardation also increases. This result confirms the trend shown in the one-dimensional simulations of Section 5.3.1. The age distributions all follow the same pattern in that the young ages are near the valleys on the surface where fresh $^{14}CO_2$ enters the system, whereas, the old ages exist at locations where the $CO_2(g)$ can only transport through diffusion. These simulations show that for a set of high fracture permeability and high $CO_2(g)$ diffusion, pH values less than 7.5 allow for relatively rapid ^{14}C vapor transport. Values of pH which are higher than 7.5 result in significant ^{14}C retardation.

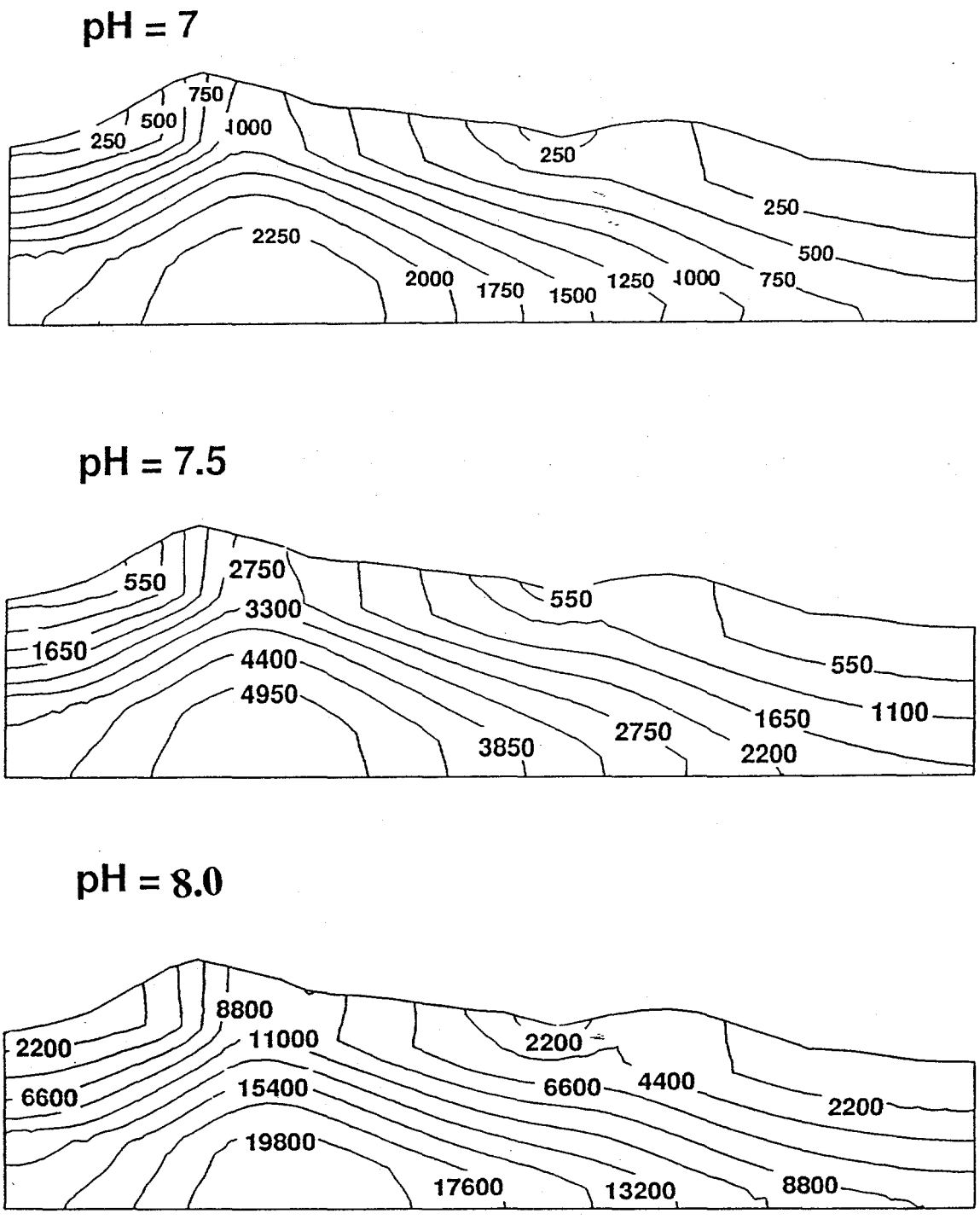

Figure 32: The effect of pH on ^{14}C apparent ages (high fracture permeabilities, $CO_2(g)$ diffusion coefficient = 1×10^{-5} m^2/s)

Measurements of pH as a function of spatial position at Yucca Mountain would be helpful in further calibrating the ^{14}C transport model. Calcium concentration distributions could also be used to generate a pH map by making the assumption that the water is in equilibrium with calcite. If calcium concentrations are available along with measurements of $CO_2(g)$ partial pressure, the reactive transport model could calculate pH by including the calcite solubility product expression (equation (41)) into the chemical model.

$CO_2(g)$ diffusion sensitivity

$CO_2(g)$ diffusion could be an important parameter which affects the modeling of $CO_2(g)$ transport. The free $CO_2(g)$ diffusion coefficient into air is 1.39×10^{-5} m^2/s (CRC, 1981). However, this constant must be adjusted in porous media due to tortuosity effects. The tortuosity of the rocks at Yucca Mountain is parameter with a large amount uncertainty associated with it. In these simulations, the effect of varying $CO_2(g)$ diffusion is examined by performing simulations for a characteristically high and low values of $CO_2(g)$ diffusion. Specifically, the diffusion coefficient was varied from 1×10^{-5} m^2/s to 1×10^{-6} m^2/s. The simulations were run at a pH of 8.0 with a high set of fracture permeabilities.

Figure 33 shows ^{14}C age profiles for a high and low set of $CO_2(g)$ diffusion. As the $CO_2(g)$ diffusion coefficient decreases, older ^{14}C ages result in the regions where there is little or no advective transport of $CO_2(g)$. For this reason, the low diffusion simulation results in much sharper age contours. $CO_2(g)$ diffusion coefficient is most critical in modeling these regions in which there is little of no advective transport of gas.

Fracture permeability sensitivity

The fracture permeability in the relative permeability model is a difficult parameter to determine experimentally. Therefore, substantial uncertainty is associated with this parameter. Two simulations were run using a high and low set of fracture permeabilities. The first simulation contains high fracture permeability parameters, whereas the second set contained low fracture permeability parameters. The values represent high and low estimates for the fracture permeability at Yucca Mountain. In each simulation, the fracture permeability varies between each of the 11 stratigraphic

$CO_2(g)$ diffusion = $1 \times 10^{-5} m^2/s$

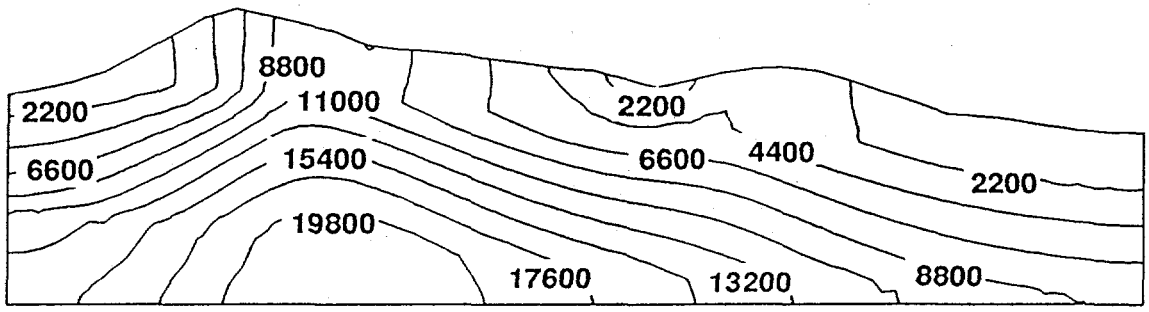

$CO_2(g)$ diffusion = $1 \times 10^{-6} m^2/s$

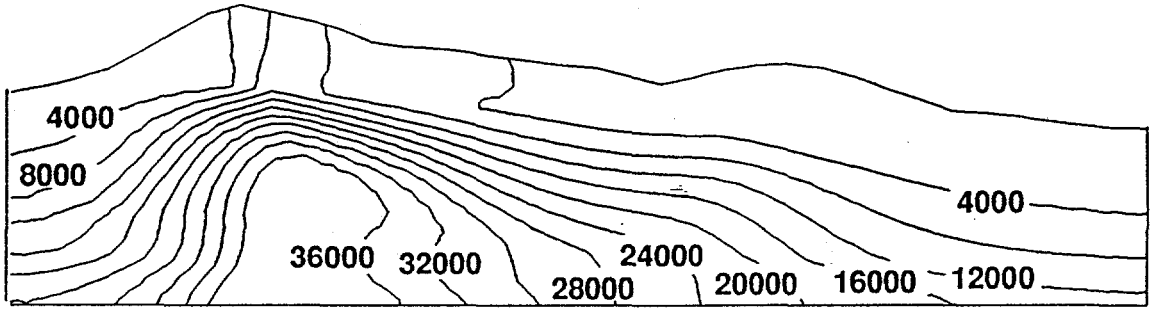

Units: all ages are in years

Figure 33: The effect of the $CO_2(g)$ diffusion coefficient on ^{14}C apparent ages (pH = 8.0, high fracture permeabilities)

units. Each stratigraphic unit in the high fracture permeability set is one order of magnitude higher than the corresponding unit in the lower set for these simulations. Both simulations used a $CO_2(g)$ diffusion coefficient of $1x10^{-5}$ m^2/s and were run at a pH of 8.

Figure 34 shows the ^{14}C age distributions for a high and low set of fracture permeabilities. Gas flow transport primarily occurs in the fractures. Therefore, the high fracture permeability set transports $CO_2(g)$ much faster than in the low set. For this reason, the ^{14}C ages are much younger in the high permeability set. As with the pH studies, the pattern of the age profiles are similar with the only difference being the magnitude of the ages.

The effect of fixing the ^{14}C age at the water table

All of the previous simulations have assumed that the only source of ^{14}C is from the $CO_2(g)$ entering with the gas flow at the surface of the mountain. This assumption was made since air flow is typically much faster than groundwater flow in the unsaturated zone. However, the water below the water table could travel much faster since saturated zone permeabilities are usually higher than unsaturated zone permeabilities. In fact, water in the unsaturated zone of Yucca Mountain has been measured to be extremely old at certain locations ($\sim$100,000 years according to the ^{36}Cl measurements), whereas, the saturated zone water may be much younger ($\sim$11,500 years according to ^{14}C ages) (Benson et al., 1983). Ages of 11,500 years are young enough for significant quantities of $^{14}CO_2(g)$ to still be dissolved in the saturated zone water considering that the half life of ^{14}C is 5730 years. Therefore, the water table can act as an additional source of ^{14}C. This hypothesis is tested in the next simulation by fixing the apparent age of ^{14}C at the bottom boundary. The assumption made by fixing the ^{14}C apparent age at the bottom boundary is that ^{14}C at the water table is in equilibrium with the $CO_2(g)$ immediately above the water table.

The pH=7 and pH=8 simulations were rerun with the additional constraint of fixing the ^{14}C age at the bottom boundary. The $CO_2(g)$ diffusion coefficient was $1x10^{-5}$ m^2/s and the high set of fracture permeabilities were used for both simulations. Figure 35 shows that adding this constraint results in much younger ages for the pH=7 and pH=8 simulations. Diffusion of $CO_2(g)$ from directly

High Set of Fracture Permeabilities

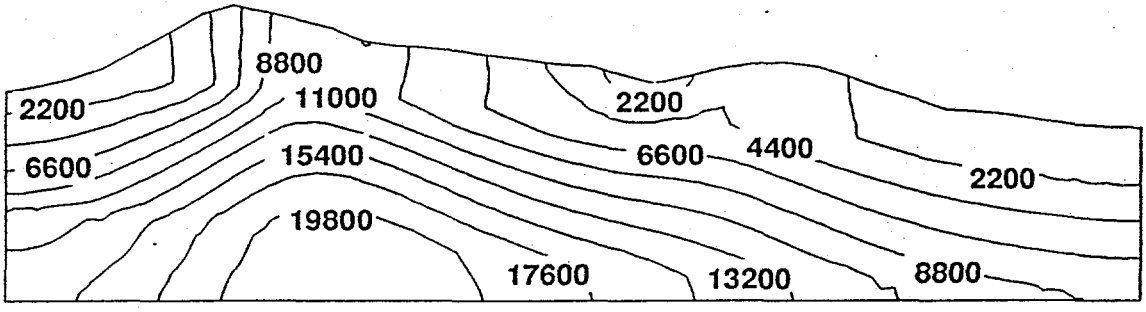

Low Set of Fracture Permeabilities

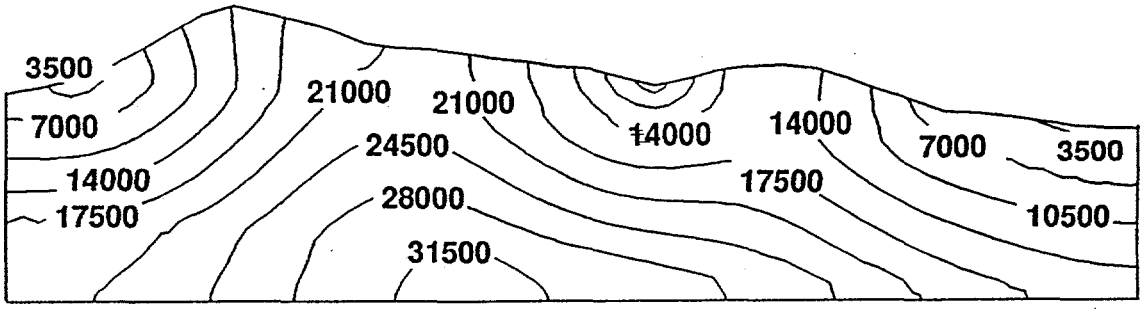

Units: all ages are in years

Figure 34: The effect of fracture permeability on ^{14}C apparent ages (pH = 8.0, $CO_2(g)$ diffusion coefficient = $1x10^{-5}$ m^2/s)

pH = 7

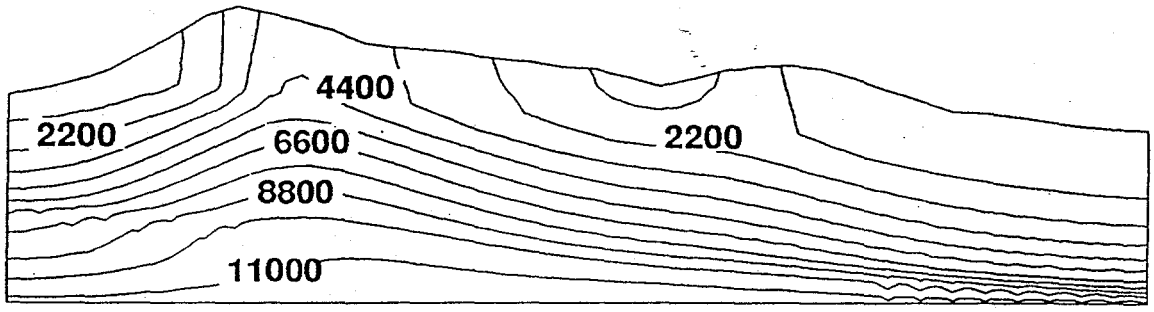

pH = 8.0

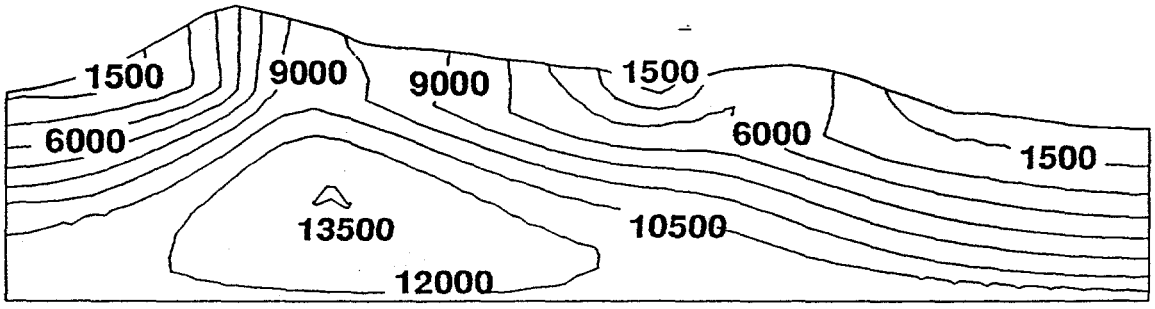

Units: all ages are in years

Figure 35: The effect of pH on ^{14}C apparent ages while fixing the ^{14}C age at the water table to 11,500 years (high fracture permeabilities, $CO_2(g)$ diffusion coefficient = 1×10^{-5} m^2/s)

above the water table acts to eliminate many of the old ages that occur in the previous simulations. This simulation shows that the oldest apparent ^{14}C ages no longer exist due to the additional source of ^{14}C.

Conclusions from the Sensitivity Analysis

These preliminary ^{14}C transport simulations have shown that gas flow through the unsaturated zone of Yucca Mountain can be a very significant factor in ^{14}C transport. In fact, simulations with no groundwater flow resulted in rather complex ^{14}C age distributions. Therefore, gas flow should definitely be considered when interpreting ^{14}C apparent ages. The only true conclusion which can be reached from these runs is that the discrepancy between ^{14}C and ^{36}Cl ages can be explained by gas transport through fractures at Yucca Mountain. However, more experimental data is required to determine whether this hypothesis is correct.

5.4 Performance of the FEHMN Reactive Transport Model

The background ^{14}C transport simulations proved to be a good introductory application for the FEHMN reactive transport model. The simulations successfully used LANL's site scale model to model the retardation of $CO_2(g)$ due to chemical reactions. The simulations proved that gas flow at Yucca Mountain could be a significant transport mechanism for ^{14}C transport. However, many of the important capabilities of FEHMN were not brought out in this example.

The coupling of the flow and transport solutions was not used in the problem. Specifically, for natural ^{14}C background simulations, the flow field is first allowed to reach steady state before the transport simulations begin. The next application of the reactive transport model, simulated ^{14}C transport from a repository breach, will take advantage of the coupling between the flow and transport model. ^{14}C transport from a breach of the potential repository can be simulated once a model of the repository is incorporated into the finite element mesh. Gas flow should be even more important for the repository calculations as heat from the repository gives rise to gas phase buoyant convection. The heating of the repository will produce time variant processes in temperature, flow, and saturation. These time variant processes will be directly coupled to the chemistry in these simulations which should result in some very interesting coupled processes.

The kinetic capability of the reactive transport solution was also not used in the ^{14}C natural background studies. The reactive transport model was designed so that both equilibrium and kinetic reactions could be modeled. However, the ^{14}C simulations conducted in this thesis assumed that all reactions were at local equilibrium since the natural background simulations are modeled for over 10,000 years. Therefore, kinetic limitations are not a consideration for these long simulations. In fact, this application could have been simulated more efficiently with a fully equilibrium formulation. However, many other FEHMN simulations will require the kinetic capabilities of the code. Kinetic limitations will play a role for the repository breach simulations. The time scales of transport will be much shorter for these simulations and kinetic sorption and precipitation/dissolution reactions may be necessary to describe the transport of contaminants such as ^{237}Np. Therefore, the fully kinetic formulation used by FEHMN should prove to be useful in the future.

The example problems shown in Chapter 4 and the application problems shown in Chapter 5 tested the FEHMN reactive transport capabilities for a wide variety of conditions. The model is capable of simulating multi-dimensional transport of small chemical systems (less than 10 species) quite rigorously. The transport models of various radioisotopes and other contaminants can now be refined using the model. At this time, the need for modeling more complex chemical systems (more than 10 species) appears to be unnecessary.

Two options exist to increase the number of species that can be modeled by FEHMN. The first option is to refine the solver technology used by FEHMN. Specifically, the limit of 10 species arises due to CPU and memory limitations incurred by the linear equation solver GZSOLVE. Methods may be available to simplify the chemical equation sets within the solver to increase the capacity of the reactive transport model. An advantage of this option is that the code development would be conducted within the solver thereby leaving the software structure of FEHMN intact. In addition, the solver is also used for the flow equation sets. Therefore, better solver technology would increase both FEHMN's flow and chemical transport capability. The second option is to incorporate a mixed equilibrium-kinetic formulation into FEHMN. The mixed formulation would make use of the local equilibrium assumption to reduce the number of coupled PDEs in the chemical equation set. As

mentioned in Section 2.2, significant software restructuring would be necessary to incorporate a mixed formulation into FEHMN. An equilibrium speciation routine would need to be constructed or borrowed from another code. In addition, the solute transport model of FEHMN would have to be modified to transport chemical components rather than chemical species. However, the mixed formulation would greatly increase the capability of the reactive transport model. Both options may be explored in the future if additional geochemical modeling capability is necessary.

REFERENCES

Allison, J.D., Brown, D.S., Novo-Gradac, K.J., MINTEQA2/PRODEFA2, A Geochemical Assessment Model for En vironmental Systems: Version 3.0 User's Manual, EPA/600/3-91/021, 1991.

Bahr, J. M., and J. Rubin, Direct comparison of kinetic and equilibrium formulations for solute transport affected by surface reactions, *Water Resources Research, 23*, 438-452.

Barret, R., M. Berry, T. Chan, J. Demmel, J. Donato, J. Dongarra, V. Eijkhout, R. Pozo, C. Romine, and H. Van der Vorst, *TEMPLATES for the solution of linear systems: Buildings blocks for iteratives methods*, SIAM Publication, 1994.

Benson, L. V., J. H. Robinson, R. K. Blankennagel, and A. E. Ogard, Chemical composition of groundwater and the locations of of permeable zones in the Yucca Mountain area, Nevada, *United States Geological Survey Open File Report Number 83-854 (USGS-OFR-83-854)*, 1983.

Brusseau, M. L., R. E. Jessup, and P. S. C. Rao, Modeling the transport of solutes influenced by multiprocess nonequilibrium, *Water Resources Research, 25*, 1971-1988, 1989.

Cederberg, G. A., R. L. Street, and J. O. Leckie, A groundwater mass transport and equilibrium chemistry model for multicomponent systems, *Water Resources Research, 21*,1095–1104, 1985.

CRC Handbook of Chemistry and Physics, 62nd edition, CRC Press, New York, 1981.

Dash, Z.V., B.A. Robinson, V&V Plan and Procedures for the FEHMN Application, *Los Alamos Document ECD-22*, Rev. 1, 1995a.

Dash, Z.V., B.A. Robinson, V&V Report for the FEHMN Application, *Los Alamos Document ECD-22*, Rev. 1, 1995b.

Dongarra, J. J., I. S. Duff, D. C. Sorenson, and H. A. Van der Vorst, *Solving linear systems on vector and shared memmory computers*, SIAM publication, 1991.

Engesgaard, P., Geochemical Modelling of Contaminant Transport in Groundwater, Ph.D. Thesis, Institute of Hydrodynamics and Hydraulic Engineering, Technical University of Denmark, 1991.

Engesgaard, P., and K. L. Kipp, A geochemical transport model for redox-controlled movement of mineral fronts in groundwater flow systems: A case of nitrate removal y oxidation of pyrite, *Water Resources Research, 28*, 2829–2843, 1992.

Fetter, C.W., *Contaminant Hydrology*, Macmillan Publishing Company, New York, 1993.

Freeze, A.R., J.A. Cherry, *Groundwater*, Prentice-Hall, Englewood Cliffs, N. J., 1979.

Goltz, M. N., and P. V. Roberts, Interpreting organic solute transport data from a field experiment using physical nonequilibrium models, *Journal of Contaminant Hydrology, 1*, 77–94, 1986.

Hutzler, N. J., J. C. Crittenden, J. S. Gierke, and A. S. Johnson, Transport or organic compounds with saturated groundwater flow: Experimental results, *Water Resources Research, 22*, 285-295, 1986.

Javandel, I., C. Doughty, and C. F. Tsang, *Groundwater Transport: Handbook of Mathematical Models*, AGU, WR Monograph 10, 1984.

Knapp, R.B., Spatial and temporal scales of local equilibrium in dynamic fluid-rock systems: *Geochimica et Cosmochimica Acta, 53*, 1955-1964, 1989.

Lasaga, A.C., and Rye, D.M., Fluid flow and chemical reaction kinetics in metamorphic systems: *American Journal of Science, 293*, 361-404, 1993.

Levenspiel, O., *Chemical Reaction Engineering*, 2nd edition, John Wiley & Sons, New York, 1962.

Light, W. B., Chambré, P. L., Lee, W.L., and Pigford, T.H., Transport of gaseous ^{14}C in a partially saturated, fractured, porous medium, presented in Boston, MA, *Scientific Basis for Nuclear Waste Management XIII*, November 27–30, 1989.

Liu, B.L., J.F. Martin, A. Wolfsberg, B. Robinson, and P. Sharma, Significance of Apparent Discrepancies in Water Ages Derived from Atmospheric Radionuclides at Yucca Mountain, Nevada, *Los Alamos Document LA-UR-95-575*, 1995.

Liu, C. W., and T. N. Narasimhan, Redox-controlled multiple-species reactive chemical transport, 1, Model development, *Water Resources Research*, *25*, 869-882, 1989.

Mangold, C. D., and C. F. Tsang, A summary of subsurface hydrological and hydrochemical models, *Rev. Geophys.*, *29*, 51-71, 1991.

Meijer, A., Far–field transport of carbon dioxide: retardation mechanisms and possible validation experiments, presented in Las Vegas, NV, Conference Proceedings FOCUS '93, September 26–29, 1993.

Nicoud, R. M., and D. Schweich, Solute transport in porous media with solid-liquid mass transfer limitations: Application to ion exchange, *Water Resources Research*, *25*, 1071-1082, 1989.

Nitsche, H., R. C. Gatti, E. M. Standifer, S. C. Lee, A. Muller, T. Prussin, R. S. Deinhammer, H. Maurer, K. Becraft, S. Leung, S. A. Carpenter, Measured Solubilities and Speciations of Neptunium, Plutonium, and Americum in a typcial groundwater (J-13) from the Yucca Mountain Region, *Los Alamos National Laboratory Report Number LA-12562-MS*, 1993.

Ortiz, T.S., R.L. Williams, F.B. Nimick, B.C. Whittet and D.L. South, A Three-Dimensional Model of Reference Thermal/mechanical and Hydrological Statigraphy at Yucca Mountain, Southern Nevada," *Sandia Report (SAND 84-1076)*, 1985

Pinder, G. And W. Gray, *Finite Element Simulation in Surface and Subsurface Hydrology*, Academic Press, New York, 1977.

Plummer, L.N., and E. Busenberg, The solubilities of Calcite, Argonite, and Vaterite in CO_2–H_2O solutions between 0 and 90 C, and an evaluation of the aqueous model for the system $CaCO_3$–H_2O, *Geochimica et Cosmochima Acta, 46*, 1101, 1982.

Press, W. H., S. A. Teukolsky, W. T. Vettering, B. P. Flannery, *Numerical Recipes in FORTRAN*, 2nd edition, Cambridge University Press, New York, 1992.

Pruess, K., J. S. Y. Wang, and Y. W. Tsang, Thermohydrologic conditions near high–level nuclear waste emplaced in partially saturated fractured tuff, *Water Resources Research*, 26, 1235–1261, 1990.

Reeves, M., N. A. Baker, and J. O. Duguid, Review and selection of unsaturated flow models, Civilian Radioactive Waste Management and Operating Contractor Report Number B00000000-01425-2200-00001, 1994.

Robinson, B.A. , C. Gable, G. Zyvoloski, Summary of recent retardation sensitivity analysis activities, *Yucca Mountain Site Characterization Number 3416 (LA–EES–5–TIP–94–001)*, 1995.

Ross, B., Gas–phase transport of carbon–14 released from nuclear waste into the unsaturated zone, presented in Boston, MA, Scientific Basis for Nuclear Waste Management XI, November 30–December 3, 1987.

Ross, B., S. Amter, N. Lu, Numerical Studies of Rock–Gas Flow in Yucca Mountain, *Sandia Report (SAND91–7034)*, 1992.

Rubin, J., Transport of reacting solutes in porous media: Relation between mathematical nature of problem formulation and chemical nature of reaction, *Water Resources Research*, *19*, 1231–1252, 1983.

Rubin, J., Solute transport with multisegment, equilibrium controlled reactions: A feedforward simulation method, *Water Resources Research*, *26*, 2029-2055, 1990.

Schweich, D., M. Sardin, Transient ion exchange and solubilization of limestone in an oil field sandstone: Experimental and theoretical wavefront analysis, *American Institute Chemical Engineering Journal*, 13, 1882–1890, 1985.

Snoeyink, V.L., D. Jenkins, *Water Chemistry*, John-Wiley & Sons, New York, 1980.

Steefel, C.I., and Lasaga, A.C., A Coupled Model for Transport of Multiple Chemical Species and Kinetic Precipitation/Dissolution Reactions with Application to Reactive Flow in Single Phase Hydrothermal Systems, *American Journal of Science, 924*, 529-592, 1994.

Szecsody, J.E., J.M. Zachara, P.L. Bruckhart, *Environmental Science and Technology, 28*, 1706–1716, 1994.

Toran, L. , Radionuclide contamination in groundwater: is there a problem?, in: *Groundwater Contamination and Control*, U. Zoller, ed., Marcel Dekker, NY, 1994.

Valocchi, A. J., and D.E. Pastor, "PDREACT, Version 1.1, Description and User's Guide," Dept. of CE, University of Illinios, DRAFT, May 1994.

Valocchi, A. J., Validity of the local equilibrium assumption for modeling sorbing solute transport through homogeneous soils, *Water Resources Research, 21*, 808–820, 1985.

van der Zee, S. F. Lens, and M. Lauer, Prediction of phosphate transport in small columns with an approximate sorption kinetics model, *Water Resources Research, 25*, 1353-1365, 1989.

van Genuchten, M. T., A closed form equation for predicting hydraulic conductivity of unsaturated soils, *Soil. Sci. Soc. Am. J., 44*, 892-898, 1980.

Vichnevetsky, R., *Computer Methods for Partial Differential Equations*: Volume 1, Prentical-Hall, 1981.

Walsh, M.P., S.L. Bryant, R.S. Schechter, L.W. Lake, Precipitation and dissolution of solids attending flow through porous media, *American Institute Chemical Engineering Journal, 30*, 317–328, 1984.

Walter, A. L., E. O. Frind, D. W. Blowes, C. J. Ptacek, and J. W. Molson, Modeling of multicomponent reactive transport in groundwater, 1, Model development and evaluation, *Water Resources Research, 30*, 3149–3158, 1994.

Wilson et al., Total-System Performance Assessment for Yucca Mountain-SNL Second Iteration (TSPA-1993), *Sandia Report (SAND93-2675)*, 1993.

Wood, W. W., T. F. Kraemer, and P. P. Hearn, Intragranular diffusion: An important mechanism influencing solute transport in clastic aquifers? *Science, 247*, 1569–1572, 1990.

Yang, I. C., Status of H–3, C–14, and stable isotope studies to date groundwater in the unsaturated zone at the proposed Yucca Mountain Site–results and interpretation, presented in Las Vegas, Nevada, to the Advisory Committee on Nuclear Waste, October 20–21, 1994.

Yeh, G. T., and V. S. Tripathi, A critical evaluation of recent developments in hydrogeochemical transport models of reactive multichemical components, *Water Resources Research, 25*, 93–108, 1989.

Yeh, G. T., and V. S. Tripathi, HYDROGEOCHEM: A coupled model of HYDROlogical transport and GEOCHEMical equilibrium of multi-component systems, *Rep. OVRL-6371*, Oak Ridge National Laboratory, Oak Ridge, Tenn, 1988.

Zysset, A., Stauffer, and T. Dracos, Modeling of chemically reactive groundwater transport, *Water Resources Research, 30*, 2217-2229, 1994.

Zyvoloski, G.A., Science and Technology Assessment and External Review Committee Meeting, May 16-18, 1994.

Zyvoloski, G.A., B.A. Robinson, Z.V. Dash, and L.L. Trease., Models and Methods Summary for the FEHMN Application, *Los Alamos National Laboratory Software Document ECD-22*, 1995a.

Zyvoloski, G.A. and B.A. Robinson, , Models and Methods Summary for the GZSOLVE Application, *Los Alamos National Laboratory Software Document ECD-97*, 1995b.